Experimental study of air-to-air heat/energy exchangers for use in Arctic housing

Colin J. Beattie

A Thesis
in
The Department
of
Building, Civil and Environmental Engineering

Presented in Partial Fulfillment of the Requirements
for the Degree of Master of Applied Science (Building Engineering) at
Concordia University
Montreal, Quebec, Canada

June 2017

CONCORDIA UNIVERSITY
School of Graduate Studies

This is to certify that the thesis prepared

By: Colin J. Beattie

Entitled: Experimental study of air-to-air heat/energy exchangers for use in Arctic housing

and submitted in partial fulfillment of the requirements for the degree of

Master of Applied Science (Building Engineering)

complies with the regulations of the University and meets the accepted standards with respect to originality and quality.

Signed by the final examining committee:

Dr. A. Athienitis Chair

Dr. H. Ge Examiner

Dr. L. Kadem Examiner

Dr. R. Zmeureanu Supervisor

Approved by _____
Chair of Department or Graduate Program Director

_____
Dean of Faculty

Date _____

ABSTRACT

Experimental study of air-to-air heat/energy exchangers for use in Arctic housing

Colin J. Beattie

The thesis presents the experimental results of an air-to-air heat/energy exchanger (HEE), tested with four different cores, to assess the performance under Arctic climate conditions. Four performance indicators are presented: (i) the outlet supply air temperature; (ii) the exhaust air flow rate; (iii) the sensible and latent heat transfer effectiveness; and (iv) UV-value. The mass of ice formed within the core was also measured at the end of each experiment. The experiments are separated into three phases: Phase 1 with one HEE without recirculation defrost, Phase 2 with one HEE with recirculation defrost, and Phase 3 with two HEEs in parallel with alternating recirculation defrost. Correlation−based models were developed that predict the change in heat transfer effectiveness in terms of the change in exhaust air mass flow rate, inlet supply air temperature and core type. The experiments with recirculation defrost proved that the factory-set defrost times are a conservative approach that manages the formation of frost. Because of the reduced operating time as controlled by the timer, all cores have almost the same sensible heat transfer effectiveness. The use of vapour-permeable cores reduced the rate of frost growth and the amount of frost at inlet supply air temperatures where core frosting was a concern. The rate of core frosting was dependant on the inlet supply air temperature. Frost formation impeded the transfer of heat between the two airstreams and reduced the adjusted sensible and latent heat transfer effectiveness for all cores. Recirculation defrost effectively managed the formation of frost in all tested exchanger cores for the duration of the tests at inlet supply air temperature down to −35°C. However, the use of recirculation defrost intermittently interrupts the supply of outdoor air resulting in reduced ventilation rates. The use of two heat/energy exchangers with alternating recirculation defrost adequately managed core frosting while providing a continuous supply of outdoor air.

ACKNOWLEDGEMENTS

First and foremost, I would like to thank the late Dr. Paul Fazio who supported and guided me throughout my thesis. Dr. Fazio's unfaltering commitment to the field of building engineering was and still is a constant motivation for myself and, without doubt, for all who had the privilege of working with him. Dr. Fazio was a true leader on so many fronts; be it through his countless research efforts, industry partnerships, or university initiatives; his legacy and contributions will continue on for generations.

I would like to thank my co-supervisor Dr. Radu Zmeureanu. This thesis would not have been possible without his guidance and direction. Thank you for trusting me and sharing your technical expertise. I would like to thank Dr. Hua Ge, Dr. Andreas Athienitis and Dr. Jiwu Rao for their support throughout my thesis, more specifically during the difficult transition after the passing of Dr. Fazio. The support of my family and fellow colleagues was invaluable. It was a real pleasure having the opportunity to meet so many motivated and truly brilliant people through the course of my studies.

I would like to acknowledge the in-kind support of our industry partners: Venmar Ventilation Inc. and dPoint Technologies Inc. Furthermore, I would like to thank Jeff Armstrong of KOTT Group (DAC International), who was always available to share his knowledge of and experiences in northern Canada. The equipment and technical expertise provided by all partners were integral to the success of this research project.

Finally, I would like to acknowledge the financial support from Natural Sciences and Engineering Research Council of Canada, through the Smart Net-Zero Energy Buildings Strategic Research Network, and the Faculty of Engineering and Computer Science of Concordia.

TABLE OF CONTENTS

LIST OF FIGURES

LIST OF TABLES

LIST OF SYMBOLS AND UNITS

Name	Symbol	Units
Cross-sectional area	A_c	m^2
Surface area	A_s	m^2
Floor area	A_{floor}	m^2
Specific heat capacity of air	c_{pa}	J kg^{-1} K^{-1}
Diameter	D	m
Enthalpy	h	J $kg_{dry\ air}^{-1}$
Heat of vapourization of water	h_{fg}	J kg^{-1}
Logarithmic mean temperature difference	$LMTD$	°C
Mass flow rate	$\dot{m}$	kg s^{-1}
Number of bedrooms	N_{br}	–
Pressure	P	Pa
Atmospheric pressure of air	p_{atm}	Pa
Dynamic air pressure	$p_{dynamic}$	Pa
Saturation pressure of air	p_{sat}	Pa
Static air pressure	p_{static}	Pa
Total air pressure	p_{total}	Pa
Vapour pressure of air	p_v	Pa
Rate of heat transfer	Q	W
Standard deviation	S_x	–
Temperature	T	°C
Test duct	TD	–
Overall heat transfer coefficient	U	W m^{-2} K^{-1}
Overall uncertainty	U_x	–
Volumetric flow rate	$\dot{V}$	m^3 s^{-1}
Effectiveness	ε	–
Latent heat transfer effectiveness	ε_l	–
Adjusted latent heat transfer effectiveness	ε'_l	–
Sensible heat transfer effectiveness	ε_s	–
Adjusted sensible heat transfer effectiveness	ε'_s	–
Total heat transfer effectiveness	ε_T	–
Density of air	ρ_a	kg·m^{-3}
Relative humidity of air	ϕ	%
Humidity ratio	ω	kg_{water} $kg_{dry\ air}^{-1}$

1. INTRODUCTION

1.1. Context and Motivation

1.1.1. Northern Canada

Inuit Nunangat spans 5 provinces and territories in northern Canada and is divided into four regions (**Figure 1.1**). The four regions are the Inuvialuit region (consisting of the northern coastal regions of the Yukon and North West Territories), the Territory of Nunavut, Nunavik (northern Quebec) and Nunatsiavut (northern coastal Labrador).

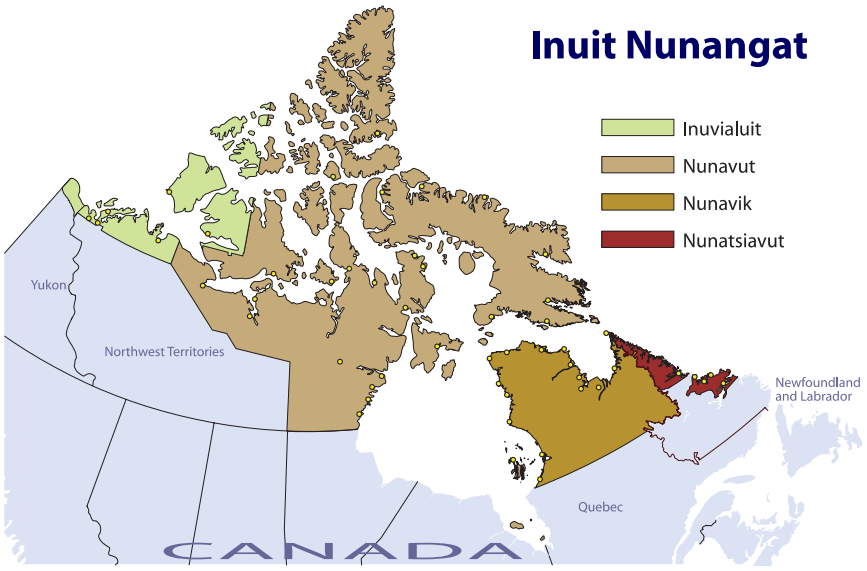

Figure 1.1: Map of northern Canada indicating the different regions of Inuit Nunangat [1]

Inuit Nunangat is the ancestral homeland of the Inuit people of Canada. In 2011, the population of Inuit Nunangat was 52,115 of which 83% identified as being Inuit [2].

The communities located in Inuit Nunangat are typically small and located near the coast. There is a limited network of roads connecting these communities, where most of the communities are accessible only by aircraft or seasonal boats. As a result of this limited mobility, the availability of materials and goods is infrequent and typically constrained to the warmer summer months. Three quarters of all fuel consumption in Northern Canada is a by-product of refined oil import-

ed from the southern provinces [3]. These fuels are primary used for heating, transportation, and electricity generation. More specifically, all electricity in Nunavut is generated from diesel fuel imported from the south [3]. The high cost of importing energy products along with the method of energy production have resulted in northern Canada having the highest end-use energy costs nationally [3]. Even with these regional limitations, the Inuit people are the least likely to consider moving from their communities. Many identify their family ties, social support of each other, and traditional activates as the primary reasons for remaining in these communities [4].

1.1.2. Housing in Northern Canada

The largest city in the region, Iqaluit, is located on Baffin Island in Nunavut. The majority Inuit city is one of the fastest growing communities in Canada with a 8.3% increase in population for the 5 year period between 2006 and 2011 [5]. The Canadian national average for the same period was 5.9%. Regionally, Arctic Canada has the youngest and fastest growing population in Canada, with a median age in 2009 nearly half that for the rest of Canada and a fertility rate more than double that for the rest of the country [6]. The increase in population, particularly in Iqaluit, has been accompanied by an increase in the demand for housing. During the same period between 2006 and 2011 the percent increase in the number of private dwellings occupied by usual residents was nearly double the national average [5]. Even though there was a significant increase in the number of *private* dwelling, the majority of housing in Nunavut is public or government housing. There are approximately 8550 regularly occupied households in Nunavut, of which 51% are public housing, 16% are government staff housing and 33% are privately-owned [7].

The need for more housing is not only linked to the increase in population. Inadequate temperature and humidity control, along with high air leakage in the building envelopes in northern

housing has been found to increase the occurrence of moisture-related problems such as mould-growth, mildew and frost [8]. Additionally, the layout of homes, typically designed based on Euro-Canadian standards, are not ideal for the activities carried out by Inuit families [9]. As a result, the state of good repair for housing in northern Canada is particularity poor and does not meet the current needs of many habitants. Eighteen percent of the households in the region require major repair with 23% of households in Nunavut requiring major repair. The average percentage of households requiring major repair in Canada is only 7.5% [10]. In these studies a household is considered to be in need of major repair if the dwelling is not able to adequately provide basic household services such as water, heat, electricity and shelter.

Primarily due to the lack of quality housing, overcrowding is another significant issue in northern Canada. Sixteen percent of households in the region are considered to be overcrowded [11]. Nunavut has the highest rates of overcrowding, with 35% of households considered overcrowded [7]. In these studies a dwelling is considered overcrowded when the number of bedrooms is not sufficient for the occupants as determined by the National Occupancy Standard (NOS).

The poor housing conditions in Northern Canada has been identified as one of many contributing socio-economic factors in the high rate of physical and mental illness. The regions higher suicide rates have been linked to the possible contributing role of several socio-economic factors, one of which is poor housing conditions [12]. Furthermore, the life expectancy for people living in Nunavut between 2005 and 2007 was nearly ten years lower when compared to the rest of the Canadian population [6]. This is all underlined by the fact that only one in two people in Arctic Canada self-identify as being in very-good health [4].

1.1.3. Household Ventilation

One of many concerns when it comes to households that are overcrowded and in need of major repair is indoor air quality (IAQ). In the past designers relied on air leakage through the building envelope as the primary source of outside air. However, in order to reduce space heating energy consumption, airtight housing construction has become common practice in Canada.

The importance of indoor air quality in northern housing is underlined in [13]. This study investigated the high rate of lower respiratory tract infections in Canadian Inuit children. The investigation included 49 homes spread over multiple communities located in the Baffin (Qikiqtaaluk) region. It concluded that the poor indoor air quality as a result of insufficient ventilation and overcrowding within the homes maybe the reason for the higher rates of infections. This particular study was followed up by [14], where air-to-air heat exchangers were installed in multiple homes in the same region to see if the rate of respiratory tract infections changed in Canadian Inuit children. The installation of the exchangers was found to reduce indoor air pollutes, more specifically carbon dioxide, and the relative humidity of indoor air. There was also a reduction in reported wheezing and rhinitis over the 6-month evaluation period. The study concluded that the use of air-to-air heat exchangers was associated with improved air quality and a reduction in reported respiratory infection symptoms in Inuit children. Models have been developed based on field measurements to investigates the effectiveness of mechanical ventilation on reducing indoor contaminants [15].

Air-to-air heat/energy exchangers are utilized extensively across Canada to reduce the energy required for heating while providing outside air to airtight housing. Limitations, however, still exist for northern Arctic regions. Due to the extremely cold inlet supply sir temperatures in these regions, moisture in the exhaust air condenses within the air exchanger core resulting in frost

formation. This phenomenon can result in a reduction in system efficiency and if allowed to propagate can lead to system failure and/or damage.

The existing operating procedure for air exchangers in northern Arctic climates typically requires the pre-heating of inlet supply air before entering the heat/energy exchanger in order to reduce the potential for frost formation. This can be costly because as previously mentioned Northern Canada has some of the highest end-use energy costs nationally. Conventional defrosting practices, while adequate in more temperate locations in Canada, are not optimal for managing the accumulation of frost in an exchanger in these regions. New preventive and retroactive frost control methods are needed to combat the operational limitations in Arctic climates [16].

1.2. Research Objectives

The main goal of this project is to evaluate the performance of residential air-to-air heat/energy exchangers in Arctic climates. For this reason, the following sub-goals are undertaken:

- Study of the formation of frost in different types of exchanger cores without frost management at different inlet supply air temperatures.
- Evaluation of the proactive management of frost formation through the use of vapour-permeable exchanger cores.
- Evaluation of air recirculation as a method of frost management at different inlet supply air temperatures.
- Evaluation of the retroactive management of frost formation through alternating recirculation between two exchanger cores.
- Evaluation of the continuous supply of fresh air to a household through the alternating operation of two exchangers in parallel.

1.3. Thesis Overview

The following is a brief overview of the sections to follow:

In section 2, air-to-air heat/energy exchangers are introduced and more specifically fixed-plate type exchangers. The different types of cross-flow fixed-plate exchanger cores are presented. The operational concerns of air-to-air heat exchangers in cold climates are reviewed detailing the effects of different environmental parameters on core frosting. Finally, traditional and alternative frost management methods are discussed.

The proposed heat/energy exchanger system is presented in section 3. The exchanger and exchanger core specifications and construction are discussed along with the proposed proactive and retroactive frost management scheme.

The performance indices are presented in section 4. The section also included the required variables and necessary measurements needed to calculate the performance indices. The experimental setup used for the tests are presented, detailing the construction and configuration of the equipment, measurement apparatus and environmental chambers. Finally the experimental conditions and different tests are tabulated.

The results for phases 1, 2 and 3 of experiments are presented in sections 5, 6, and 7, respectively. The measurement results were used in the determination of the performance indices and the results for all cores were compared at the different inlet supply air temperatures.

The conclusions of the experiments are presented in section 8. Design recommendations based on the conclusions of this thesis are presented for heat/energy exchanger applications in northern climates. Finally, opportunities for future work are discussed for further research in the field.

2. LITERATURE REVIEW

2.1. Air-to-air Heat/Energy Exchangers

There are many types of air-to-air heat/energy exchangers (HEE), all of which are traditionally divided into two categories:

i. Air-to-air heat exchangers that allow the exchange of sensible heat between two air-streams.

ii. Air-to-air energy exchangers that allow the exchange of both sensible heat and latent heat (through the transfer of water-vapour) between two airstreams.

Air-to-air heat exchangers and air-to-air energy exchangers are often referred to as HRVs and ERVs, respectively. Where HRV stands for "heat recovery ventilator" and ERV stand for "energy/enthalpy recover ventilator".

Both heat and energy exchangers are used in residential and commercial buildings for the pre-heating and/or pre-cooling of supply air. There are multiple types of air-to-air heat/energy exchangers (rotary, recovery loop, heat pipe, etc.), however fixed-plate heat/energy exchangers are the most common equipment used in low-rise residential housing. This type of exchanger will be the focus of this thesis.

2.1.1. Fixed-plate Heat/Energy Exchangers

Fixed-plate heat/energy exchangers (**Figure 2.1**) consist of a core constructed of laminated fixed-plates. Within these plates are several channels where the supply and exhaust airstreams travel. The flow of the supply and exhaust air alternates between each plate of the core allowing for the transfer of heat and/or water-vapour between airstreams.

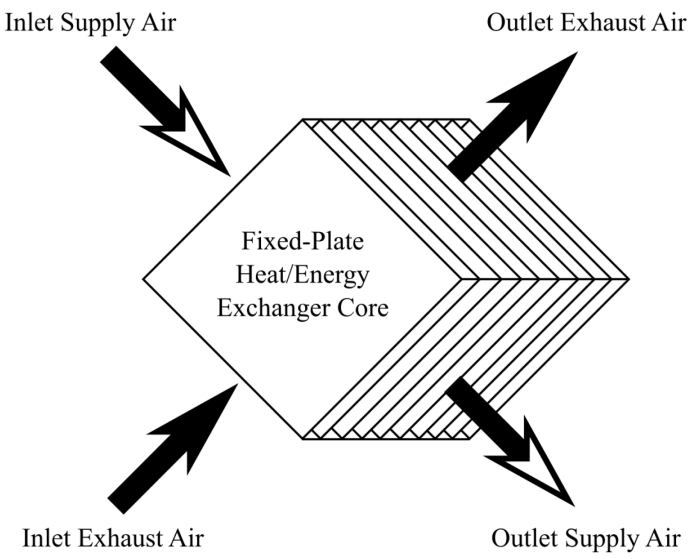

Figure 2.1: Simplified airflow diagram of a cross-flow fixed-plate exchanger core

The direction of the supply and exhaust air as it passes through the core depends on the orientation of the plates. The two most common orientations are *cross-flow* and *counter-flow*. This study focuses on cross-flow cores, as they are the most commonly used cores for residential applications. Heat recovery technologies for applications in buildings have been extensively reviewed in [17]; covering, but not limited to, the different types of technologies and system integrations. This review was followed by [18], which reviews the physical and performance parameters of heat recovery systems for applications in buildings.

2.1.2. Fixed-plate Exchanger Cores

The geometry and material of the cores varies depending of design constraints and the intended purpose of the air-to-air heat/energy exchanger. Exchanger cores that transfer only sensible heat are typically constructed of corrugated plastic sheets (commonly referred to as Coroplast®) made of polycarbonate. Metal (aluminum or stainless steel) fixed-plate cores are also available, however are more expensive and not as easy to manufacture as the corrugated plastic alternative.

Corrugated plastic cores are durable, waterproof and are thermally stable for typical residential ventilation applications.

Vapour-permeable core are typically recommended for hot and humid climates where they have been proven to provide considerable energy savings [19]–[21]. Conversely, even though the cores have been recommended for over 30 years [22], little research has been completed for applications in very cold climates. There are many types of vapour permeable materials available, however most of which are proprietary designs owned by the respective manufacturer. Typically, vapour permeable materials consist of a substrate that is treated to allow for water-vapour transfer. One of the most common types of vapour permeable core materials is polymerized paper. Membrane-based cores are becoming more popular as research in the vapour transfer performance progresses. One commonly used membrane core consist of porous desiccant-loaded polymer substrate that is coated on one surface with a thin layer of water permeable polymer [23]. The porous polymer substrate provides structural rigidity while different types of water permeable polymer coats are applied for different applications. The permeability of the material is highly dependent on the sorption curve, which is influenced by the temperature of the material itself. For the membrane exchanger cores, materials with linear sorption curves perform better under typical conditions [24]. Thinner membranes increase heat and water-vapour transfer between airstreams [25].

When it comes to the performance of membrane cores at different inlet supply air temperatures approaching freezing (0°C to 10°C), the inlet supply air temperature and relative humidity has little to no effect on the sensible effectiveness of membrane cores. However, the latent heat transfer effective increases as the inlet supply air temperature decrease and decreases as relative humidity level decreases [26], [27].

Membrane exchanger cores have low containment ratios. The mass transfer of contaminant between the supply and exhaust airstream is not influenced by inlet indoor and outdoor air temperatures and relative humidity. Air leakage due to core construction, not through the membrane material itself, is the primary concern regarding the mass transfer of contaminants [27]. The use of membrane materials for heat and moisture recovery has been extensively reviewed in [28]; covering, but not limited to, the progress of heat and mass transfer analysis, exchanger structures and membrane design.

2.2. Operational Concerns in Cold Climates

The primary concern for heat/energy exchangers operating in cold climates is the formation of frost in the exchanger core. At cold inlet supply air temperatures, moisture in the warm and relatively humid exhaust air condenses and freezes on the internal surfaces of the exchanger core. In sensible-only heat exchanger cores, frosting is observed when inlet supply air temperature decreases below -5°C for typical indoor air relative humidity levels [29]. However due to the transfer of water-vapour from the exhaust airstream to the supply airstream, vapour-permeable cores begin to frost at inlet supply air temperatures below -10°C. Frost formation in the exchanger core reduces the amount of warm exhaust air entering the exchanger because of the reduction in the cross-sectional area and the increase in the dynamic resistance caused by the roughness of the accumulated frost. This reduces the amount of energy available to be recovered by the supply airstream. The formation of frost, also reduces the efficiency of the unit due to the increased thermal resistance caused by frost accumulation [30], [31]. Additionally, if core frosting is allowed to propagate without control it can lead to system failure and/or damage. Frosting in air-to-air energy exchangers has been extensively reviewed in [32]. The authors cover many

topics including frosting in different types of air-to-air heat/energy exchangers, research related to frost properties, and different frost management strategies.

2.2.1. Frost formation process

The frost formation process can be divided into three distinct periods [33]. The first phase is the crystal growth period involving the vertical and liner growth of the frost crystals that are far apart from each other. If frosting is allowed to continue the next period of growth is the frost layer growth period. This stage involves the formation of a uniform mesh-like frost surface through three-dimensional growth that results in increased frost density and internal diffusion of water-vapour. Finally, the frost layer full growth period is a cyclic process of melting at the surface. The melting at the surface is due to an increase in the frost thermal resistance, which results in internal frost densification.

2.2.2. Effects of environmental parameters on frost formation

With respect to heat/energy exchangers, the key environmental parameters that affect the formation of frost are air velocity, air relative humidity, surface temperature, and location on the surface [34]. Additionally, how these parameters vary over time is of importance as frost formation is dependant of time and the history of the frost layer [35]. For flow through an annulus or parallel plates, frost growth shows little dependence on the Reynolds number of the air when above a certain critical value [34]. Below this critical value, approximately 12000-16,000, frost formation increases with an increase in air flow Reynolds number [34], [36]. Air turbulence has little to no effect of the rate of frost formation on horizontal flat plates [31].

The thickness and mass of frost growth is strongly dependent of the humidity of the air [31], [37]. As the humidity of the air increases so does the thickness and mass of the frost layer.

The thickness of frost growth is strongly dependent on the contact surface temperature [37]. As the temperature of the surface decreased there is an increase in the thickness of the accumulating frost. However, the contact surface temperature showed little influence on the mass growth rate of the frost. Additionally, the transfer of heat and water-vapour is not uniform on the surface of the exchanger core. The heat and moisture transfer is greatest near the inlets of the fluids [38]; accounting for the increase in frost formation is these same regions. For flat plate design, [33] concluded that frost growth was faster up-stream from the flow, while slower down-stream. It has also been noted that, when air flow rates are relatively high, frost growth appeared to be more evenly distributed over the surfaces [34].

2.3. Traditional frost management methods

Methods for managing core frosting are divided into two categories: 1) the proactive approach of "frost control" and 2) the retroactive approach of "defrost" [39]. The benefits of optimizing freeze control strategies are greater for cold climates since there is a greater need to recover energy from the exhaust airstream due to the lower outside air temperatures which occur for longer periods [39]. Additionally, the higher the effectiveness of an exchanger core the greater the need for frost control optimization. This is due to the greater amount of energy to be recovered and the fact that frosting tends to occur at higher inlet supply air temperatures as the effectiveness increases [39].

2.3.1. Reducing System Effectiveness or Supply Airflow Rates

Reducing the thermal conductivity of the air exchanger during potential frosting conditions can prevent frost growth. Thermal conductivity of the systems would be reduced to prevent the temperature of the exchanger-exhaust interface surfaces from decreasing beyond freezing. A consequence of this frost control measure is that overall system efficiency is decreased; colder outlet-

supply air is provided to the building. In addition to reducing the system effectiveness frost formation can be prevented or defrosting can be accomplished by reducing the supply airflow rates and maintaining the exhaust airflow rate.

2.3.2. Preheat

Preheat is an effective frost control method that is used in arctic applications. Preheat involves heating, by means of electricity or fossil fuels, the cold supply air prior to entering the heat/energy exchanger. Preheating can be achieved through variable control or step ON/OFF control. While preheat is one of the most adaptable frost control methods, it is also the most detrimental to the overall system efficiency [39]. Additionally, in locations where energy sources are limited (arctic Canada), this method of frost control can become very expensive.

2.3.3. Bypass Loop

This method of dealing with frost formation is classified as defrost. When the frost growth within the air exchanger reaches a critical level the cold supply air is diverted around the heat/energy exchanger, directly to an auxiliary heating system. The relativity warmer exhaust air is now able to defrost the frost that has accumulated in the exchanger core. This method results in a drop in the overall system efficiency, since during defrost supply air is not pre-heated by the exhaust air, increasing heating requirements.

2.3.4. Recirculation

The recirculation of exhaust air within the heat/energy exchanger is the most commonly used defrost mechanism for low-rise residential applications because is it considered the most energy efficient defrost strategy [40]. When frost formation within the exchanger core reaches a critical level, the unit stops the supply of outside air allowing exhaust air to circulate through the exhaust and supply air channels of the exchanger core. The warm exhaust air melts the accumulated

frost in the exchanger core. The frequency of the defrost cycle has little effect of the amount of heat recovered [40]. One disadvantage of this method of defrost is that higher outside air volumetric flow rates are required when in normal operation to compensate for the periods of time when supply is not provided during defrost.

According to manufacturer specifications [41], when exterior temperatures are below -25°C a typical system can running 50% in recirculation defrost mode and 50% in normal operation. As a result, for airtight building construction, the lack of outside air under poses indoor air quality concerns. Finally, for very cold exterior temperatures (i.e. below -35°C) the recirculation method may not be sufficient to defrost the system, which could lead to exchanger core damage due to uncontrolled frost propagation. Recirculation, while better than other retroactive frost control methods, still consumes a significant amount of energy and is far from the ideal in Arctic climates [16].

2.4. Alternative frost management methods

The following are examples of recent research investigating cold weather heat/energy exchanger operation. There is a clear trend towards the use of two heat/energy exchangers for the management of core frosting.

2.4.1. Serial connection of two heat exchangers

Researchers from the Technical University of Denmark have developed a heat exchanger design that connects two fixed-plate heat exchangers in series, alternating the supply and exhaust airflow directions [42]. **Figure 2.2** illustrates the two positions of the system.

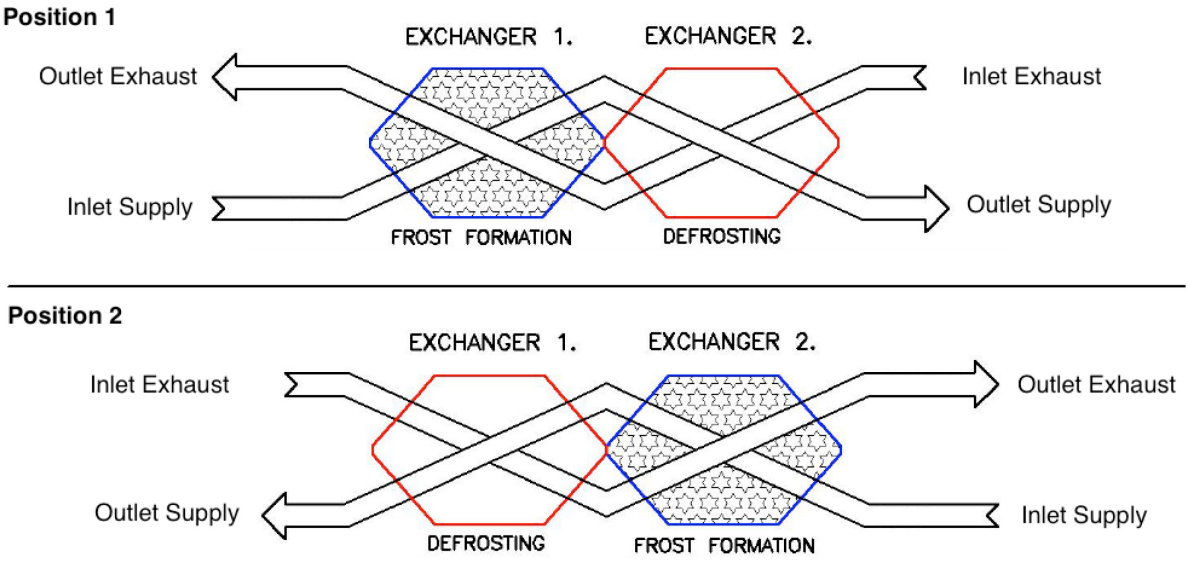

Figure 2.2: Illustration of the operation of two heat exchangers arranged in series (adapted from [43]

The heat exchanger consists of two high-efficiency fixed-plate heat exchangers cores arranged in series. When the system is in position 1 (**Figure 2.2**), frost will start to form on the exhaust channels of heat exchanger no.1 due to the cold supply air. After a pre-determined period of time, a series of dampers redirect the supply and exhaust airflow in the opposite directions (Pos. 2 in **Figure 2.2**). Heat exchanger no.1 is now directly exposed to the warm inlet exhaust air re-

sulting in the defrost of the accumulated frost. The opposite is the case for heat exchanger no.2 where frost begins to form in the exchanger core. The reversal of airflow is repeated when defrosting is necessary.

The system was installed in a low-energy house in Sisimiut, Greenland and evaluated over a five-year period [44]. The theoretical temperature efficiency (the ratio between the difference in the inlet and outlet supply air temperatures and the difference in the inlet exhaust and inlet supply air temperatures) of the system was estimated at 90%. During in-field operation, however, the temperature efficiency fluctuated from 55% to 80%, with an annual average of 60%. The operation and control of the damper proved to be the main source of temperature inefficiency. It was suggested that the damper should only be engaged when defrosting was necessary, not at pre-determined time set point (i.e. 1hr, 2hr, etc.) as was the case for the five-year observation period. It was noticed that there was significant heat loss from ducting due to the placement of the heat exchanger unit in an unconditioned space. It was recommended that future installation of the unit be done in a conditioned space.

2.4.2. Multi-section system (parallel configuration)

The multi-section system, as presented in [45] is a heat exchanger meant to recovery sensible heat in cold climates. The system consists of two identical side-by-side polycarbonate heat exchangers. A simplified schematic of the system operation is presented in **Figure 2.3**.

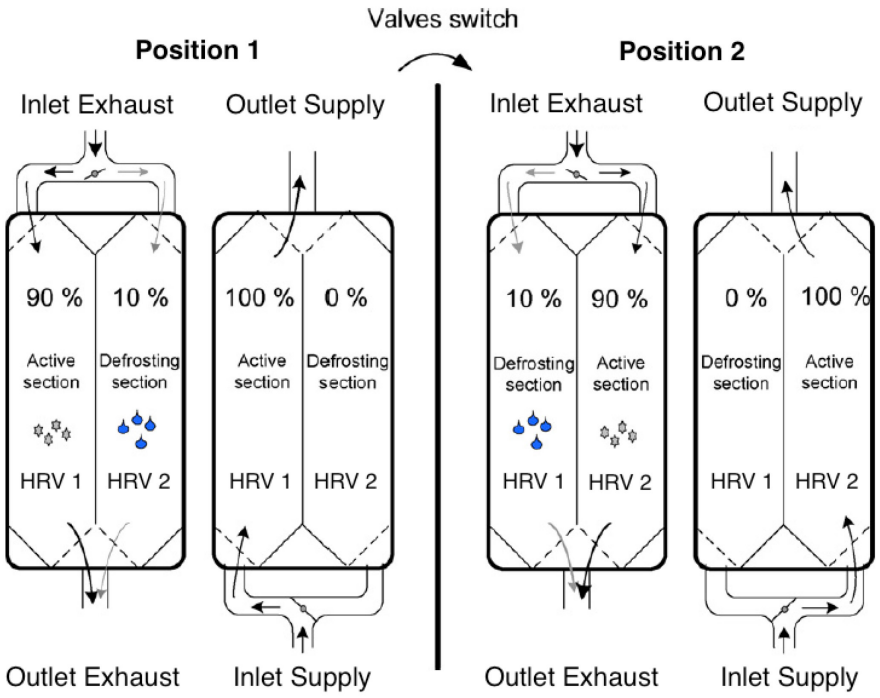

Figure 2.3: Multi-section system schematic (adapted from [45])

In the Position 1 arrangement, 90% of the inlet exhaust air is allowed to exchange with 100% of the inlet supply air in HRV 1. The remaining 10% of the warm exhaust air is diverted to HRV 2, where the air is used to defrost of accumulated frost in the previously active section. After a set period of time the system switches to Position 2. In Position 2, 10% of the inlet exhaust air is diverted to defrost the previously active sections in HRV1. 100% of the inlet supply air is now diverted to HRV 2 where it is exchanged with the remaining 90% of the inlet exhaust air. The alternating between positions 1 and 2 continues when operating under frosting conditions. This

defrosting method allows for cyclic defrosting of the stand-by heat exchanger and continuous ventilation.

The system was evaluated for long-term operation under laboratory set-up while operating under frosting conditions and was able to achieve a temperature efficiency (the ratio between the difference in the inlet and outlet supply air temperatures and the difference in the inlet exhaust and inlet supply air temperatures) of 88%. The exterior supply temperature was held constant at minus 6°C while interior conditions were approximately 20°C with a relative humidity of 55-60%. Due to limitations of the test apparatus, the airflow rate was set lower then desired, 25 l/s, in order to maintain a constant inlet supply air temperature. Under these conditions the system was capable of performing for the four days utilizing cyclic defrost. It was noted that the section switch time of 60 minutes was not sufficient for total defrost in the corresponding section. This raises the issue of the capability of the system to operate at temperatures well below the tested conditions. Insufficient defrost of the sections could result in uncontrolled frost in both sections, in turn eventually leading to system failure.

The researchers concluded that the relatively large size of the system poses an issue for immediate implementation, and identified the possibility of integrating the system into a building envelope. Additionally, they identified the possibility of controlling the section switch time as a function of the inlet temperature and a variable diversion of inlet exhaust air for defrost.

2.4.3. VENTIREG system

The VENTIREG system, as presented in [46], aims to achieve sensible and latent heat recovery. The system consists of a single duct where the airflow alternates between supply and exhaust direction. Within the channel there is a layer of heat storage material and a layer of moisture

absorbing material. A simplified schematic of the design and operation of the VENTIREG is shown in **Figure 2.4**.

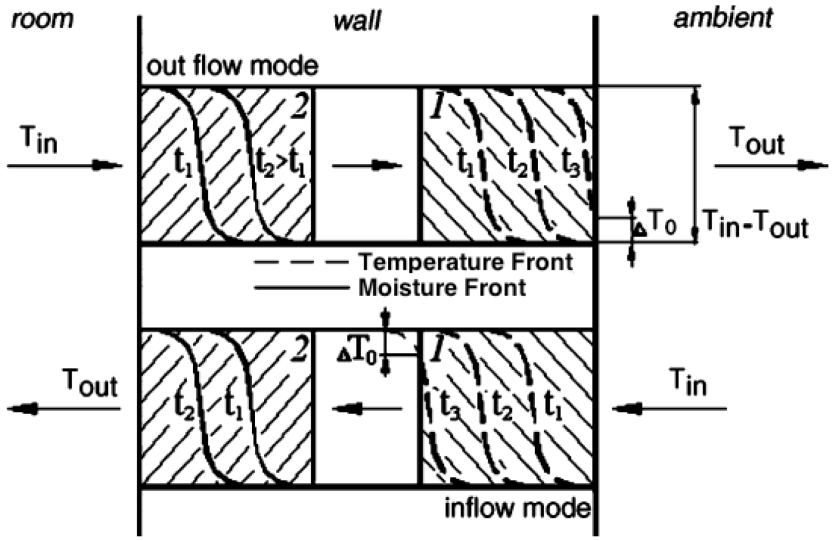

Figure 2.4: Schematic showing VENTIREG design and operation (adapted from [46])

The operation of the system can be divided into two phases: 1) charging and 2) discharging. During the charging phase, the warm humid air from the interior (exhaust air) first travels through the water absorbent material resulting in a decrease in the moisture content of the air. The air then passes through the thermal storage material where the exhaust air is cooled down. At a predetermined temperature drop across the system, the system is reversed resulting in the discharge of both thermal and moisture storage. The benefit of this system is that the cold supply air is heated prior to reaching the moisture absorbent material, reducing the chances for freezing and frost formation. The pulse-like action of the system allows for any frost that might form within the moisture discharge material to be melted with the passing of the warm exhaust air.

The primary focus of [46] was to determine the feasibility of the system and the efficiencies of the processes. The system was capable of recovering up to 95% of the sensible heat and 70-90% of the moisture from the exhaust air. It was also noted that the system performance increased as

the difference in the inlet supply and exhaust air temperature increased. Indicating that the system is better suited for cold climate applications.

Very little information was presented with regards to the formation of frost. However, results were presented for inlet supply air temperatures approaching minus 8°C with no mention of frost formation. Two alternating systems are required in order to provide continuous airflow, which might lead to concerns over the size of the units and required space. Additionally, the system requires greater electric power input to fans due to the dynamic resistance of the heat storage and moisture absorbing materials.

2.5. Literature review conclusions

The current housing stock in northern Canada is not suitable for the occupants and the climatic conditions. Overcrowding, faulty design and inadequate temperature and relative humidity control has resulted in a building stock that is costly to maintain/operate, uncomfortable, and in some cases hazardous to the health of the occupants. The use of air-to-air heat/energy exchangers has shown to improve the health of occupants, increase occupant comfort and reduce the operational costs for occupants.

The formation of frost within an exchanger core is the primary concern when operating in very cold climates. The formation of frost is dependent of many environmental factors of which the relative humidity of the exhaust air and the surface temperature of the exchange surface play a significant role. Both of these parameters are exacerbated in Arctic climates due to the very low inlet supply air temperatures and consequently the relatively high humidity of exhaust air.

Traditional frost management methods, while effective at mitigating frost, can significantly reduce system efficiency and in some cases, as is the case for pre-heat, can prove to be very costly

in Arctic regions. The recirculation of exhaust air is the most common retroactive method of defrost; used across multiple climate zones.

Alternative methods of defrost have focused on the use of multiple heat/energy exchangers to mitigate frost formation in cold climates. Some have investigated the use of water-vapour permeable or absorbent materials as a method to proactively prevent frost formation. Vapour permeable cores have traditionally been recommended for hot and humid climates. However, research has shown that the use of water vapour permeable cores may also be desirable for very cold climates.

This thesis builds on the findings of previous works, using the fundamentals gathered through the literature, to further investigate the use water-vapour permeable exchanger cores to proactively mitigate frost formation in air-to-air heat/energy exchangers operating in very cold climates. This thesis also investigates the use of two heat/energy exchangers operating in parallel with alternating recirculation to retroactive control frost formation within exchanger cores.

3. PROPOSED HEAT/ENERGY EXCHANGER SYSTEM

Figure 3.1 shows the airflow definitions that will be used throughout this document. **Figure 3.1** is based on [47] and has been modified for the geometry of the exchanger being utilized in the experiments.

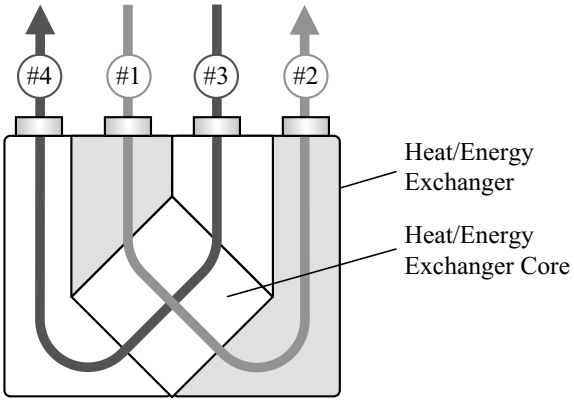

Figure 3.1 - Airflow definitions

Where:

#1 = inlet supply air

#2 = outlet supply air

#3 = inlet exhaust air

#4 = outlet exhaust air

Since the equipment will be tested with both sensible heat-only and heat and vapour-permeable cores the terminology of heat/energy exchanger will be used. This is also in keeping with the terminology used in [47]

3.1. Exchanger Specifications

The exchangers used in the experiments are Venmar EKO 1.5 air-to-air heat/energy exchangers. The specific exchanger used in the experiments and detailed below is not necessarily required for the proposed system. However, a high efficiency type exchanger, similar to the EKO 1.5, is recommended for the proposed system. **Figure 3.2** shows a diagram of the EKO 1.5.

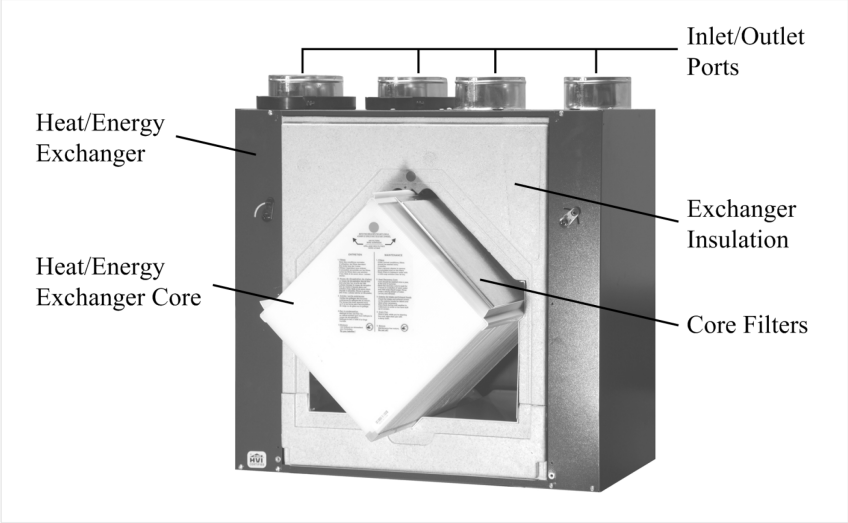

Figure 3.2: Venmar AVS EKO 1.5 heat/energy exchanger

The exchanger has a fixed-plate cross-flow exchanger core. It consists of vertically aligned inlet/outlet ports located on the top of the exchanger. The exchanger is insulated from the ambient conditions with expanded polystyrene. As shown in **Figure 3.2**, core filters are located at the inlet supply and exhaust air channels. The core filters have a minimum efficiency reporting value (MERV) of 9, preventing the transfer of particles larger than 1.0 – 3.0 μm in size.

The exchangers are equipped with electronically commutated (EC) motors. The EC motors provide variable speed control and are highly efficient. Additionally, EC motors typically have longer life and lower maintenance requirements than traditional DC motors [48]. This characteristic is of particular interest due to the limited availability of skilled labour and replacement parts

in northern Canada. The EKO 1.5 air-to-air heat/energy exchanger has two factory airflow rate settings: High (74 l/s) and Low (37.75 l/s).

The defrosting of the exchanger core is accomplished through the recirculation of the exhaust air through the exchanger (**Figure 3.3**). When recirculation is triggered, the inlet supply air (#1) and outlet exhaust air (#4) ports are closed and the inlet exhaust air (#3) is redirected to the inlet supply air (#2) channel.

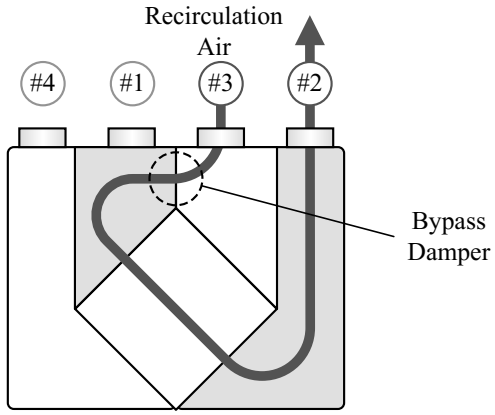

Figure 3.3: Airflow path during recirculation defrost

The relatively warm inlet exhaust air melts the accumulated frost in the exchanger core and the resulting liquid is collected in a condensation pan and ultimately drained out the bottom of the exchanger. The by-pass damper and condensation pan are shown in **Figure 3.4**.

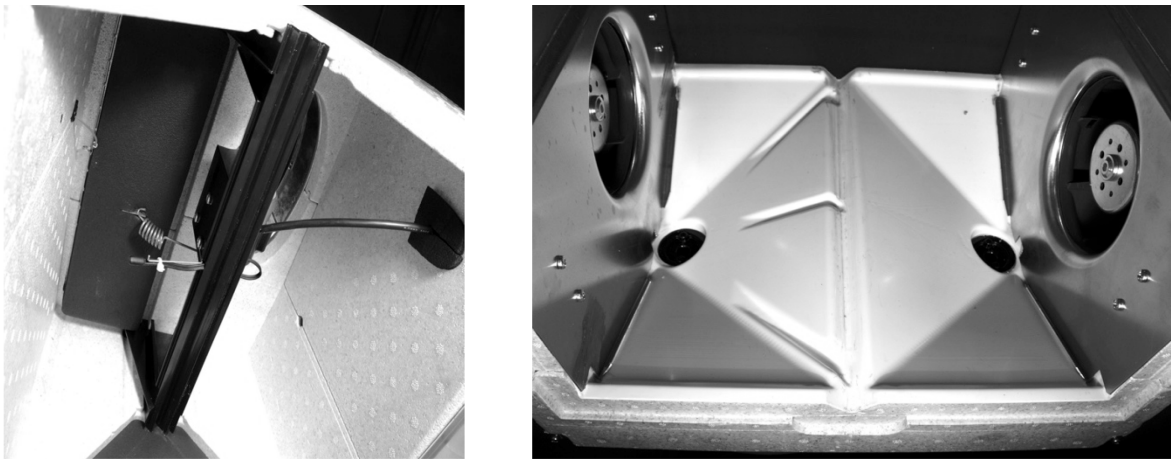

Figure 3.4: Left: inlet exhaust air bypass damper in activated position; Right: condensation pan with drainage openings

The recirculation of exhaust air is triggered based on the inlet supply air temperature (#1). The defrost schedule is divided into different operational bands based on the inlet supply air temperature. The factory settings for the EKO 1.5 are tabulated in **Table 3.1**.

Table 3.1: Factory set operating schedule [41], [49]

Inlet Supply Air Temperature [°C]	Heat Exchanger Core Defrost/Operating [min]	Energy Exchanger Core Defrost/Operating [min]
Warmer than −5	No Defrost	No Defrost
−5 to −10	7/25	No Defrost
−10 to −27	7/25	7/25
Lower than −27	10/22	10/22

The defrost schedule are the same for the heat and energy exchanger cores when inlet supply air temperatures are lower than −10°C, while they are different for inlet supply air temperatures greater than −10°C. For instance, when the inlet supply temperature is about −12°C, the heat or energy exchanger operates normally for 25 min, and then switches to defrost mode for seven minutes. The heat exchanger core requires defrost when inlet supply air temperatures drop below −5°C. While energy exchanger cores can operate without defrost until temperatures of

−10°C. This is due to the differences in the temperature at which frost formation is of concern in the exchanger core, as previously discussed.

3.2. Exchanger Cores

Four different exchanger cores were tested with the exchangers. All cores are cross-flow fixed-plate type and have dimensions of 254 mm x 254 mm 362 mm (width x height x length). The cores are listed in **Table 3.2**.

Table 3.2: Exchanger core specifications

Core ID#	Transfer between Airstreams	Core Material	Approx. Exchange Surface Area, *A*
HRV Core	Heat only	Polypropylene	9.7m^2
ERV Core	Heat and Moisture	Polymerized Paper	9.5m^2
MERV1 Core	Heat and Moisture	Substrate with vapour-permeable coating	8.8m^2
MERV2 Core	Heat and Moisture		8.8m^2

The only difference between cores MERV1 and MERV2 is the type of vapour-permeable coating applied to the membrane substrate. The construction varies between the different types of cores. **Figure 3.5** shows the different constructions of each core.

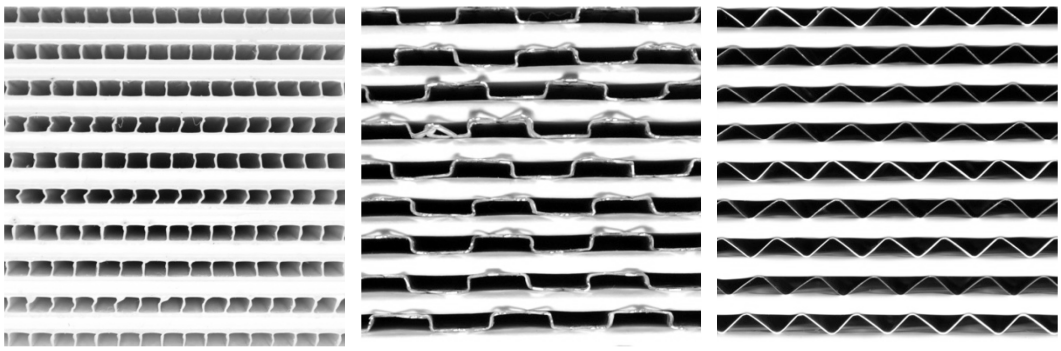

Figure 3.5: Heat/energy exchanger core construction; Left: HRV core, Centre: ERV core, Right: MERV1 and MERV2 cores

All the cores feature a sandwich-style structure. The HRV core consists of corrugated polypropylene sheets separated and supported by spacers of the same material. All vapour-permeable cores have a similar construction; heat and moisture permeable material separated and supported by a corrugated metal sheet. The HRV and ERV cores were supplied with the heat/energy exchangers, while the MERV1 and MERV2 were custom made by the respective manufacturer. The construction of the cores results in different exchange surface areas. The HRV core has the largest exchange surface area due to the smaller height of each air channel in the corrugated polypropylene. The opposite can be said about the MERV1 and MERV2 cores.

3.3. Frost Management

The frost management strategies for the proposed system are twofold. The strategies are divided in (1) the use of vapour-permeable core to proactively reduce the onset and amount of core frosting and (2) the use of alternating recirculation to remove frost that has formed in the exchanger core and provide continuous ventilation.

3.3.1. Proactive frost management

The use of vapour-permeable core allows for the transfer of moisture between airstreams. In cold climates this results in the transfer of moisture from the relatively humid inlet exhaust air to the dry and cold inlet supply air. The transfer of moisture from the exhaust to supply airstreams avoids condensation in the core and if the exchanger core surface temperatures are below freezing it avoids the formation of frost in the core. The other benefit of vapour-permeable cores is the reduction in the amount of vapour in the exhaust airstream. This reduces the amount of moisture that could potentially condense and freeze.

3.3.2. Retroactive frost management

The proposed system consists of two heat/energy exchangers (#1 and #2) operating in parallel. The operation can be divided into periods where core frosting in not a concern and when defrosting is required.

3.3.2.1. No Defrosting

The exchangers operate similarly to conventional systems when there is no risk of frost formation. **Figure 3.6** shows the potential operation of the proposed system during periods when defrost in not necessary.

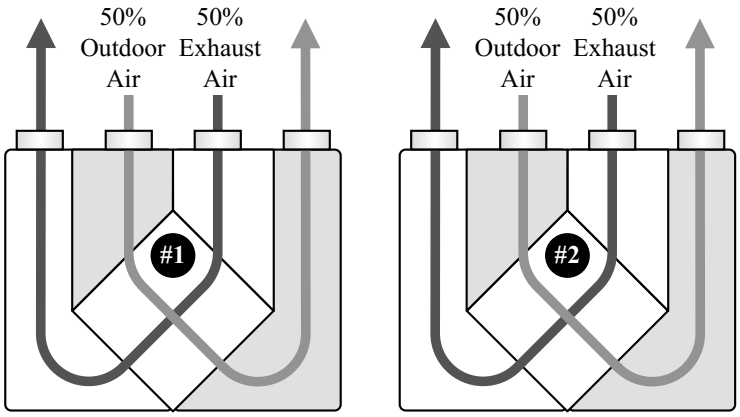

Figure 3.6: Operation of proposed system when defrost is not required

As depicted in **Figure 3.6**, the supply and exhaust airstreams are split equally between the two exchangers. This is done in order to increase the effective area of heat/energy exchange between the supply and exhaust airstreams. As previously stated the operation of the proposed system when defrost is not required is outside of the scope of this study.

3.3.2.2. Defrosting

A method of defrost control is necessary when inlet supply air temperatures fall within the operation bands listed in **Table 3.1**. When this occurs the two exchangers will start to alternate according to **Figure 3.7**.

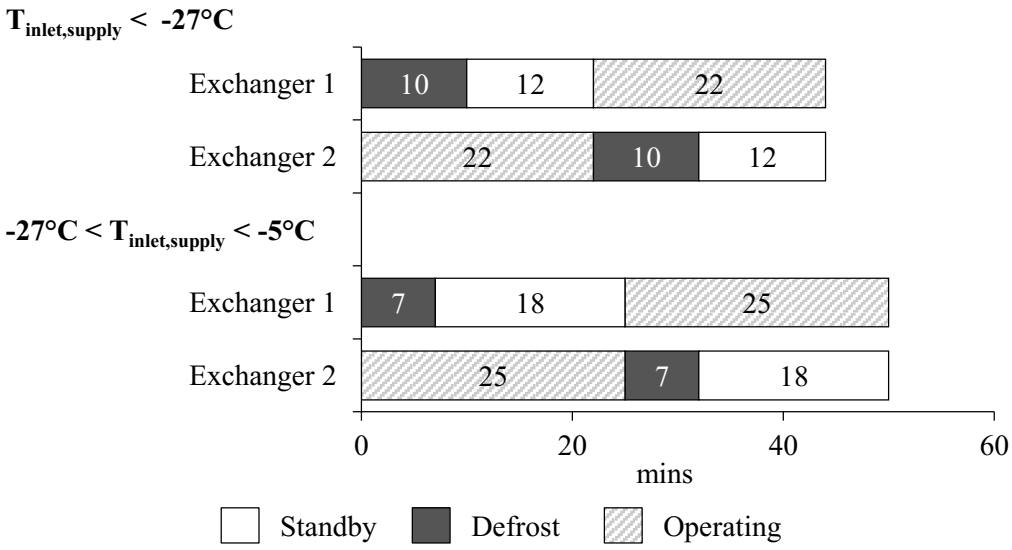

Figure 3.7: Defrosting operational schedule

Figure 3.7 shows the durations of the defrosting, operating and standby periods for each exchanger for one cycle. The durations of each mode presented in **Figure 3.7** is based on the factory set schedule for the heat/energy exchanger. It can be seen that when the inlet supply air temperature drop below −27°C the duration of the defrost mode increases from seven minutes to 10 minutes. This is to provide more time to remove the expected increase in the amount of frost formed due to the colder inlet supply air temperatures. **Figure 3.8** and **Figure 3.9** show the airflow for the two defrosting scenarios.

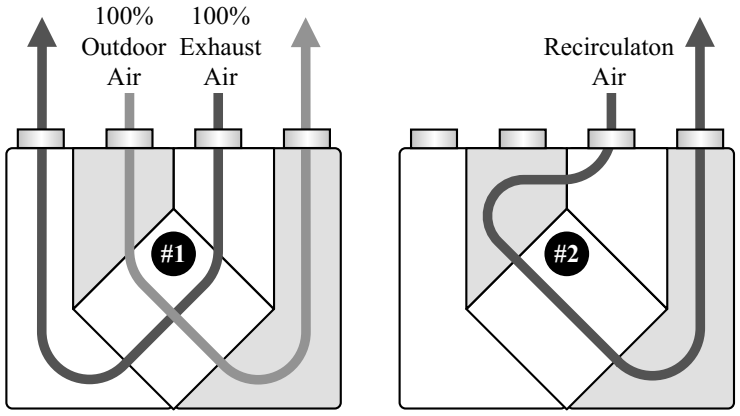

Figure 3.8: Exchanger operation with heat/energy exchanger #2 in defrost (recirculation)

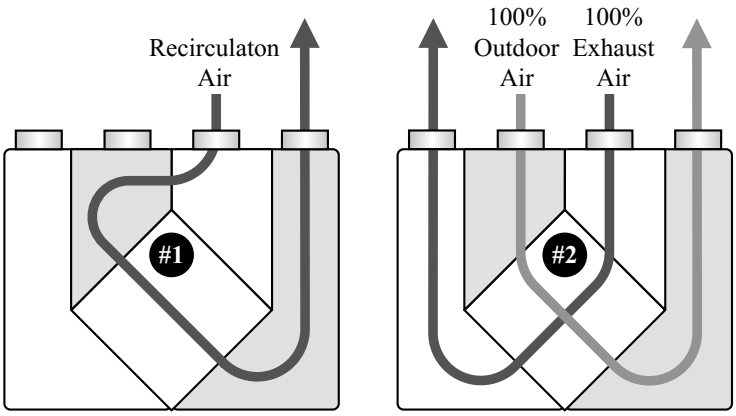

Figure 3.9: Exchanger operation with heat/energy exchanger #1 in defrost (recirculation)

Since one exchanger is always in use the supply of outdoor air to the home is continuous.

4. METHODOLOGY

4.1. Overview

This section outlines the methodology for the experiments undertaken.

- Firstly, the performance indicators as to which the heat/energy exchangers were evaluated on are presented in Section 4.2. This includes the sensible and latent heat transfer effectiveness, changes in outlet supply air temperature and humidity ratio, air flow rate and UA value of the cores.
- The measurement variables are introduced in Section 4.3 along with the instrumentation needed for measurement. These measurements were used for the aforementioned performance indicators. The uncertainty analysis for each measured variable and resulting propagation error are presented in Section 4.4.
- The experimental setup is presented in Section 4.5; detailing the apparatus used to measure the required variables.
- The experimental conditions are presented in Section 4.6, including indoor and outdoor air conditions as well as heat/energy exchanger volumetric airflow rates.
- Finally the individual experiments are tabulated in Section 4.7; outlining the test durations, conditions, operation and the different exchanger cores used.

4.2. Performance Indicators

The testing of the air-to-air heat/energy exchangers and cores were in compliance with the procedures outlined in the following industry standards:

- ASHRAE Standard 84-2013: Method of Testing Air-to-Air Heat/Energy Exchangers [47]
- CAN/CSA-C439-09: Standard laboratory methods of test for rating the performance of heat/energy-recovery ventilators [50]

The performance of the air-to-air heat/energy exchanger and exchanger cores were evaluated based on four categories:

- Sensible and latent heat transfer effectiveness (ε_s and ε_l)
- Change in outlet supply air temperature and humidity ratio over time
- Air flow rates
- UA-value

Reference [47] outlines other parameters used to evaluate the performance of air-to-air heat/energy exchangers. The recovery efficiency ratio (RER) takes into consideration the fan and drive efficiencies along with the auxiliary power required to operate and control the exchanger. The RER was not considered because this study focuses on the performance of different cores operating in the same heat/energy exchangers. Additionally, the exhaust air transfer ratio (EATR) considers the leakage between airstream in the exchanger. For the purpose of this study the EATR was not evaluated primarily due to the complexity of the experiments; requiring the measurement of tracer gas concentrations within the airstreams.

4.2.1. Sensible and Latent Heat Transfer Effectiveness

The effectiveness (ε) of an air-to-air heat/energy exchanger is defined as the ratio between the actual energy transferred and the potential maximum energy transferred between the airstreams [47]. The effectiveness can be divided into three different parameters: sensible, latent, and total heat transfer effectiveness. The sensible heat transfer effectiveness (ε_s), latent heat transfer effectiveness (ε_l) and total heat transfer effectiveness (ε_T) of an air-to-air energy exchanger are defined in Eq. (4.1), Eq. (4.2) and Eq. (4.3), respectively.

$$\varepsilon_s = \frac{\left(\dot{m}c_{pa}\right)_s (T_2 - T_1)}{\left(\dot{m}c_{pa}\right)_{min} (T_3 - T_1)} \qquad [-] \qquad (4.1)$$

$$\varepsilon_l = \frac{\left(\dot{m}h_{fg}\right)_s (\omega_2 - \omega_1)}{\left(\dot{m}h_{fg}\right)_{min} (\omega_3 - \omega_1)} \qquad [-] \qquad (4.2)$$

$$\varepsilon_T = \frac{\dot{m}_s (h_2 - h_1)}{\dot{m}_{min} (h_3 - h_1)} \qquad [-] \qquad (4.3)$$

Where:

T_1 = inlet supply air temperature, °C

T_2 = outlet supply air temperature, °C

T_3 = inlet exhaust air temperature, °C

ω_1 = inlet supply air humidity ratio, $kg_{water}\ kg_{dry\ air}^{-1}$

ω_2 = outlet supply air humidity ratio, $kg_{water}\ kg_{dry\ air}^{-1}$

ω_3 = inlet exhaust air humidity ratio, $kg_{water}\ kg_{dry\ air}^{-1}$

h_1 = inlet supply air enthalpy, $J\ kg_{dry\ air}^{-1}$

h_2 = outlet supply air enthalpy, J $kg_{dry\ air}^{-1}$

h_3 = inlet exhaust air enthalpy, J $kg_{dry\ air}^{-1}$

$\dot{m}$ = mass flow rate, kg s^{-1}

$\dot{m}_{min}$ = lowest of the mass flow rate of dry air for airflow #1 and #3, kg s^{-1}

h_{fg} = heat of vaporization of water, J kg^{-1}

c_{pa} = specific heat capacity of air, J kg^{-1} K^{-1}

If the exchanger core does not allow for moisture transfer (i.e. HRV) between the two airstreams the latent heat transfer effectiveness is equal to zero. The specific heat capacity of air, c_{pa} was assumed at 1.005 J kg^{-1} K^{-1}, as all test temperatures were between −35°C and 30°C. The total effectiveness (ε_T) of each core was not evaluated because the focus of this study was on the heat and vapour transfer performances of each core rather than the total energy transferred by each exchanger core.

For the purpose of this study, Eq 4.1, and Eq 4.2 are adjusted to take into consideration the effects of frost formation on the sensible and latent heat transfer effectiveness. This was necessary because both equations do not take into consideration the actual potential maximum energy when there is no frost on the exhaust air flow. The adjusted sensible and latent heat transfer effectiveness (ε_s' and ε_l') equations are presented below in Eq. (4.4) and Eq. (4.5).

$$\varepsilon_s' = \frac{\left(\dot{m}c_{pa}\right)_s (T_2 - T_1)}{\left(\dot{m}c_{pa}\right)_{min,initial} (T_3 - T_1)} \qquad [-] \qquad (4.4)$$

$$\varepsilon_l' = \frac{\left(\dot{m}h_{fg}\right)_s (\omega_2 - \omega_1)}{\left(\dot{m}h_{fg}\right)_{min,initial} (\omega_3 - \omega_1)} \qquad [-] \qquad (4.5)$$

Where, $(\dot{m}c_{pa})_{min,initial}$ and $(\dot{m}h_{fg})_{min,initial}$ are the average values of the first 5 minutes of the evaluation period, when there is no frost. The evaluation period is the time interval when measurements used in the calculation of the sensible and latent heater transfer of the cores are gathered.

4.2.2. Outlet Supply Air Conditions

The primary purpose of a heat/energy exchanger is to pre-condition the outdoor supply air for a residence. Therefore, the temperature and humidity ratio of the outlet supply air was monitored for the duration of the tests. The measurements were compared versus time to see any change in the values due to core frosting. The outlet supply air conditions for each core were also compared to see the effect of core sensible and latent heat transfer effectiveness.

4.2.3. Air Flow Rates

The air flow rates of all four airflows (supply inlet/outlet and exhaust inlet/outlet) for both heat/energy exchangers were measured. In addition to being a required variable in the previously presented effectiveness equations, the measured air flow rates were used to indirectly evaluate the formation of frost in the exchanger cores. As frost forms in the exchanger core there is a corresponding decrease in the exhaust air flow rate. This decrease in the exhaust air flow rate is due to the decrease in cross-sectional area and increase in the dynamic resistance caused by the rough frost covered surfaces. The exhaust air mass flow rate was plotted versus time and the results for each core were compared at different inlet supply air temperatures. Alternatively, the formation of frost could have been evaluated visually however this was not practical when the heat/energy exchangers were in operation.

The air flow rate measurements were also used to evaluate the operation of the heat/energy exchangers. When the exchanger enters a defrost cycle the inlet supply air and outlet exhaust air is

temporarily blocked allowing for the recirculation of exhaust air through the exchange core. By monitoring the air flow rates of all airflows it was possible to determine if the heat/energy exchanger was in defrost, operating or stand-by modes.

4.2.4. UA-value

The effect of frost formation on the heat transfer between airstreams was evaluated by calculating the UA-value for each core over time. UA-value was calculated as follows:

$$UA = \frac{Q}{LMTD} \qquad [\mathrm{W\ K^{-1}}] \qquad (4.6)$$

Where:

Q = rate of heat transfer, W

A = heat transfer surface area of exchanger core, m^2

U = overall heat transfer coefficient, $W/(m^2 \cdot K)$

$LMTD$ = logarithmic mean temperature difference, K

Using the previously defined notation for the different airflows, the logarithmic mean temperature difference, *LMTD*, was calculated using Eq. (4.7).

$$LMTD = \frac{(T_3 - T_2) - (T_4 - T_1)}{\ln\left(\frac{T_3 - T_2}{T_4 - T_1}\right)} \qquad [\mathrm{K}] \qquad (4.7)$$

By plotting the UA-value for the cores versus time it was possible to not only see the effect of frost formation but also the effect of vapour-permeability on the UA-value. .

4.3. Measurements

The following air properties and characteristics were measured in order to evaluate the performance of the system.

- Temperature
- Relative humidity
- Air flow rate

4.3.1. Temperature Measurement

Temperature measurements were conducted in accordance with ASHRAE Standard 41.1-2013: Standard Method for Temperature Measurement [51].

4.3.1.1. Instrumentation

The air temperatures were measured using T Copper and Constantan thermocouples. T Copper and Constantan thermocouples were selected based on the suitable operating temperature range and relatively low limits of error. **Table 4.1** tabulates these values.

Table 4.1: Thermocouple Properties [51]

Thermocouple Materials	Temperature Range	Accuracy
T Copper & Constantan	−200°C to 0°C	±1.0°C ± 1.5%
	0°C to 350°C	±1.0°C ± 0.75%

Multiple thermocouples were used in order to determine the average air temperature across the cross-section of the test-ducts. The thermocouples were arranged in accordance with **Figure 4.1**.

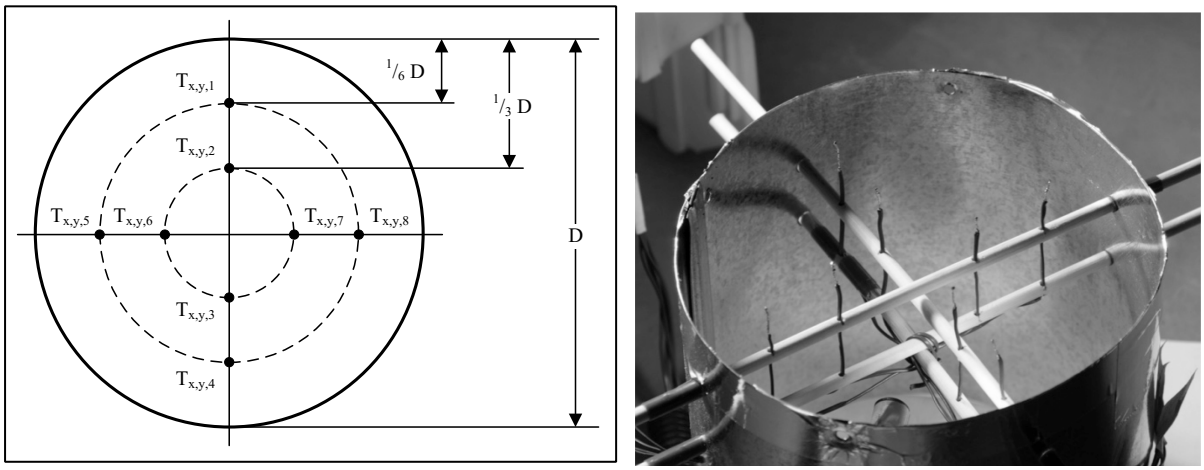

Figure 4.1: LEFT: Thermocouples placement dimensions; RIGHT: Thermocouples as installed

Two thermocouples are placed on four radii in each test-duct. The measurements from the eight thermocouples were used to determine the average temperature of the air passing through the duct. The use of eight thermocouples in each inlet/outlet airstream configurations results in a total of 64 thermocouples. The 64 thermocouples are labeled according to the following nomenclature:

$T_{x,y,\#}$
- → Thermocouple placement: 1 through 8
- → Airflow: 1 through 4
- → Exchanger number: 1 or 2

For example, $T_{1,3,4}$ would be the thermocouple measurement for exchanger #1 in the inlet exhaust airstream in placement 4 as depicted in **Figure 4.1** and displayed in Appendix A.

The thermocouples were supported across the duct using wooden skewers. The skewers were selected to be very thin in order to reduce conduction along the axis of the skewer. This was not expected to be of great concern since the differences in the temperature distribution over the cross-section of the test-duct would not be significant. The thermocouples were also supported by two sets of wooden skewers in order to ensure that 6 cm of each thermocouple wire was with-

in the isotherm of the cross-section. Additionally, each thermocouple was calibrated before the experiments were conducted. The calibration procedure and results are presented in APPENDIX A

4.3.2. Relative Humidity Measurement

The measurement of moist air properties was conducted in accordance with ASHRAE Standard 41.6-1994: Standard Method for Measurement of Moist Air Properties [52].

The relative humidity (φ) of air is the ratio between the vapour pressure (p_w) of the air and the saturation pressure (p_{sat}) of the same air at temperature (T). This relationship is shown in Eq. (4.8).

$$\varphi = \frac{p_w}{p_{sat}(T)} \times 100 \qquad [\%] \qquad (4.8)$$

The humidity ratio (ω) of an air sample is calculated using Eq. (4.9).

$$\omega = 0.62198 \frac{p_w}{p_{atm} - p_w} \qquad [kg_w\ kg_{da}^{-1}] \qquad (4.9)$$

Where:

p_{atm} = atmospheric air pressure, Pa

The humidity ratios of the airstreams are used in the latent heat transfer effectiveness calculations presented in Section 4.2.1.

4.3.2.1. Instrumentation

The relative humidity of the airstreams will be determined using a collection of capacitive thin film hygrometer sensors. According to [52], the advantages of thin-film hygrometers are that they are small in size, have fast response times and have relatively high accuracy. The meas-

urement device consists of two components, a sensor probe and a transmitter**.** **Table 4.2** shows the specifications for the sensors that were used in the experimental setup.

Table 4.2: Hygrometer probe specifications

Manufacturer & Model	RH Range	Temp. Range	Accuracy
Vaisala - HMT333	0 to 100 %RH	−40 to 180 °C	±(1.5 + 0.015 x reading) %RH

Figure 4.2 shows HMT333 transmitter alongside the corresponding hygrometer probe.

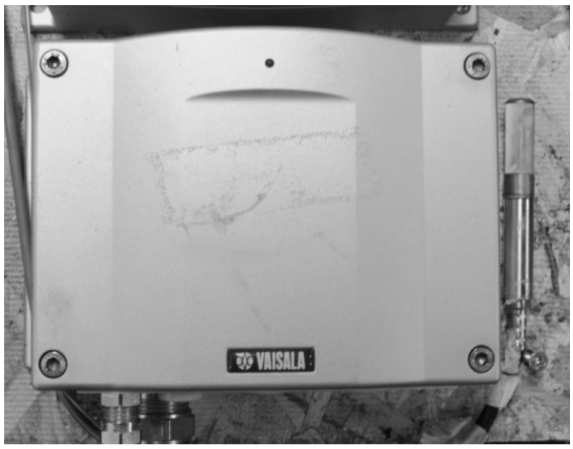

Figure 4.2: Hygrothermal transmitter with probes

Only one hygrometer was be used across the cross-section of the ducts to determine the moisture properties of the air. **Figure 4.3** shows the placement of the measurement probe within the cross-section of the duct.

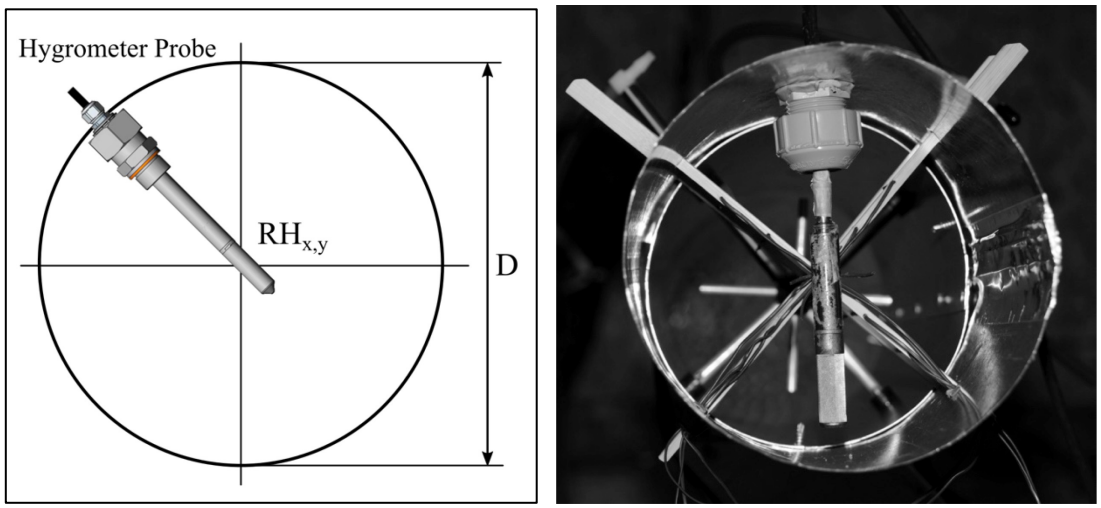

Figure 4.3: LEFT: Hygrothermal probe placement; RIGHT: Hygrothermal probe installed.

The probe is mounted to the wall of the duct using a cable gland and sealed with duct seal compound. The hygrometer probes (total 6) were installed in the inlet and outlet supply air and inlet exhaust air test-ducts. A probe was not installed in the outlet exhaust air test-duct because the moisture properties of the air are not required to evaluate the performance of the exchanger system. The six probes were labeled following the notation below:

$RH_{x,y}$
- → Airflow: 1 through 3
- → Exchanger number: 1 or 2

4.3.3. Mass Flow Rate

The mass flow-rate of the airstreams can be calculated indirectly using the total and static pressure measurements of the cross-sectional area. Air pressure measurements were conducted in accordance with the following ASHRAE standards:

- ASHRAE Standard 41.2-1987: Standard Methods for Laboratory Air-flow Measurement [53]

- ASHRAE Standard 41.3-1989: Standard Method for Pressure Measurement [54]

The average air speed, V in the cross-sectional area is calculated according to Eq. (4.10).

$$V = \sqrt{2\frac{(p_{total} - p_{static})}{\rho_a}} = \sqrt{2\frac{p_{dynamic}}{\rho_a}} \qquad [\text{m s}^{-1}] \qquad (4.10)$$

Where:

p_{total} = total air pressure, Pa

p_{static} = static air pressure, Pa

$p_{dynamic}$ = dynamic air pressure, Pa

ρ_a = air density, kg/m^3

Finally, the mass flow rate ($\dot{m}$) is calculated using the cross-sectional area (A_c) of the test duct and the density of the air as shown in Eq (4.11).

$$\dot{m} = \rho_a(V \cdot A_c) \qquad [\text{kg s}^{-1}] \qquad (4.11)$$

4.3.3.1. Instrumentation

The total and static air pressures were measured using an airflow measurement station. The station allows for the measurement of the average differential pressure across the cross-section of a duct through the use of a traverse Pitot-tube arrangement. The differential pressure measurement is then converted to a voltage ranging from 0-5V by a pressure transmitter and sent to a data acquisition (DAQ) system. Each airflow measurement station was connected to a differential pressure multiplexer resulting in only one pressure transmitter being required. The multiplexer cycles though pairs of pressure inputs (high and low) allowing for multiple differential pressure measurements with only one transmitter.

Table 4.3 lists the manufacturer's specifications for the different equipment being used for the airflow pressure measurements.

Table 4.3: Airflow Pressure Measurement Equipment

Device	Manufacturer & Model	Operating Range	Response Time	Accuracy
Airflow Measurement Station	ENVIRO-TEC FlowStar	6.6 to 66 L/s	-	-
Diff. Pressure Multiplexer	Scanivalve CTLR2/S2-S6	0 to 3447 kPa	5-8 ms	-
Diff. Pressure Transmitter	OMEGA PX655-0.5DI	0 to 125 Pa	250 ms	±0.25% FS

The airflow measurement station, differential pressure multiplexer and differential pressure transmitter are shown in **Figure 4.4** and **Figure 4.5**, respectively.

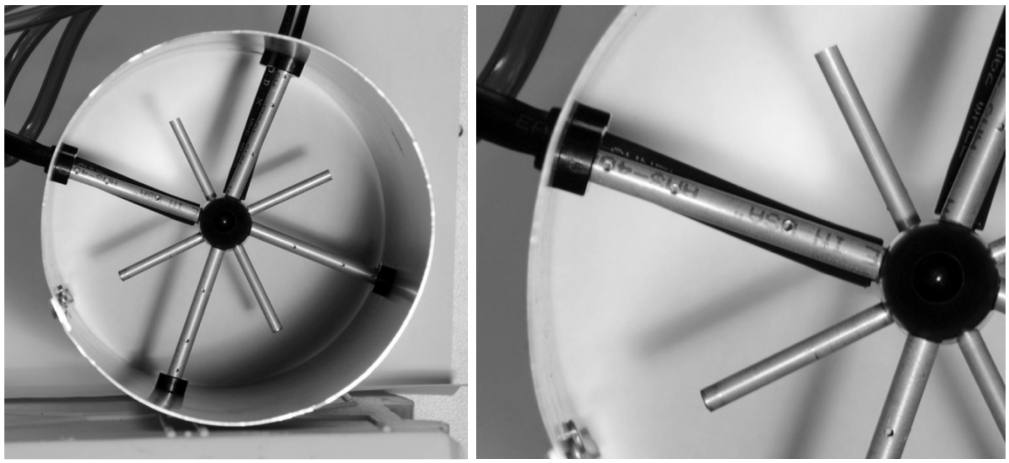

Figure 4.4: LEFT: airflow measurement station cross-section; RIGHT: Traverse Pitot-tube arrangement detail

Figure 4.5: LEFT: 24 port differential pressure multiplexer; RIGHT: Differential pressure transmitter

The calibration procedure and results for the airflow measurement stations can be found in APPENDIX A. There is one airflow measurement station per test-duct, resulting in a total of eight stations. The pressure measurements are labeled according to the following notation:

$P_{x,y}$

- Airflow: 1 through 4
- Exchanger number: 1 or 2

4.4. Measurement Uncertainty and Propagation of Error

The overall uncertainty of a measured variable consists of two components 1) bias error and 2) random error. Bias errors are offsets that are constant overtime and multiple measurement points [55]. The equipment manufacturer provided the bias error for each measurement device. Random errors are the random differences in the measurement observations, such as sensor noise or extraordinary conditions [55]. The random error for each measurement device was determined based on a sample selection of the measurement data.

The propagation of error was considered when determining the uncertainty of a variable (i.e. humidity ratio, w or sensible heat transfer effectiveness, ε_s) that was calculated using measured

variables. The methodology outlined in [55] was used for the propagation of error and ultimately for calculating the overall uncertainty, U_x of all measured and calculated variables.

The overall uncertainty of all measured and calculated variables are summarized in **Table 4.4** and the calculations are shown in APPENDIX B.

Table 4.4: Overall uncertainty for measured and calculated variables

Variable	Overall Uncertainty, U_x	
Average air temperature, T	± 0.4	℃
Saturation pressure, p_{sat}	± 10.7	Pa
Relative humidity, ϕ	± 1.43	%
Humidity ratio, ω	± 0.00083	g kg_{da}^{-1}
Volumetric flow rate, $\dot{V}$	± 0.0013	$m^3\ s^{-1}$
Mass flow rate, $\dot{m}$	± 0.002	kg s^{-1}
Sensible heat transfer effectiveness, ε_s	± 0.04	–
Latent heat transfer effectiveness, ε_l	± 0.03	–
Exchanger core weight	± 0.02	kg

4.5. Experimental Setup

4.5.1. Test-ducts

A test-duct setup was used for the measurement of air temperature, relative humidity, and differential pressure. This setup is recommended in [53]. There are two different test-duct configurations: inlet and outlet test-ducts. Both the supply and exhaust airstreams used the same configurations. **Figure 4.6** and **Figure 4.7** show the test-duct with dimensions for the exchanger inlet and outlet airflows, respectively.

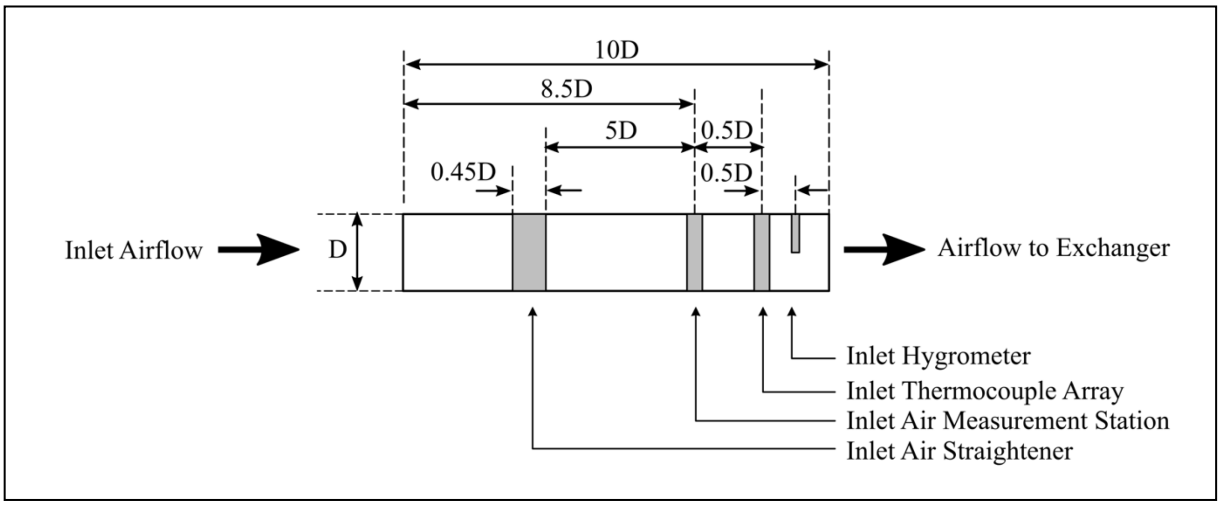

Figure 4.6: Inlet test-duct plan adapted from [53]

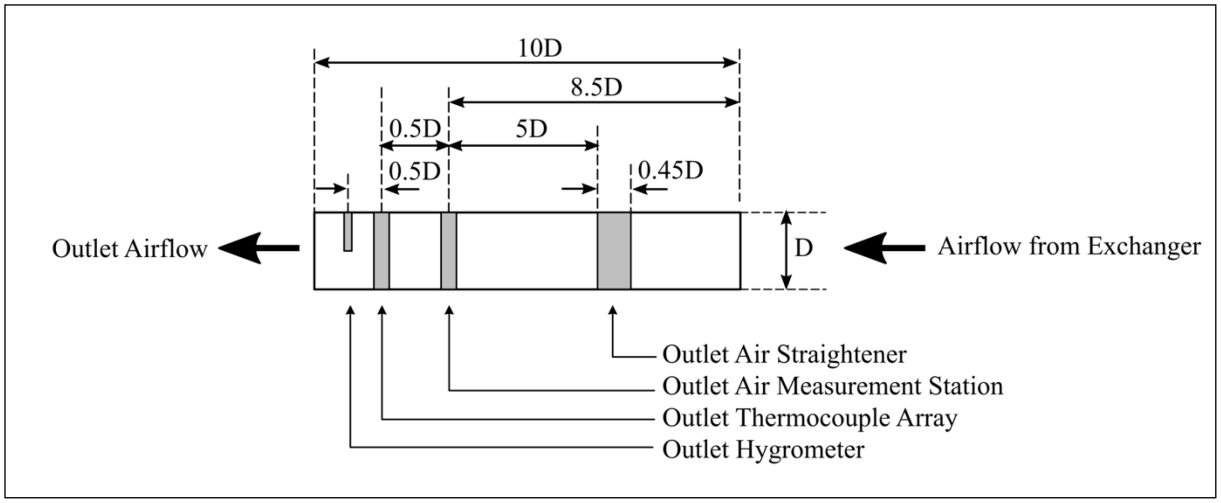

Figure 4.7: Outlet test-duct plan adapted from [53]

Figure 4.6 and **Figure 4.7** have been adapted slightly with respect to [53] to include air moisture measurements with a hygrometer. The tests duct were 152.4 mm in diameter, *D* and constructed of galvanized steel (**Figure 4.8**). The test-ducts were wrapped with mineral wool insulation and vapour barrier (**Figure 4.9**) in order to reduce the heat loss/gains from the ambient air in the laboratory and reduce the potential for condensation on the ducts.

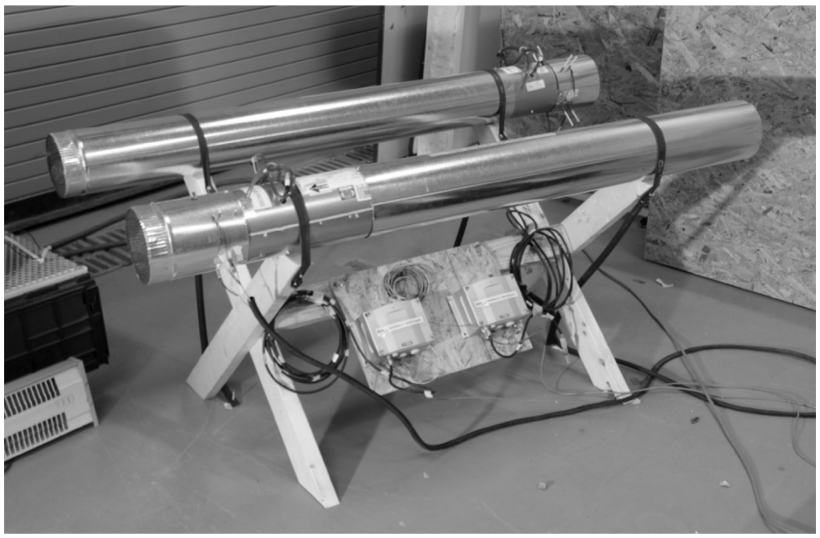

Figure 4.8: Inlet and outlet test-ducts on stand without insulation

The test-ducts are referred to according to the following notation.

$TD_{x,y}$

- Airflow: 1 through 4
- Exchanger number: 1 or 2

4.5.1.1. Air Mixing and straightening devices

The use of air mixers and straighteners are recommended in order to improve the uniformity of the air properties (temperature and humidity) and conditions (air flow) across the cross-section of the airstream.

Air mixers were not used in the experimental setup because the temperature, humidity and airflow measurements were taken after the internal fans of the heat/energy exchangers. Air

straighteners were used in each of the test-ducts to reduce air turbulence before the measurement stations. As shown in both Figure 4.6 and Figure 4.7, [53] recommends that the length of the air straightener be 45% of the duct diameter. Figure 4.9 shows the air straightener installed in the test-duct.

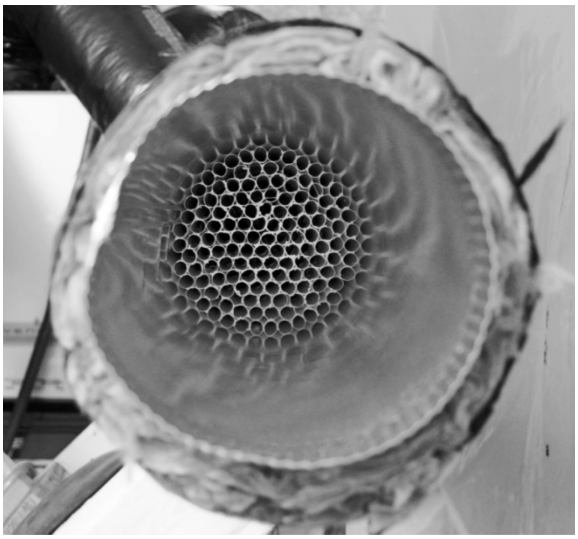

Figure 4.9: Air straightener installed in a test-duct

4.5.2. Environmental Chamber

The outdoor climatic conditions experienced in northern Canada were replicated using the environmental chamber located in the Building Envelope Performance Laboratory at Concordia University. The chamber consists of a SIP enclosure and an ESPEC – MAPX-6CWL temperature and relative humidity conditioner. The chamber is capable of obtaining temperatures between −65°C and 50°C. Figure 4.10 shows the placement of the ducts that lead to and from the chamber and heat/energy exchangers.

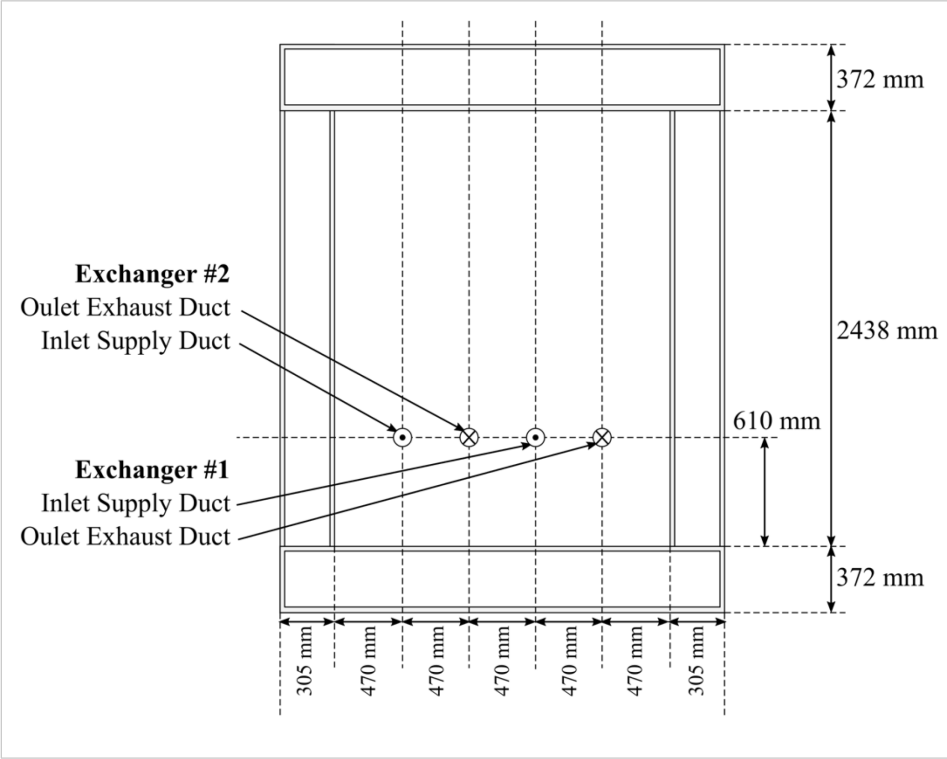

Figure 4.10: Environmental chamber dimensions and duct locations

Holes were cut into the SIP panels to accommodate the inlet and exhaust air ducts. The air conditioning system is not equipped with a defrost function. Consequently, the exhaust air ducts were extended in the chamber with flexible ducting (**Figure 4.11**) to promote condensation and ultimately frosting. This significantly reduced the amount of frost in the air conditioner evaporator.

Figure 4.11: LEFT: Flexible duct for the frost collection in the exhaust airstream; RIGHT: Frost accumulation in flexible duct

The ducts were positioned at the bottom of the wall to reduce the pressure losses within the ductwork. Since the ducts are installed side-by-side a plywood partition was place between the outlets in the chamber. This was to reduce the chance of airflow shortcuts between inlet and outlet airstreams that would result in temperature variations. The high turbulence of the air within the chamber also helped to mix the relatively warm outlet exhaust air from the heat/energy exchangers.

4.5.3. "Room" Chamber

The indoor air conditions (temperature and relative humidity) were maintained through the use of a secondary room chamber. The room chamber was constructed using a gantry crane. Using the crane as a support structure, wood framing was place on the top to create a secure "roof" for polyethylene plastic sheeting to be attached. Rope strung between the wood studs supported the vapour barrier around the top perimeter of the chamber. The vapour barrier draped down to the ground where it was secured and sealed with tape and additional wood studs. The dimensions of the chamber were approximately 3.7 m x 3.6 m x 4.3 m (WxLxH) and 56 m^3.

Figure 4.12: LEFT: Room chamber showing construction; CENTRE: Temperature and hygrometer probes at the inlet exhaust air ducts; RIGHT: Outlet supply air ducts and heating equipment.

The air temperature within the chamber was controlled using a PID controller. The PID controller measured the room chamber air temperature with a temperature probe and controlled a baseboard heating element and two oil radiators. The relative humidity of the air was controlled by a data acquisition system that measured the room chamber air relative humidity with a hygrometer (the same hygrometer model installed in the test-ducts). The DAQ controlled multiple fan-induced evaporative humidifiers in the chamber based on the measurements and the desired set-point of 35%. Fans were used to improve the uniformity of the air conditions throughout the room chamber.

4.5.4. System Schematic

A schematic diagram of the experimental setup is shown in **Figure 4.13**.

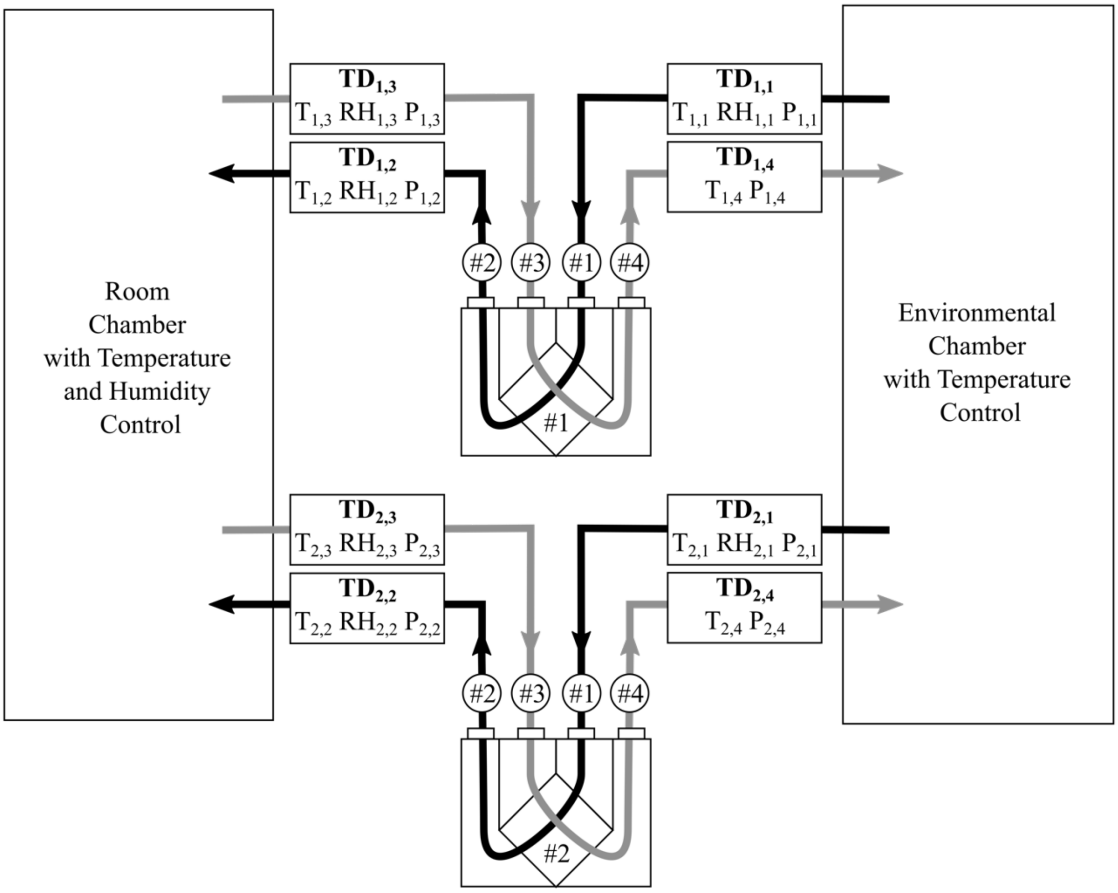

Figure 4.13: Schematic diagram of the experimental setup

The heat/energy exchangers, test-ducts, chambers were connected by flexible ducting that was then insulated with mineral wool and covered with vapour barrier. The diagram shows the different measurements that were collect at each test-duct. The exchangers were installed in parallel; connecting the environmental chamber with the room chamber. The nomenclature follows what has been previously presented.

The actual experimental setup as it was installed in the laboratory is shown in **Figure 4.14**. The specific location of the equipment differs from what is presented in **Figure 4.13** due to the space

limitation in the laboratory. However, the experimental setup functions as it is presented in the schematic diagram.

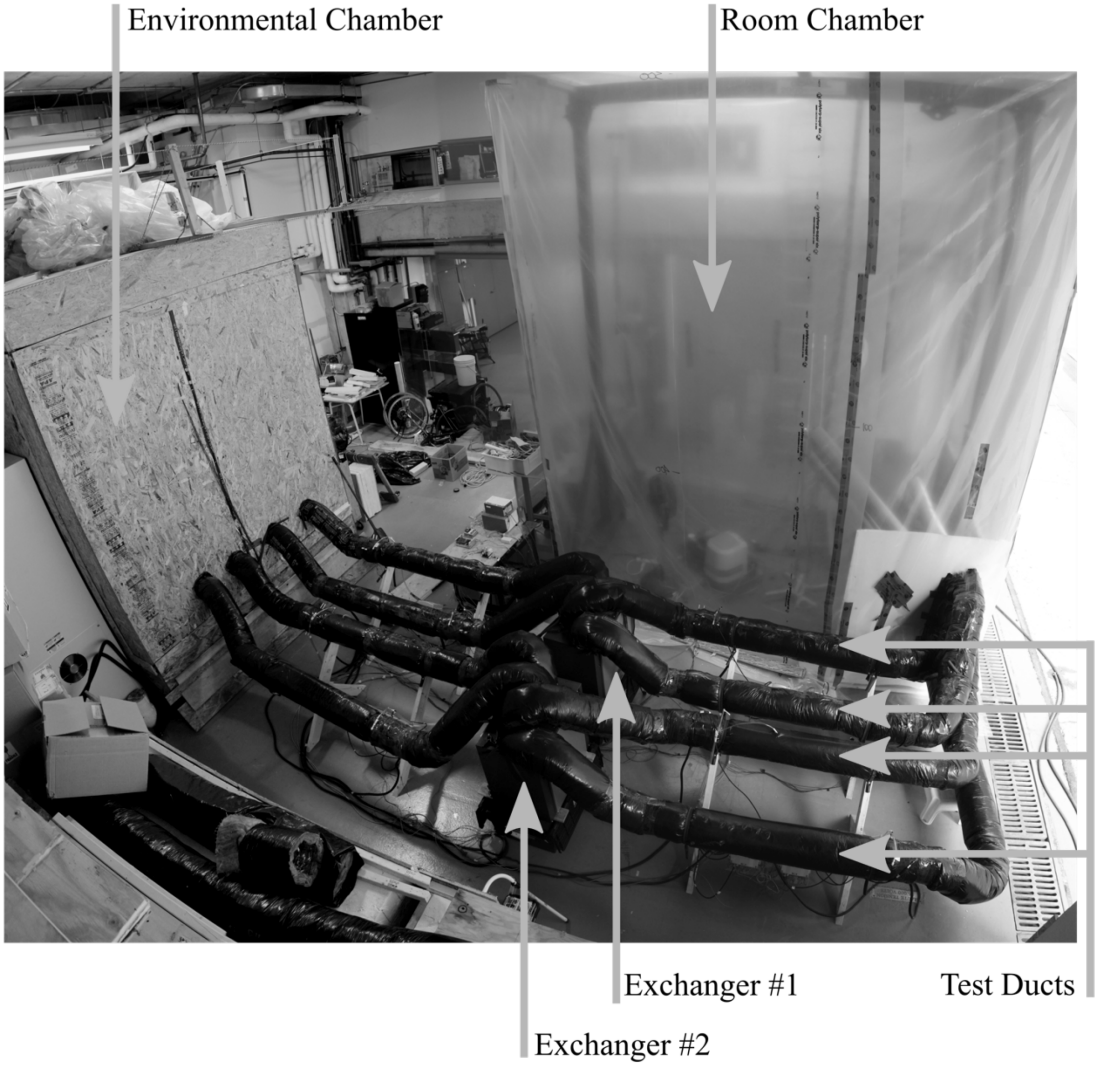

Figure 4.14: Actual experimental setup as installed

4.6. Experimental Conditions

4.6.1. Reference Location and House

The regional focus of this study is Northern Canada, however the results and conclusions of this work can be applied to other regions with a similar climates and comparative housing requirements.

Iqaluit, Nunavut was selected as the reference location in northern Canada. This was due to the city being the most populous in the region and the limited availability of weather, census, research, and housing data for other locations in northern Canada. Iqaluit is also the location of a high performance house designed by KOTT North (**Figure 4.15**). The *KOTT house* was used as the reference for housing construction and size for this study.

Figure 4.15: The KOTT house located in Iqaluit, Nunavut

The house is designed to be modular and can be constructed on site within a few days. The building envelope is made of structural insulated panels (SIPs) consisting of expanded polystyrene (EPS) sandwiched between two pieces of oriented strand board (OSB). The house is a duplex, however for the purpose of this study, ventilation requirements for only one apartment unit were considered. Heating is provided by a hydronic system with radiators located throughout the

home. The fuel used is heating oil stored on site in a tank adjacent to the home. Ventilation is provided mechanically through the use of a heat exchanger located in a second storey closet.

Permafrost is continuous in most of Inuit Nunangat and more specifically in Iqaluit year-round [56]. This requires homes to be elevated to prevent the melting of the permafrost, which could lead to unstable soil conditions. This design restriction means that there are no underground utilities (electrical, water, sewage, gas, etc.) and limited space for HVAC equipment. Equipment is typically stored in mechanical closets or in small crawl spaces between the floor and ground surface.

4.6.2. Inlet Supply Air Conditions

The inlet supply air conditions must reflect the conditions experienced in northern Canada. As previously mentioned the reference location was selected to be Iqaluit, Nunavut. **Figure 4.16** and **Figure 4.17** show the annual outdoor temperature and humidity ratio, respectively, for a representative year for Iqaluit [57].

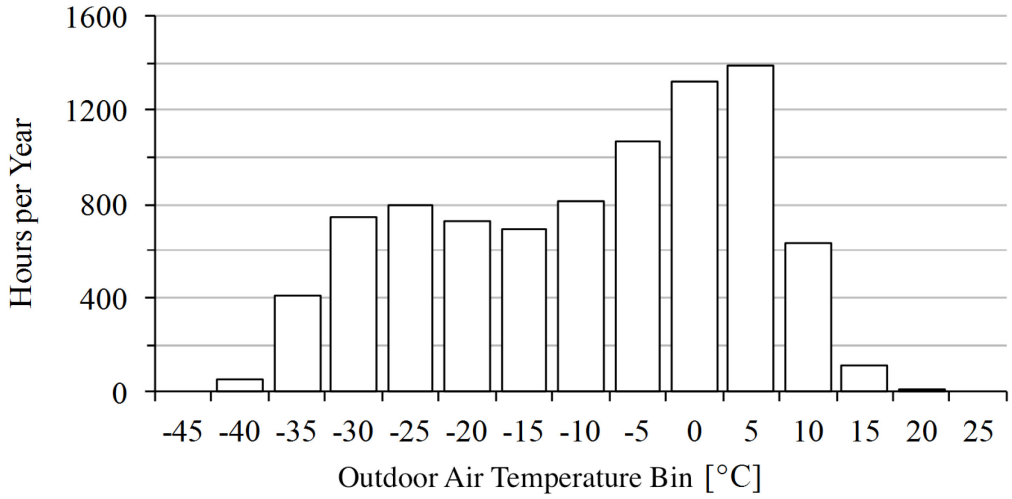

Figure 4.16: Annual outdoor temperature bin data for Iqaluit, Nunavut, Canada [57]

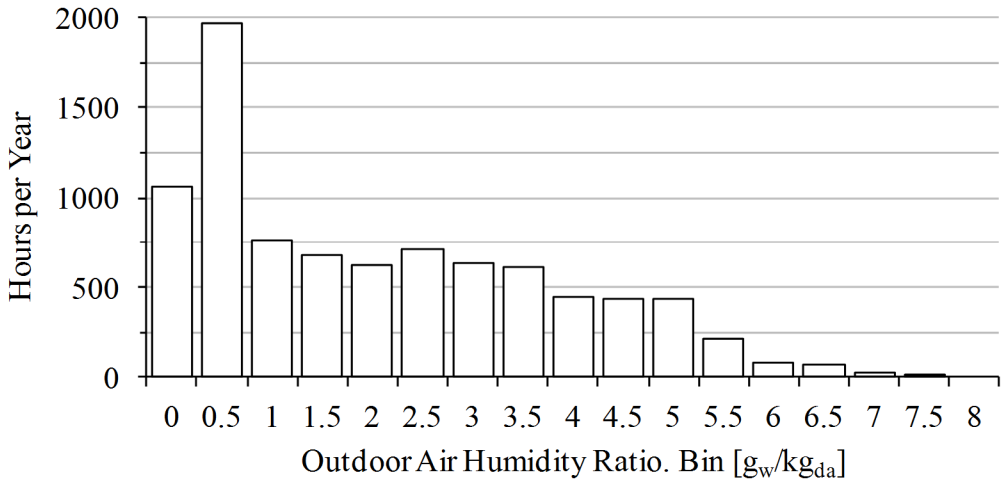

Figure 4.17: Annual outdoor humidity ratio bin data for Iqaluit, Nunavut, Canada [57]

The bin data was used to identify the most appropriate inlet supply air conditions for the experimental tests. Figure 4.16 illustrates the wide temperature range experienced in Iqaluit. The outdoor temperature ranges from 19.8°C to −39.8°C; a nearly 60°C range. Six temperatures were selected for the experiments: −5°C, −10°C, −15°C, −20°C, −25°C and −35°C. The experimental temperatures reflect the spread of outdoor air temperatures experienced in Iqaluit during periods when frost is of concern. Air temperatures above 0°C were not selected because the scope of this project is limited to periods when frost is of concern.

Due to the proximity of Iqaluit to the coast, the climate is relatively humid. However considering the cold air temperatures, the moisture content (humidity ratio) of the air is typically low. This is illustrated in **Figure 4.17**. Since the environmental chamber cannot reliably control the humidity of the air at temperatures below 0°C, control of the inlet supply air humidity was not possible for the experimental tests. A summary of the experimental inlet supply air conditions is listed in **Table 4.5**.

Table 4.5: Experimental inlet supply air conditions

Inlet Supply Air Condition	Inlet Supply Air Temperature [°C]	Inlet Supply Air Relative Humidity [%]
1	−5	N/A
2	−10	
3	−15	
4	−20	
5	−25	
6	−35	

4.6.3. Inlet Exhaust Air Conditions

As shown in [8], the indoor air conditions of Arctic housing can vary widely due to many factors. These factors include but are not limited to the type of housing construction, the condition of housing, the type of heating source and system, the occupant behaviour, etc. The results for Inuvik, NWT showed that the relative humidity of the indoor air was low for the majority of the monitoring period. The average relative humidity during the monitoring period ranged from 9% to 29% with measurements rarely going beyond 35% of relative humidity. This limit of 35% is used for the purpose of the laboratory experiments. The experimental inlet exhaust air condition is summarized in **Table 4.6**.

Table 4.6: Experimental inlet exhaust air conditions

Inlet Exhaust Air Condition	Inlet Exhaust Air Temperature [°C]	Inlet Exhaust Air Relative Humidity [%]
1	22°C	35%

4.6.4. Exchanger Air Flow Rate

The outdoor airflow rate for which the proposed exchanger system was tested was based on the requirements outlined in [58]. This standard outlines the minimum ventilation requirements for low-rise residential buildings based on two variables: floor area, A_{floor}, and number of bedrooms, N_{br}. For whole-building ventilation the total required ventilation rate is determined using Eq. (4.12).

$$\dot{V} = 0.15A_{floor} + 3.5(N_{br} + 1) \qquad [\text{L s}^{-1}] \qquad (4.12)$$

The number of bedrooms is used in the calculation with the assumption that each building occupant has one room. Since this assumption is not necessarily the case in arctic Canada due to overcrowding, the average number of occupants in the building will be used to replace the number of bedrooms.

The total required ventilation rate for a 140 m^2 house (approx. area of the *KOTT house* as presented in Section 4.6.1) with 4.1 occupants (the average house area and occupancy for arctic Canada) is calculated as follows:

$$\dot{V} = 0.15(140) + 3.5(4.1 + 1) = 38.9 \text{ L s}^{-1} \qquad (4.13)$$

The total required ventilation rate calculated above is used in the experiments.

4.7. Experiments

The experiments are separated into three phases.

- Phase 1: One heat/energy exchanger without recirculation defrost.
- Phase 2: One heat/energy exchanger with recirculation defrost.
- Phase 3: Two heat/energy exchangers with alternating recirculation defrost.

4.7.1. Phase 1: One Heat/Energy Exchanger without Recirculation Defrost

The first phase involved the evaluation and comparison of the accumulation of frost and the effect of frost formation of the effectiveness of each core with only one heat/energy exchanger at different inlet supply air temperatures. The exchanger operated with no recirculation defrost, which allowed unrestricted frost formation in the cores for the duration of the tests. The recirculation defrost capability of the exchanger was disabled by extending and moving the thermistor, that measures the inlet air temperature and initiates defrost, from inside the unit to outside the unit.

Table 4.7 lists the different tests that were conducted for this phase.

Table 4.7: Phase 1 tests with one HEE and no recirculation defrost

Inlet Supply Air Temperature [°C]	Duration* [hr]	Cores Tested
−5	2	HRV only
−10	3	All four
−15	3	All four
−20	3	ERV/MERV1/MERV2
−25	2	All four
−35	1	All four

* The HRV core was tested for only two hours for all experiments.

The durations of the tests for all cores were reduced at −25°C and −35°C to prevent core damage caused by frosting. The HRV cores were tested for only two hours at all inlet supply air temperatures, other than −35°C, to prevent core damage caused by frosting. The inlet exhaust air conditions were maintained at 22°C and 35% RH.

The air temperature, humidity and flow rate were measured for the duration of the tests. These measurements allowed for the comparison of the frost formation temperatures for each core. These tests also provided the opportunity to observe the relationship between the effectiveness and core frosting.

4.7.2. Phase 2: One heat/energy exchanger with recirculation defrost

Phase 2 involved the operation of one heat/energy exchanger with recirculation enabled.

Table 4.8 lists the different tests that were conducted for this phase.

Table 4.8: Phase 2 tests with one HEE with recirculation defrost

Inlet Supply Air Temperature [°C]	Duration [hr]	Cores Tested
−25	3	All four
−35	3	All four

All cores were tested at the inlet supply air temperatures of −25°C and −35°C for three hours with recirculation defrost enabled. The inlet exhaust air conditions were maintained at 22°C and 35%RH. The primary objective for the second phase of testing was to evaluate the performance of each core for the two different factory-set recirculation defrost schedules (as presented in **Figure 3.7**).

4.7.3. Phase 3: Two heat/energy exchangers with alternating recirculation defrost

The top two performing cores from the first and second phases were selected to continue to the third phase. The HRV core was tested as well for reference. Each core was tested with the proposed system involving the use of two exchangers with alternating recirculation defrost. **Table 4.9** lists the different test conditions for the long-term experiments.

Table 4.9: Phase 3 tests with two exchangers and alternating defrost

Inlet Supply Air Temperature [°C]	Duration [hr]	Cores Tested
−25	3	ERV/MERV1/HRV
−35	3	ERV/MERV1/HRV

The three cores were tested at the inlet supply air temperatures of −25°C and −35°C for three hours. The test consisted of six switches between exchangers and six recirculation defrost cycles. The inlet exhaust air conditions were maintained at 22°C and 35%RH. The purpose of these experiments was to determine if the system was capable of managing the propagation of frost over the duration of the tests while at the same time provide continuous outdoor supply air. The effectiveness of the system using the different cores was evaluated and compared.

5. RESULTS AND ANALYSIS OF ONE HEE UNIT WITHOUT DEFROST

5.1. Results - One HEE unit without defrost

This section presents the results for one HEE unit with ERV, MERV1, MERV2 and HRV cores, operating with defrost disabled, and at different inlet supply air temperatures.

5.1.1. Outlet supply air temperature

Figure 5.1 shows the change with time of the measured outlet supply air temperature, T_2 for the different cores operating at different inlet supply air temperatures, T_1.

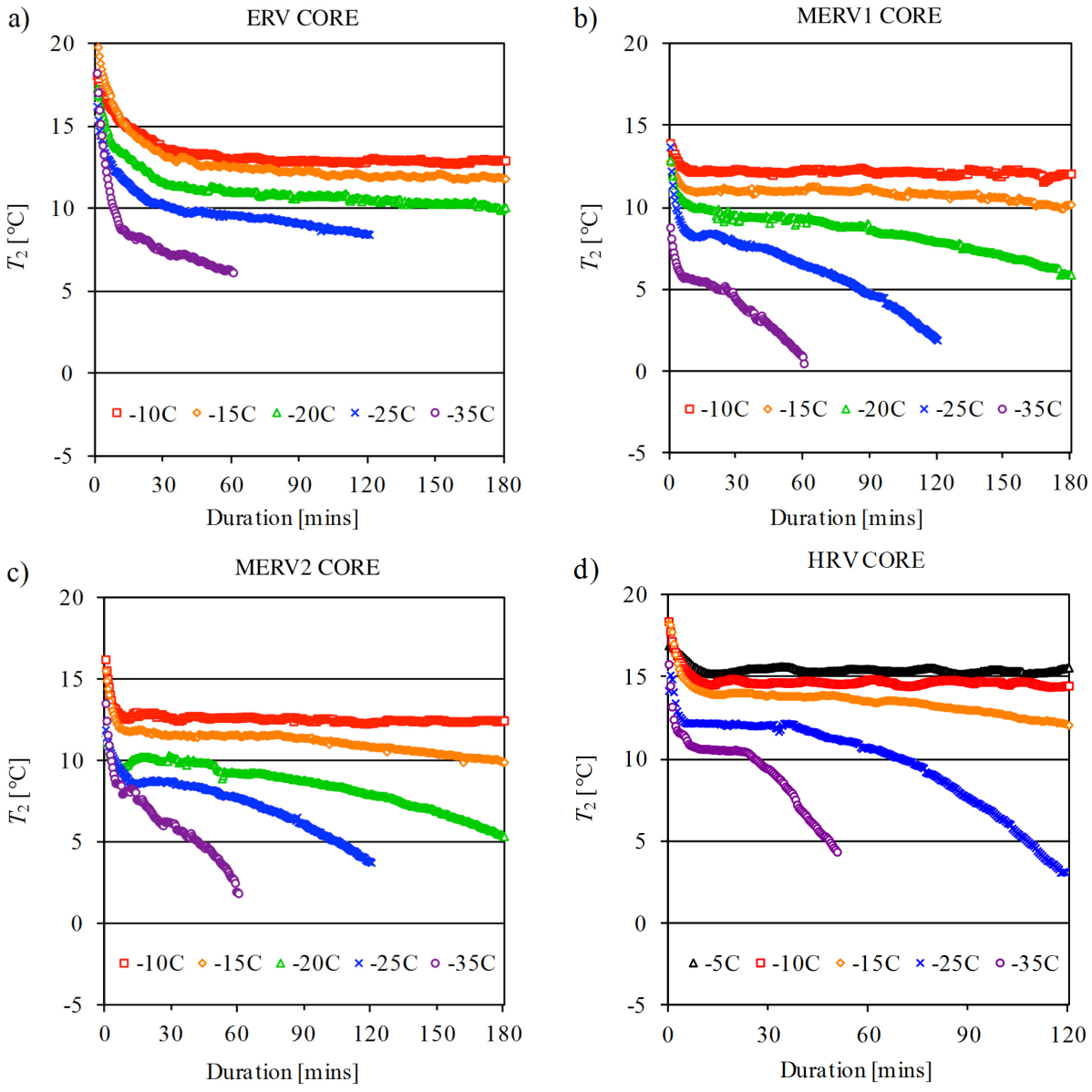

Figure 5.1: Measured outlet supply air temperature, T_2 versus time for a) ERV b) MERV1 c) MERV2 and d) HRV cores at different inlet supply air temperatures, T_1

At lower inlet supply air temperatures there is a corresponding decrease with time in the measured outlet supply air temperature. This behaviour is observed for all exchanger cores regardless of type. The measured outlet supply air temperature sees little to no change over time for the inlet supply air temperatures equal to −10°C for all vapour-permeable cores (ERV, MERV1, and MERV2) for the duration of the tests. This was also observed for the HRV core, however the tests only lasted for 2 hours compared to 3 hours for the vapour-permeable cores. The lower the inlet supply air temperature the larger the decrease over time in the outlet supply air temperature.

5.1.2. Outlet supply air humidity ratio

Figure 5.2 shows the change with time of the measured outlet supply air humidity ratio, ω_2 for the different cores operating at different inlet supply air temperatures, T_1.

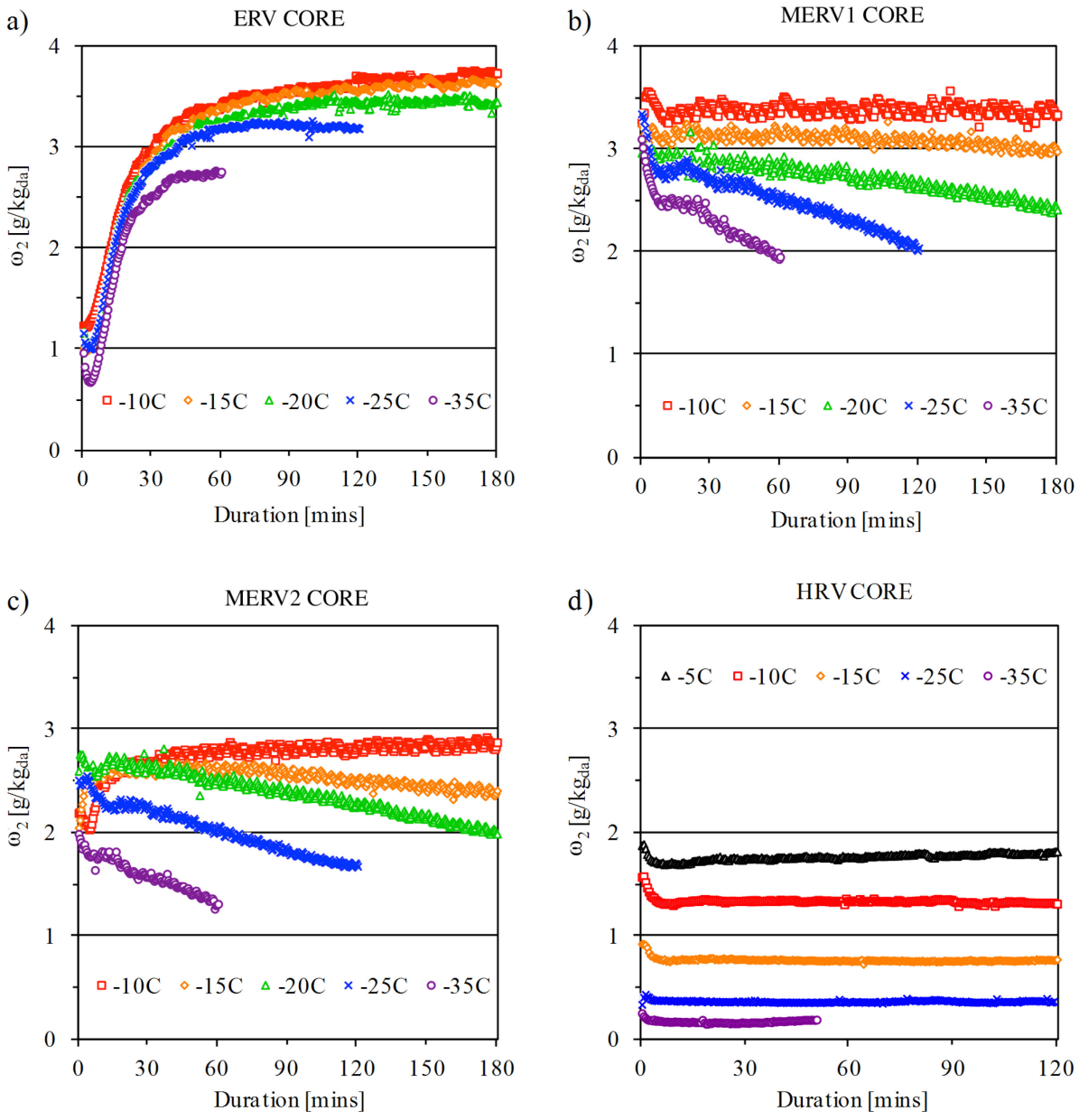

Figure 5.2: Calculated outlet supply air humidity ratio, ω_2 based on relative humidity and temperature measurements for a) ERV b) MERV1 c) MERV2 and d) HRV cores at different inlet supply air temperatures, T_1

The measurements show that ω_2 decreased for cores MERV1 and MERV2 over time when T_1 is equal or lower than −10°C. The rate of decrease over time of the humidity ratio of outlet air increases as T_1 decreases. The decrease in ω_2 over time was not witnessed for Core ERV. Instead, ω_2 measurements slowly reach a plateau, which was maintained for the duration of the tests. The outlet supply air humidity ratio remains almost constant for the HRV core because there is no moisture transfer between airstreams.

5.1.3. Exhaust Air Mass Flow Rate

Figure 5.3 shows the change with time of the mass flow rate of exhaust air expressed as the ratio between the instantaneous mass flow rate, $\dot{m}_3$ at any given time and the average initial mass flow rate, $\dot{m}_{3,i}$ calculated during the first 10 minutes of the test. This reduction of exhaust air flow rate is due to the formation of frost.

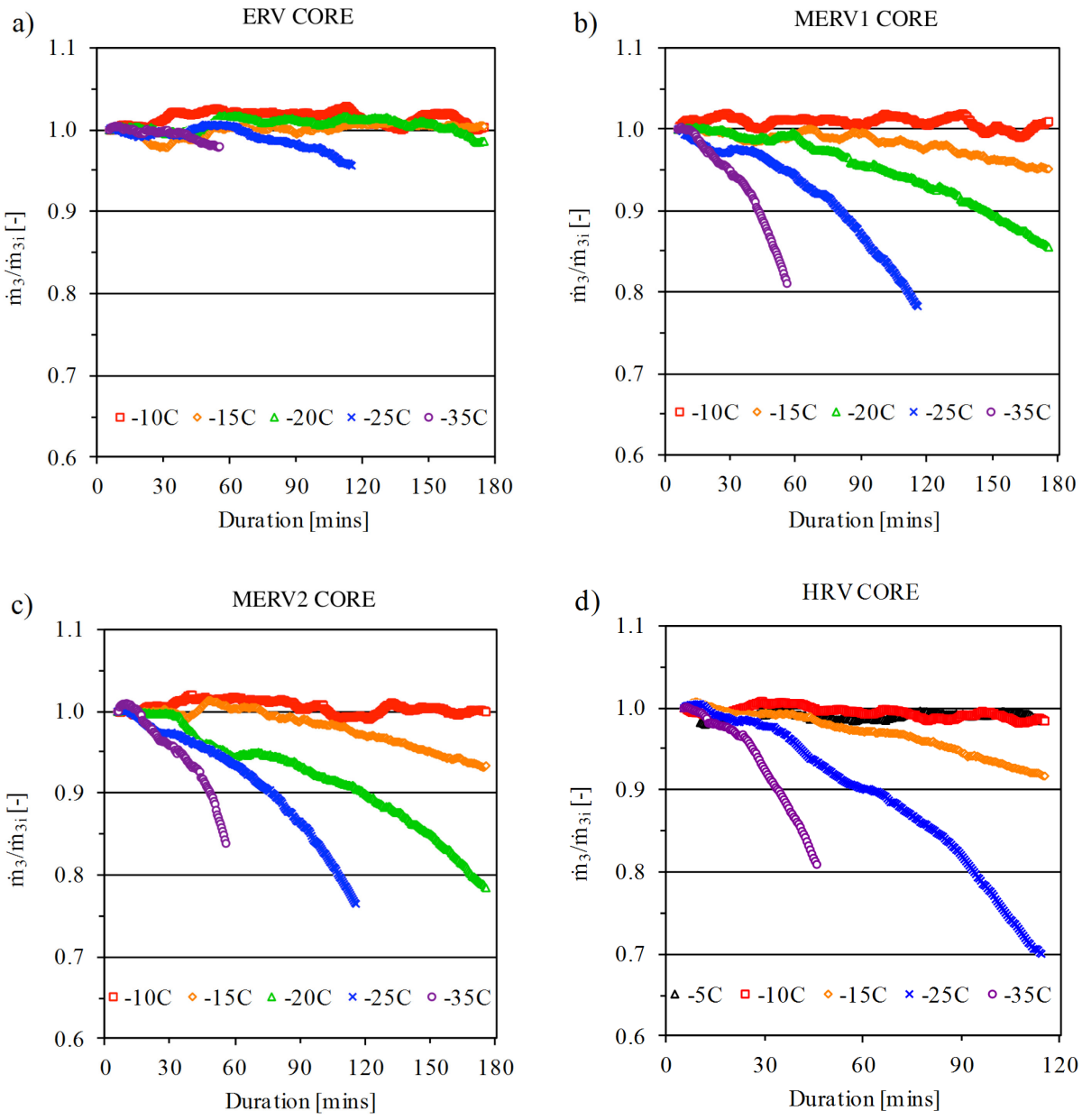

Figure 5.3: Change in the mass flow rate of exhaust air, $\dot{m}_3/\dot{m}_{3,i}$ for a) ERV b) MERV1 c) MERV2 and d) HRV cores at different inlet supply air temperatures, T_1

The exhaust air mass flow rate remains stable for all cores with little to no decrease when T_1 is equal or greater than −10°C. When T_1 is below −10°C all cores experience a decrease in $\dot{m}_3$ when compared to the initial measurements. The rate and magnitude of the decrease in $\dot{m}_3$ vary between cores, with the HRV core seeing the highest decrease in $\dot{m}_3$ when the inlet supply air temperature is lower than and equal to −25°C. Core ERV sees the smallest drop in the mass flow rate at all tested inlet supply air temperatures when compared to the other cores.

The decrease in the mass flow rate depends heavily on the inlet supply air temperature. For example, the HRV core experiences a 1.6%, 8.3% and 29.9% reduction in $\dot{m}_3$ after three hours when T_1 is equal to −10°C, −15°C and −25°C, respectively. This behaviour is witnessed for all cores, however at varying magnitudes (**Table 5.1**).

Table 5.1: Percent reduction in $\dot{m}_3$ for each core at different T_1 values

Inlet supply air temp., T_1	Reduction in $\dot{m}_3$ [%]			
	ERV	MERV1	MERV2	HRV
−5°C	*no decrease*	*no decrease*	*no decrease*	*no decrease*
−10°C	*no decrease*	*no decrease*	*no decrease*	1.6
−15°C	*no decrease*	4.8	6.6	8.3
−20°C	1.4	14.4	21.5	n/a
−25°C	4.4	21.7	23.5	29.9
−35°C	2.0	18.9	16.1	19.0

Test durations varied according to the inlet supply air temperature. The test durations were 3hrs, 2hrs and 1hrs for inlet supply air temperatures of −5°C to −20°C, −25°C and −35°C, respectively. This explains why the reduction in $\dot{m}_3$ for T_1 equal to −35°C was lower than for T_1 equal to −25°C. The HRV test at T_1 equal to −35°C was prematurely stopped at 50 minutes due to the potential for core damage.

5.1.4. Core weight

The cores were weighed before and after each experiment to monitor the amount of ice formed within the core. The results are tabulated in **Table 5.2**. The initial dry weight of the ERV, MERV1, MERV2 and HRV cores are 4.24 kg, 1.50 kg, 1.50 kg and 3.30 kg, respectively.

Table 5.2: Change in core weight for each experiment

Inlet supply air temp., T_1	Increase in core weight [kg]			
	ERV	MERV1	MERV2	HRV
−5°C	n/a	n/a	n/a	0.28
−10°C	0.26	0.06	0.14	0.42
−15°C	0.32	0.14	0.24	0.56
−20°C	0.40	0.24	0.36	n/a
−25°C	0.50	*0.40	0.40	0.70
−35°C	0.46	0.24	0.42	0.44

* Measurement recorded after 3 hour experiment instead of 2 hours

The post experiment weight of all cores increased as the inlet supply air temperature decreased. Once again the results for T_1 equal to −35°C were lower than for T_1 equal to −25°C because the duration of the tests were shorter, resulting in less time for core frosting to occur.

5.2. Analysis - One HEE unit without defrost

This section includes the analysis of the results for the first phase of experiments conducted.

5.2.1. Core frosting

The accumulation of frost in the cores impeded the flow of air in the exhaust airstream. Core frosting can be evaluated based on the decrease in the exhaust air mass flow rate and the increase in core weight.

Based on these two measurements, the HRV core experienced the most core frosting compared to the other cores because there is no water vapour transferred to the supply airstream. The HRV core had the largest reduction in the exhaust air mass flow rates at all tested inlet supply air temperatures. The HRV core also had the largest increase in core weight for inlet supply air temperatures between −10°C and −25°C. The exception being the case of T_1 equal to −35°C where the test was aborted after 50 minutes due to concerns regarding core damage.

The MERV1 core and the MERV2 core saw lower accumulations of frost when compared to the HRV core. When compared to each other, for inlet supply air temperatures between −10°C and −20°C the MERV1 core had a smaller reduction in the exhaust air mass flow rates and a lower increase in core weight. When T_1 was equal to −25°C the measured change in core weights for both MERV1 and MERV2 were equal. This was due to the duration of the experiments being different. The MERV1 core was, in error, tested for 3 hours instead of the planned 2 hours. However, it can be assumed that if the experiment had been stopped after 2 hours, the increase in the MERV1 core weight would have been less than what was measured for MERV2. This is further supported by the 21.7% and 23.5% measured decrease in exhaust air mass flow rate for MERV1 and MERV2 core, respectively, after 2 hours of testing.

The ERV core did not follow the same pattern as the other cores. The core saw the smallest reduction in exhaust air mass flow rates for all tested inlet supply air temperatures. However, the results show that the increase in core weights for the same tests were second only to the HRV core. There may be two explanations for these seemingly contradictory results. First, the construction geometry of the core could be reducing the impact of core frosting on the exhaust mass flow rate or more likely, the material of the core not only transfers but absorbs and retains a certain portion of the moisture in the exhaust airstream. This absorption theory is supported by the slow rise in the outlet supply air humidity measurements as depicted in **Figure 5.2**. This phenomenon is discussed further in the sections to come.

5.2.2. Sensible and Latent Heat Transfer Effectiveness

Figure 5.4 and **Figure 5.5** show the adjusted sensible and latent heat transfer effectiveness for each core over the duration of the experiments at different inlet supply air temperatures.

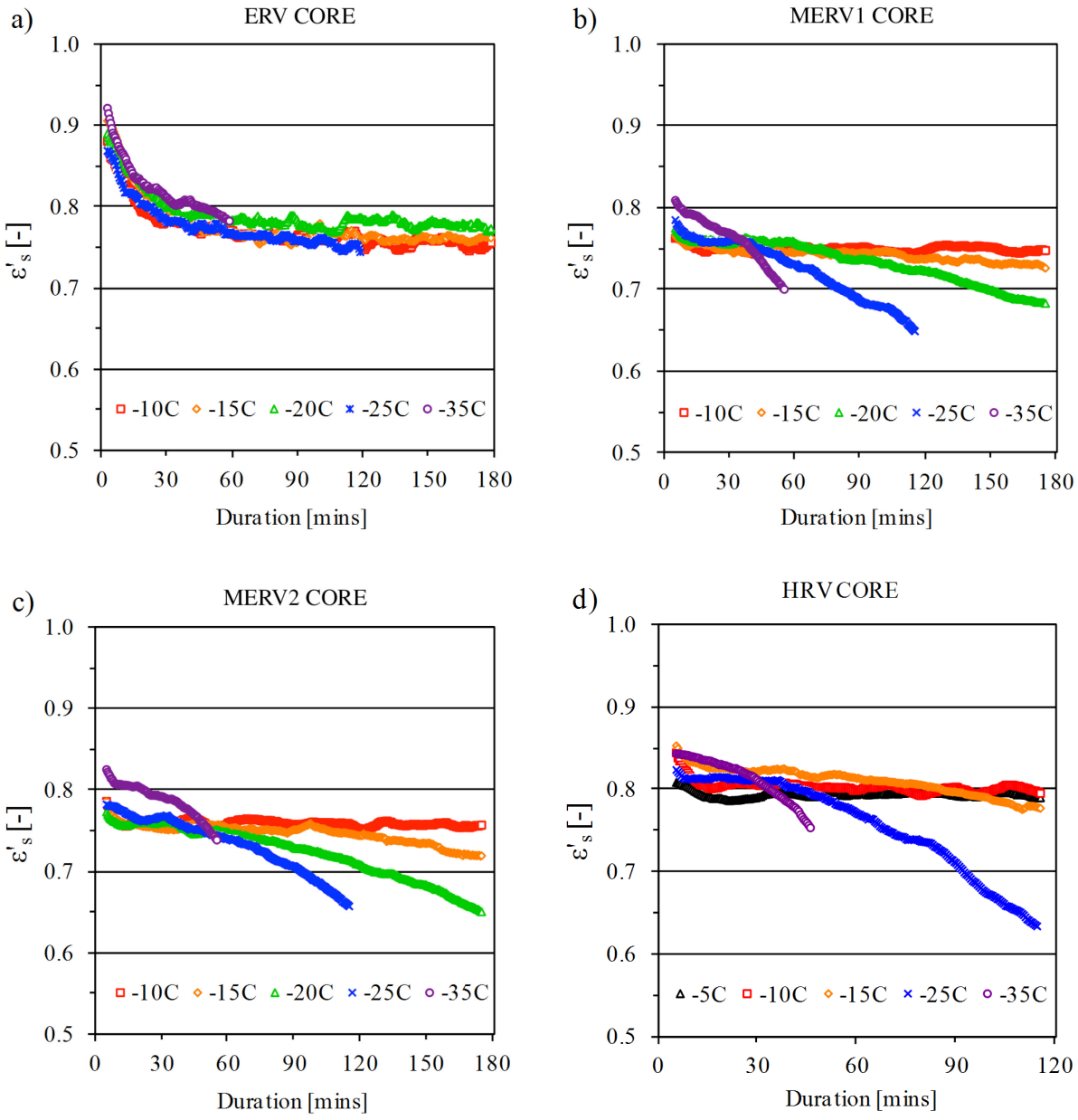

Figure 5.4: Change with time of the adjusted sensible heat transfer effectiveness, ε'_s for a) ERV b) MERV1 c) MERV2 and d) HRV cores at different inlet supply air temperatures, T_1

The sensible heat transfer effectiveness for all cores remained constant for the duration of the test for T_1 equal to −10C. However, below this temperature core frosting begins to decrease the sensible heat transfer between airstreams. The HRV core saw a significant decrease in ε'_s for inlet supply air temperatures below −15°C. This decrease in ε'_s was witnessed for inlet supply air temperatures below −20°C for the membrane-based cores. The ERV core did not exhibit a decrease in ε'_s for any of the tests.

The sensible heat transfer effectiveness during the initial minutes of the tests were highly influenced by the temperature of the core upon insertion into the exchanger. The thermal masses, due to differences in construction, of the cores vary and in-turn the influence of the initial temperature and on the sensible heat transfer effectiveness is different for each core. The effect of the thermal mass on ε'_s is best demonstrated by the results for core ERV. Compared to the cores, which are of lower weight, the ε'_s for ERV takes considerably (approximately 1 hour) longer to reach steady state.

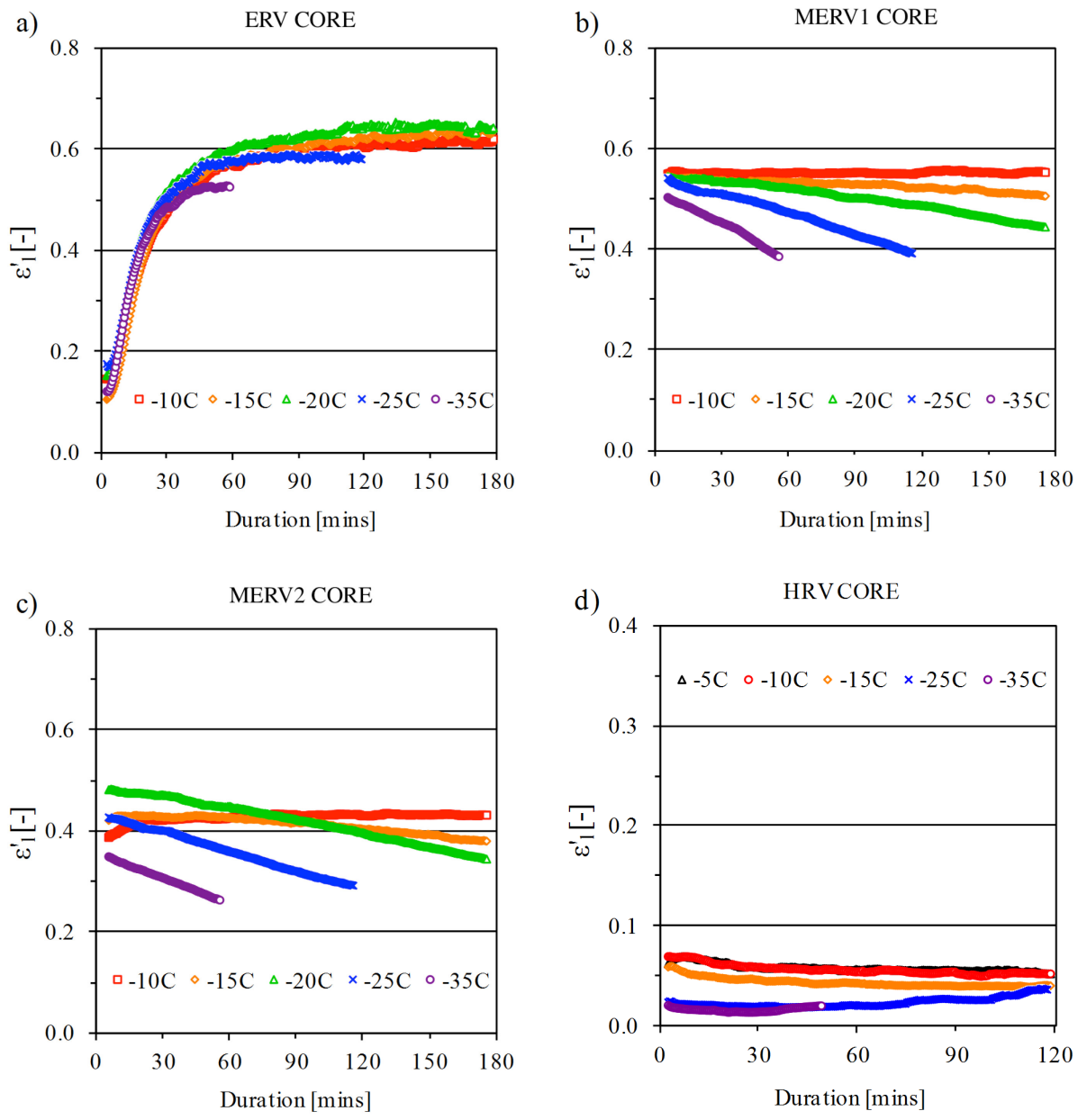

Figure 5.5: Change with time of the adjusted latent heat transfer effectiveness, ε'_l for a) ERV b) MERV1 c) MERV2 and d) HRV cores at different inlet supply air temperatures, T_1

The HRV core had the lowest ε'_l for all tests because the transfer of water vapour between the two airstreams is not permitted by the core materials.

MERV1 and MERV2 experienced little change in ε'_l for the duration of the tests when $T_1 = -10$C. Core MERV1 and Core MERV2 had an average ε'_l of 0.55 and 0.43 over the dura-

tion of the −10°C tests, with core MERV1 out performing core MERV2 by 12%. The latent heat transfer effectiveness of the two cores began to decrease over time for inlet supply air temperature below −10°C. This decrease in ε_l becomes progressively more significant as the inlet supply air temperature decreases. This is best illustrated by the decrease in the slope of the ε'_l data points as the inlet supply air temperature decreases.

The decrease in ε'_l for core MERV2 was lower than for MERV1 for nearly all inlet supply air temperatures except for −20°C. The results are shown in **Table 5.3**.

Table 5.3: Decrease in ε'_l for MERV1 and MERV2

Inlet supply air temperature, T_1	Decrease in ε'_l [%]	
	MERV1	MERV2
−15°C	5.5	0.1
−20°C	10.5	13.8
−25°C	17.0	14.0
−35°C	13.4	9.5

The results indicate that frost accumulation in the MERV2 core, while more significant compared to MERV1, may not affect the latent heat transfer effectiveness as much as for the MERV1 core.

Cores MERV1 and MERV2 saw a near instantaneous transfer of water vapour between airstreams. This was not the case for core ERV, where the ε'_l at all tested temperatures required a period of time to reach steady state. While not confirmed, it is assumed that this delay, as show in **Table 5.6**a as a ramp, is due to the absorption of moisture by the core materials (polymerized paper). The absorption of water vapour reduces the amount of vapour available to be transfer to the exhaust airstream and in turn could explain the lower ε'_l values experienced in the beginning

stages of the tests. After reaching steady state, the latent heat transfer effectiveness for core ERV were the highest compared to all cores at all tested inlet supply air temperatures.

5.2.3. Change in Heat Transfer Effectiveness versus Change in Exhaust Air Mass Flow Rate

Figure 5.6 shows the change in the sensible heat transfer effectiveness with respect to the value of initial conditions ($\varepsilon'_s/\varepsilon'_{s,i}$) versus the change in the exhaust air mass flow rate with respect to the value of initial conditions ($\dot{m}_3/\dot{m}_{3,i}$) for cores MERV1, MERV2 and HRV at different inlet supply air temperatures. The initial valves ($\varepsilon'_{s,i}$ and $\dot{m}_{3,i}$) were average values calculated for the first 10 minutes of the tests. The results for all cores when $T_1 = -10$°C have been excluded because there was little to no change in the sensible heat transfer effectiveness and exhaust air mass flow rates for the duration of the tests.

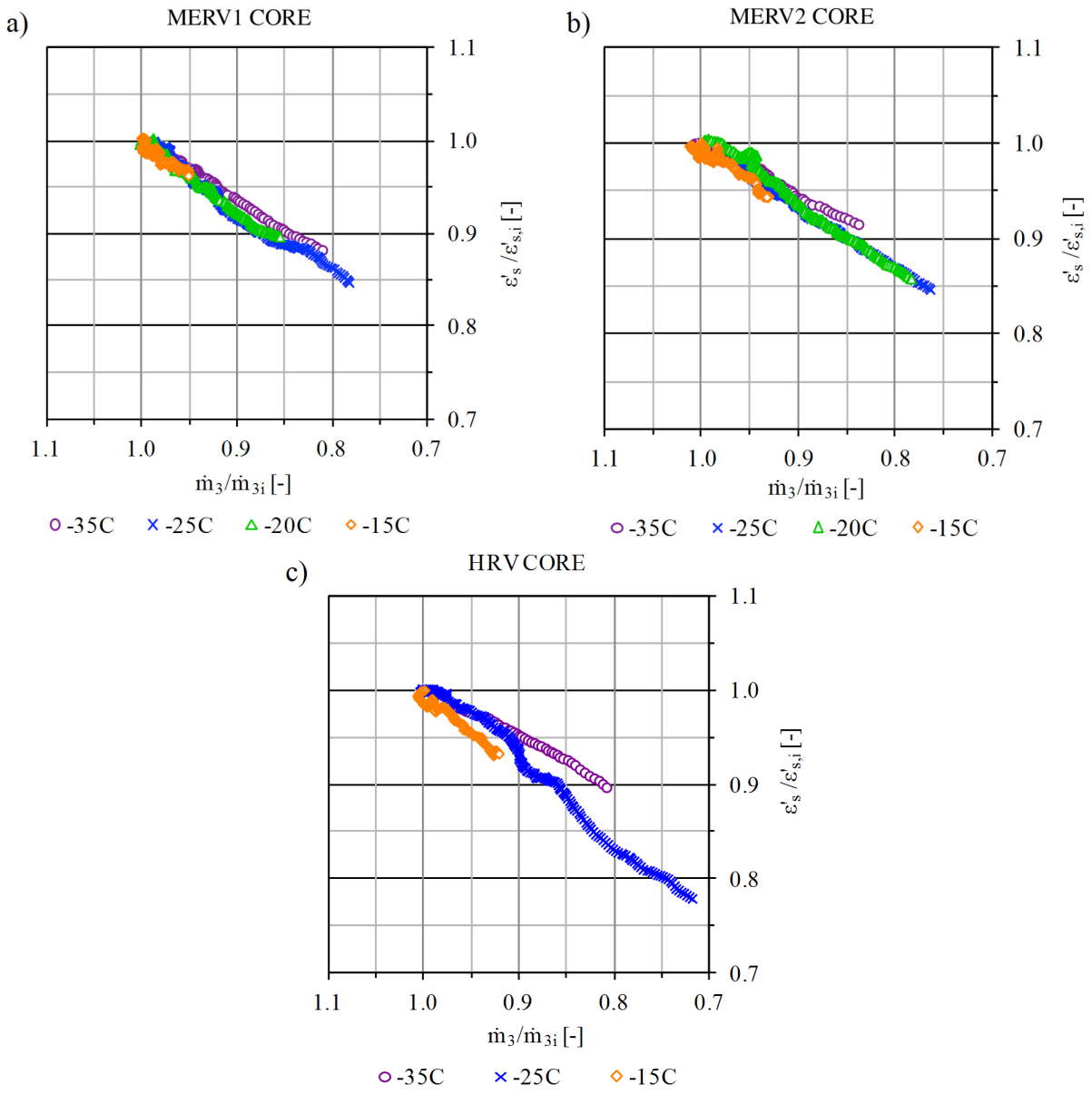

Figure 5.6: The change in the sensible heat transfer effectiveness versus the change in the exhaust air mass flow rate for cores a) MERV1, b) MERV2 and c) HRV

Core ERV was excluded from this analysis because for all tested inlet supply air temperatures there was little to no change in the sensible heat transfer effectiveness and exhaust air mass flow rates.

The inlet supply air temperature did not affect the change in ε'_s versus the change in $\dot{m}_3$ for both membrane-based cores (MERV1 and MERV2). There was a slight difference in the trajectory of

the change in ε'_s versus the change in $\dot{m}_3$ for the HRV core at different inlet supply air temperatures.

There was a linear relationship between the change in ε'_s and the change in $\dot{m}_3$ for all three cores. **Table 5.4** shows the linear trend-line equations for each core at the different inlet supply air temperatures.

Table 5.4: Change in adjusted sensible heat transfer effectiveness versus change in exhaust air mass flow rate trend-line equations

Inlet supply air temperature	**MERV1**		**MERV2**		**HRV**	
	Trend-line	R^2	Trend-line	R^2	Trend-line	R^2
$T_1 = -15°C$	y = 0.61x + 0.38	0.84	y = 0.62x + 0.37	0.91	y = 0.75x + 0.25	0.96
$T_1 = -20°C$	y = 0.77x + 0.23	0.99	y = 0.72x + 0.29	0.98	n/a	–
$T_1 = -25°C$	y = 0.75x + 0.25	0.98	y = 0.66x + 0.34	0.99	y = 0.84x + 0.16	0.99
$T_1 = -35°C$	y = 0.66x + 0.34	0.99	y = 0.55x + 0.45	0.98	y = 0.53x + 0.48	0.99

* where y represents $\varepsilon'_s/\varepsilon'_{s,i}$ and x represents $\dot{m}_3/\dot{m}_{3,i}$

Using these equations the expected change in the heat transfer effectiveness can be assess based on the variation of the exhaust mass for rate, or the change in the exhaust air mass flow rate for each core can be determined for a given reduction in sensible heat transfer effectiveness. For instance, **Table 5.5** shows the expected change in the exhaust air mass flow rates ($\dot{m}_3/\dot{m}_{3,i}$) for each core when the heat transfer effectiveness ($\varepsilon'_s/\varepsilon'_{s,i}$) reaches 90% of the initial value.

Table 5.5: Change in exhaust air mass flow rate at 10% reduction in the sensible heat transfer effectiveness

Core	Reduction of exhaust air mass flow rate when $\varepsilon_s/\varepsilon_{s,i}$ = 0.90 [-]			
	$T_1 = -15$°C	$T_1 = -20$°C	$T_1 = -25$°C	$T_1 = -35$°C
MERV1	0.85*	0.87	0.87	0.85
MERV2	0.85*	0.85	0.85	0.82*
HRV	0.87*	n/a	0.87	0.79

* Extrapolated

The change in exhaust air mass flow rate when $\varepsilon'_s/\varepsilon'_{s,i}$ = 0.90 is very similar for all cores at the tested inlet supply air temperatures, of 0.85−0.87, except when $T_1 = -35$°C When $T_1 = -35$°C, the HRV core had the largest change in exhaust air mass flow rate, while core MERV1 had the smallest. In other words, when the exhaust air mass flow rate is reduced by 13−15% from the initial value, the sensible heat transfer effectiveness is expected to be reduced by 10%.

While the relationship between $\varepsilon'_s/\varepsilon'_{s,i}$ and $\dot{m}_3/\dot{m}_{3,i}$ appears to be linear for the duration of the tests, however, it is not known what would happen if the tests were allowed to continue.

Figure 5.7 shows the change in the latent heat transfer effectiveness with respect to the value of initial conditions ($\varepsilon'_l/\varepsilon'_{l,i}$) versus the change in the exhaust air mass flow rate with respect to the value of initial conditions ($\dot{m}_3/\dot{m}_{3,i}$) for cores MERV1 and MERV2 at multiple inlet supply air temperatures. Once again, the results for $T_1 = -10$°C have been excluded because there was little to no change in either variable over the duration of the tests.

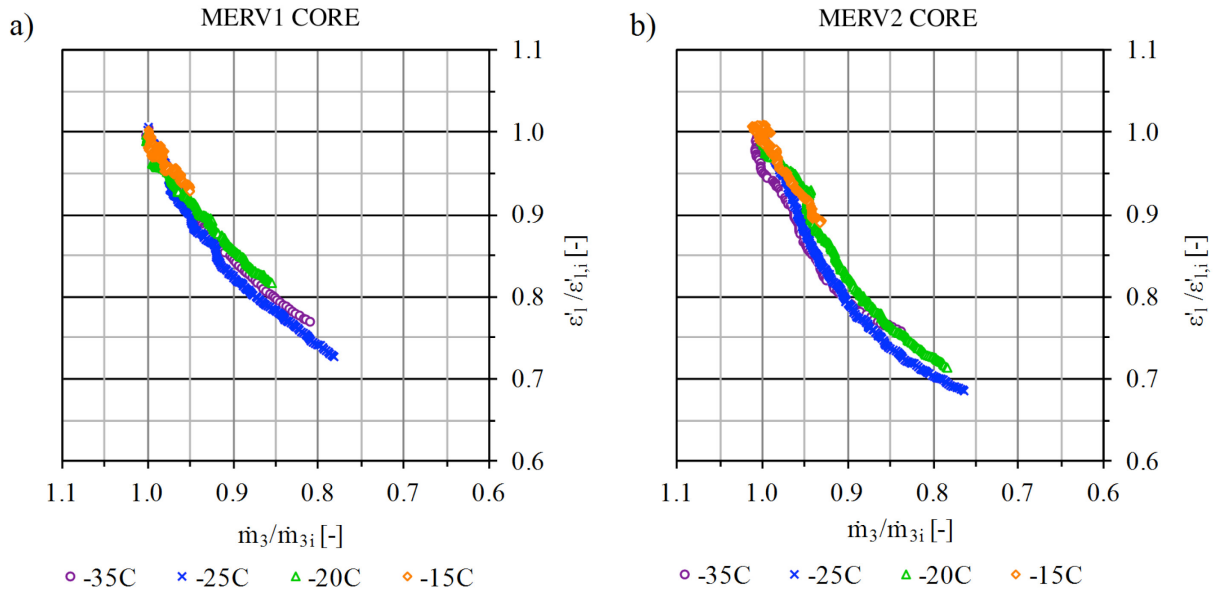

Figure 5.7: The change in the latent heat transfer effectiveness versus the change in the exhaust air mass flow rate for cores a) MERV1 and b) MERV2

Core ERV was not included in this analysis due to the moisture absorption of the core prohibiting the determination of a suitable initial adjusted latent heat transfer effectiveness value, $\varepsilon'_{l,i}$.

The $\varepsilon'_l/\varepsilon'_{l,i}$ for both cores appears to decrease exponentially with a decreasing $\dot{m}_3/\dot{m}_{3,i}$. This is unlike the case for the change in adjusted sensible heat transfer effectiveness where the relationship with predominantly linear. As with the adjusted sensible heat transfer effectiveness, the trend-line equations for the adjusted latent heat transfer effectiveness are presented in **Table 5.6**.

Table 5.6: Change in the adjusted latent heat transfer effectiveness versus change in exhaust air mass flow rate trend-line equations

Inlet supply air temperature	**MERV1**		**MERV2**	
	Trend-line	R^2	Trend-line	R^2
$T_1 = -15°C$	$y = 2.68x^2 - 4.05x + 2.35$	0.89	$y = -0.03x^2 + 1.67x - 0.64$	0.96
$T_1 = -20°C$	$y = 2.80x^2 - 4.01x + 2.20$	0.99	$y = 2.55x^2 - 3.21x + 1.65$	0.98
$T_1 = -25°C$	$y = 4.42x^2 - 6.70x + 3.28$	0.99	$y = 5.63x^2 - 8.65x + 4.02$	0.99
$T_1 = -35°C$	$y = 3.27x^2 - 4.75x + 2.48$	0.99	$y = 6.13x^2 - 9.96x + 4.79$	0.98

* where y represented $\varepsilon'_l/\varepsilon'_{l,i}$ and x represents $\dot{m}_3/\dot{m}_{3,i}$

Second-order polynomial equations (quadratic equations) were used because of the non-linear relationship between the two variables. Similarly to the equations presented in **Table 5.4**, these equations can be used to determine the expected change in the exhaust air mass flow rate for each core for a given reduction in latent heat transfer effectiveness. For example, **Table 5.7** shows the calculated change in the exhaust air mass flow rate for a 10% reduction in the adjusted latent heat transfer effectiveness for cores MERV1 and MERV2 at different inlet supply air temperatures.

Table 5.7: Change in exhaust air mass flow rate at 10% reduction in the adjusted latent heat transfer effectiveness

Core	Reduction of exhaust air mass flow rate when $\varepsilon'_l/\varepsilon'_{l,i}$ = 0.90 [-]			
	$T_1 = -15$°C	$T_1 = -20$°C	$T_1 = -25$°C	$T_1 = -35$°C
MERV1	0.93*	0.94	0.95	0.94
MERV2	0.94	0.95	0.96	0.97

* Extrapolated

It can be seen that the reduction in the exhaust air mass flow rate is nearly the same for both cores at all inlet supply air temperatures. Conversely, it can be concluded that the inlet supply air temperature does not have a significant effect on the total decrease in ε'_l as a result of a decrease in $\dot{m}_3$.

5.2.4. Change in UA value

Figure 5.8 shows the change in the UA value, UA/UA_i, for the different cores at the different tested inlet supply air temperatures. The UA/UA_i is the ratio between the calculated instantaneous UA at any given time and the average initial UA value, UA_i calculated during the first 10 minutes of the test.

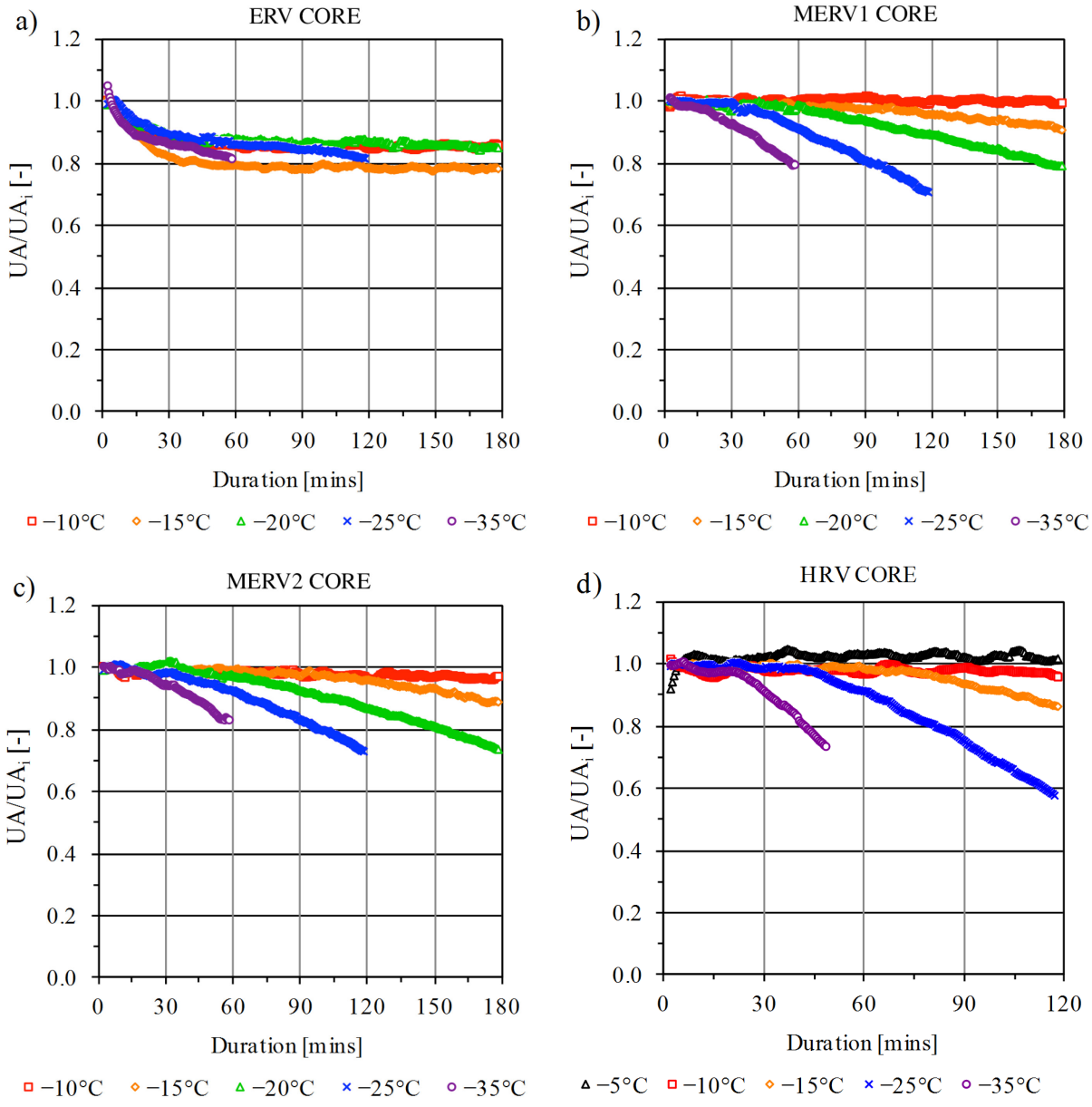

Figure 5.8: Calculated change in UA/UA_i for a) ERV b) MERV1 c) MERV2 and d) HRV cores at different inlet supply air temperatures, T_1

For cores MERV1, MERV2, and HRV there was a decrease in the UA value over the duration of the tests for inlet supply air temperatures lower than −10°C. At lower inlet supply air temperatures, the decrease in the UA value was more pronounced. This is primarily due to the larger accumulation of frost in the core, which as shown inhibits the transfer of heat between the supply and exhaust airstreams. The results for core ERV were different than for the other cores. Unlike the other cores, the UA values took a considerable longer time to over come the influence of the initial conditions. This made it difficult to select initial UA values for comparison with the instantaneous UV values.

Table 5.8 shows the initial UA values for each core at different inlet supply air temperatures. The initial values are the average for the first five minutes of each test.

Table 5.8: Initial UA values for each core at different inlet supply air temperatures

Core	Initial UA values [W/K] *					
	$T_1 = -5°C$	$T_1 = -10°C$	$T_1 = -15°C$	$T_1 = -20°C$	$T_1 = -25°C$	$T_1 = -35°C$
ERV	n/a	122.8 ± 2.1	136.9 ± 2.4	123.0 ± 2.5	127.6 ± 3.5	144.8 ± 8.1
MERV1	n/a	92.5 ± 4.1	95.8 ± 1.9	97.5 ± 1.1	101.2 ± 1.8	102.6 ± 1.4
MERV2	n/a	98.5 ± 1.4	99.3 ± 1.2	99.5 ± 2.8	101.9 ± 1.8	108.8 ± 1.2
HRV	108.0 ± 6.9	117.5 ± 3.5	118.3 ± 2.6	n/a	121.3 ± 2.5	132.2 ± 3.1

* Average and plus/minus standard deviation for the first 5 minutes of each test

As previously mentioned the high initial UA values for core ERV are due to the influence of the initial test conditions as a result of the thermal mass of the core. Disregarding core ERV, the HRV core had the highest initial UA values for all inlet supply air temperatures. However, the HRV core also had the largest decrease in the UV values over the duration of the tests. The initial UA values for cores MERV1 and MERV2 were very similar at the tested inlet supply air temperatures.

The change in the UA value versus the change in the exhaust air mass flow rate for each core and different inlet supply air temperatures are presented in **Figure 5.9**.

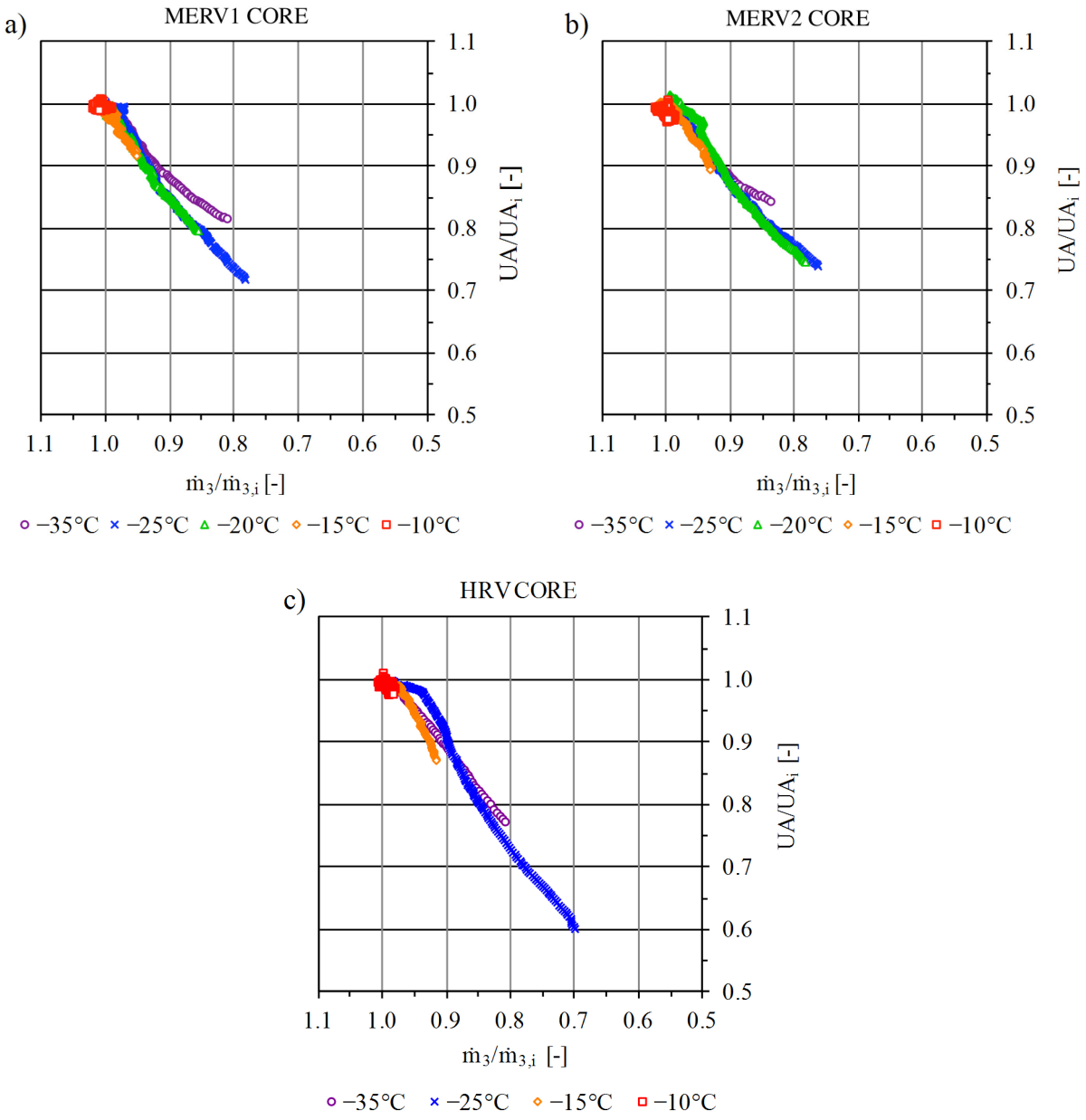

Figure 5.9: The change in UA/UA_i versus the change in exhaust air mass flow rate, $\dot{m}_3/\dot{m}_{3,i}$ for a) MERV1 b) MERV2 and c) HRV cores at different inlet supply air temperatures, T_1

The results show that the inlet supply air temperature did not have a significant effect on the expected reduction in UA values as a function of the reduction in exhaust air mass flow rate. There was a slight difference for T_1 equal to −35°C, where the reduction in UA values for the mem-

brane cores were not as large when compared to the reduction at warmer inlet supply air temperatures. This could be due to the shorter duration of the tests.

It can be concluded that core frosting, as measured by the reduction in the exhaust air mass flow rate, reduces the UA values of the exchanger cores.

6. RESULTS AND ANALYSIS OF ONE HEE UNIT WITH DEFROST

6.1. Results - One HEE unit with defrost

This section presents the results for one HEE unit with ERV, MERV1, MERV2 and HRV cores, operating for 3 hours with defrost enabled, and at the inlet supply air temperatures of −25°C and −35°C.

6.1.1. Outlet supply air temperature

Figure 6.1 shows the measured outlet supply air temperature for a single HEE with defrost for each core at $T_1 = -25$°C and $T_1 = -35$°C.

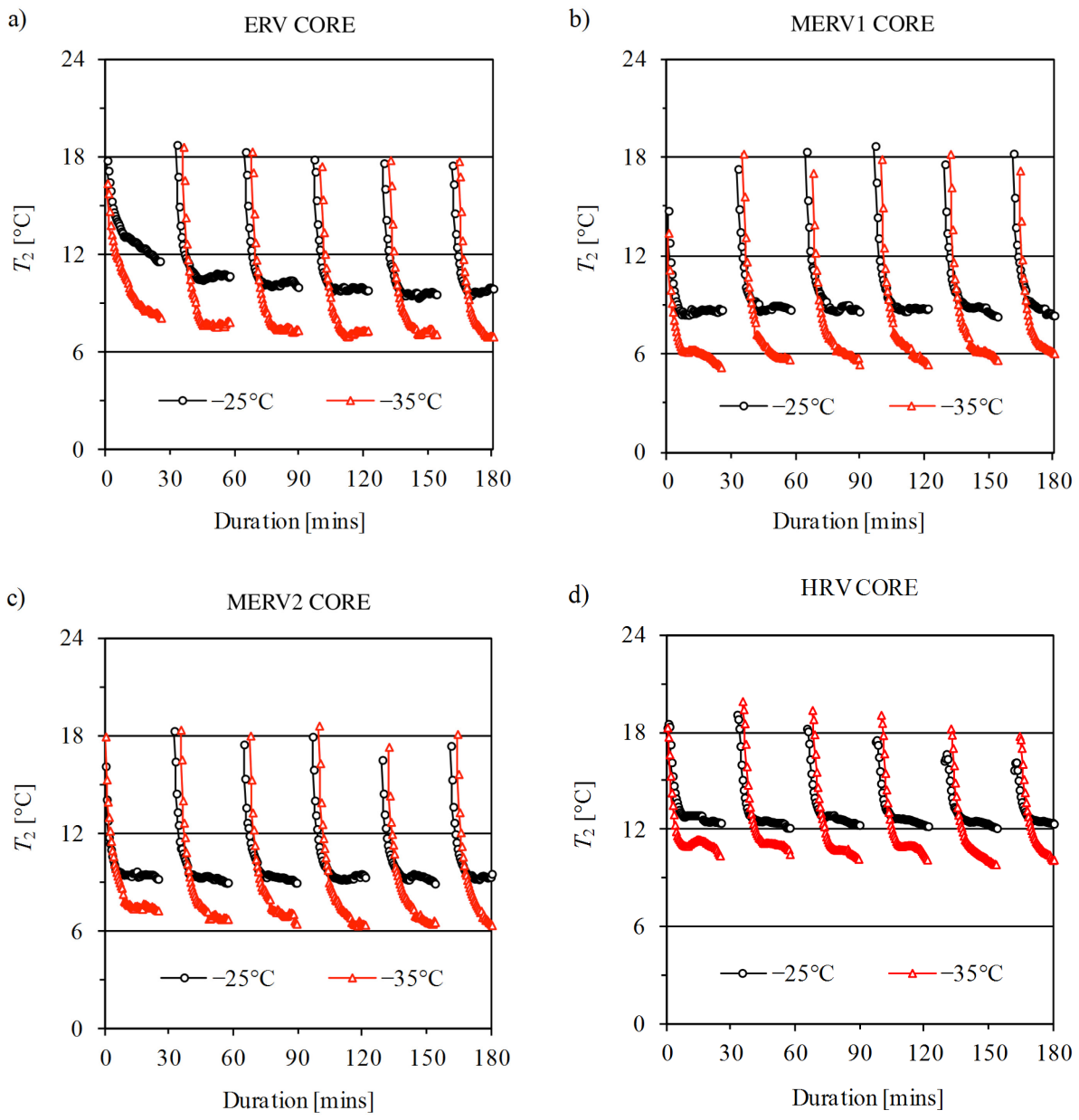

Figure 6.1: Measured outlet supply air temperature for one HEE with defrost for a) ERV b) MERV1 c) MERV2 and d) HRV cores at $T_1 = -25°C$ and $T_1 = -35°C$

The measurements presented in **Figure 6.1** show the outlet supply air temperatures for the periods when the HEE is not in defrost and outdoor supply air is being provided. The measurements during the defrost-cycles have been omitted.

The inlet supply air temperature is affected by the warming of the cores during the defrost cycle. After each defrost cycle the inlet supply air temperature decreases over time; approaching a plateau. This is observed for all cores at both tested inlet supply air temperatures.

The outlet supply air temperatures for the HRV core were the highest compared to the other cores for both tested inlet supply air temperatures. The outlet supply air temperature measurements over time were similar for the ERV, MERV1, and MERV2 cores. The ERV core required a longer period of time to reach quasi-steady state compared to the other cores.

6.1.2. Outlet supply air humidity ratio

Figure 6.2 shows the calculated outlet supply air humidity ratio for a single HEE with defrost for each core at T_1=−25°C and T_1 = −35°C.

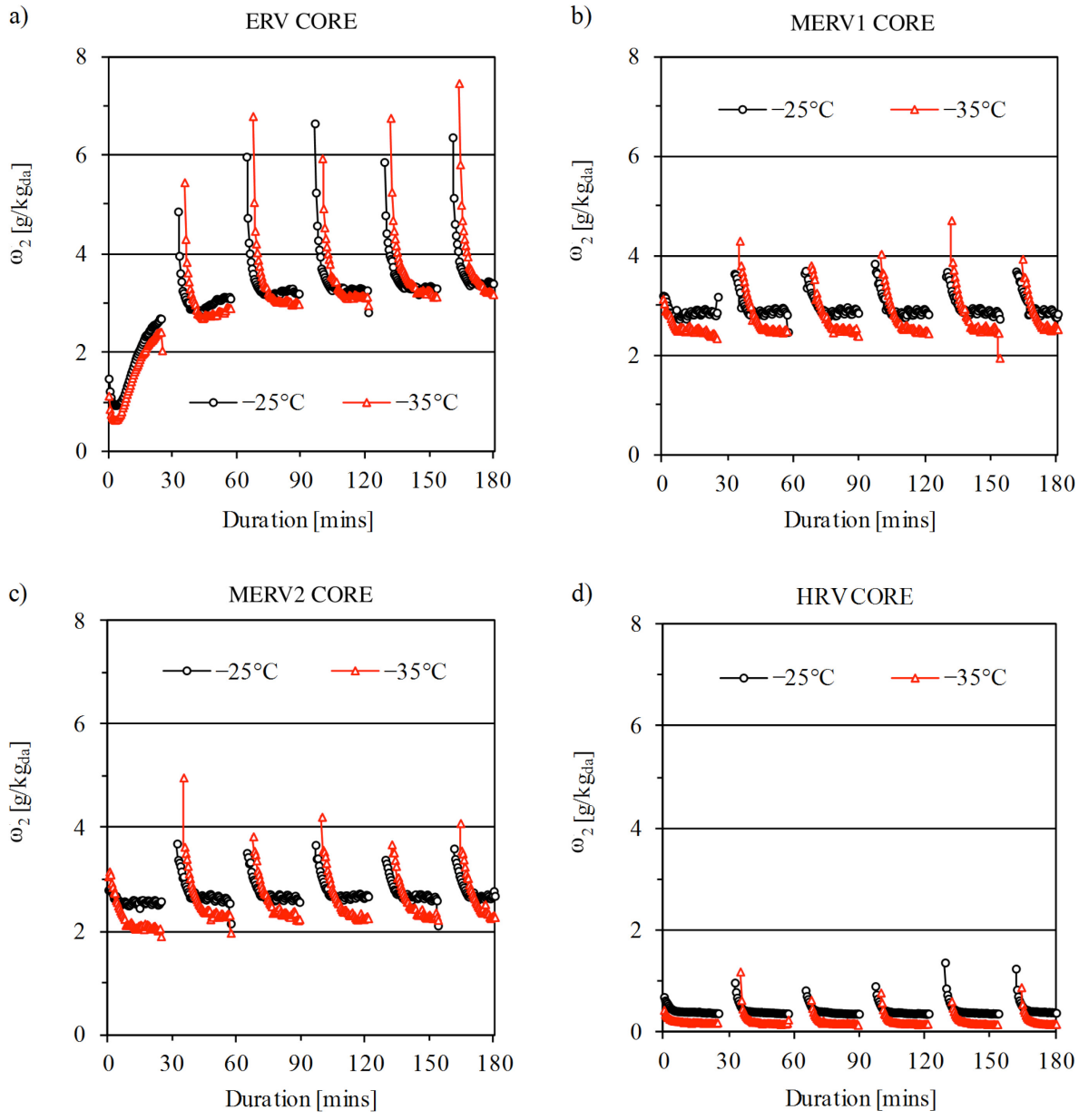

Figure 6.2: Calculated outlet supply air humidity ratio for a single HEE with defrost enabled for a) ERV b) MERV1 c) MERV2 and d) HRV cores at T_1 = −25°C and T_1 = −35°C

The measurements presented in **Figure 6.2** show the outlet supply air humidity ratio for the periods when the HEE was not in defrost and outdoor supply air was provided.

The outlet supply air humidity ratio measurements were very low for the HRV due to the core not being water vapour-permeable. For the vapour-permeable cores the outlet supply air humidity ratio was comparably higher.

The outlet supply air humidity ratio over time for the ERV core was the highest amongst all cores. However the humidity ratio took the longest time to reach steady repeatability.

The outlet supply air humidity ratio measurements for the MERV1 and MERV2 cores were very similar, with the MERV1 core measurements slightly higher than the MERV2 measurements.

The same decrease in the outlet supply air temperatures after each defrost cycle was observed for the outlet supply air humidity ratio. The ERV core saw the largest decrease compared to the other cores. This phenomenon was witnessed for the HRV core even though no moisture is transferred between airstreams.

6.1.3. Air mass flow rates

Figure 6.3 shows the calculated inlet supply and exhaust air mass flow rates for a single HEE with defrost for a HRV core at $T_1 = -25°C$ and $T_1 = -35°C$.

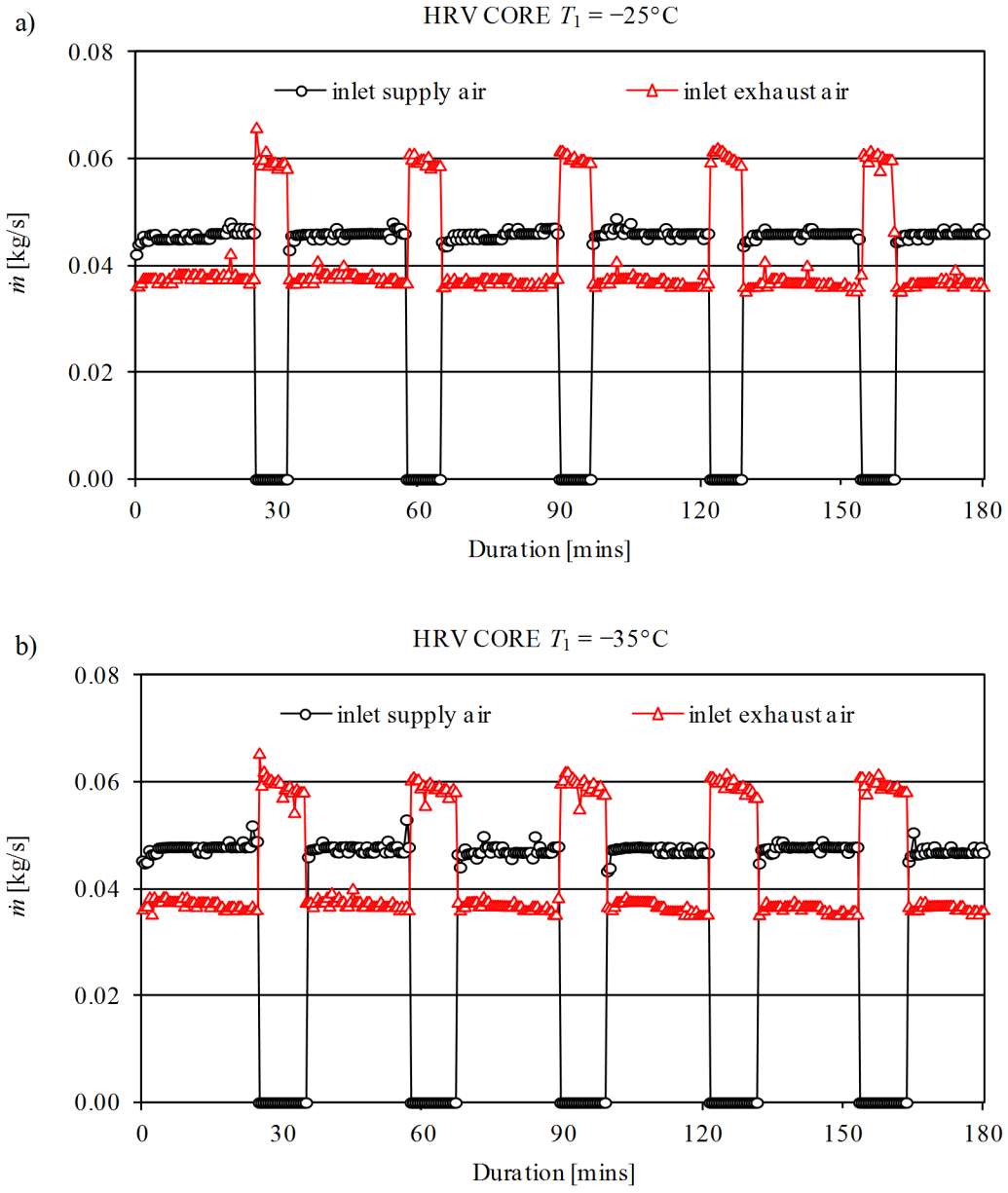

Figure 6.3: Calculated inlet supply and exhaust air mass flow rates for single HEE with defrost for a HRV core at a) $T_1 = -25°C$ and b) $T_1 = -35°C$

The inlet supply and exhaust air mass flow rate results for the ERV, MERV1, MERV2 cores can be found in APPENDIX C.

The pattern of operation at both inlet supply air temperatures for all cores was very similar. After the manufacturer's set period of time for the exchange-cycle the inlet supply air is stopped and the inlet exhaust air is used to defrost the exchanger core. As per the manufacturer's settings, the defrost cycles lasted for approximately seven and nine minutes for T_1 equal to −25°C and −35°C, respectively. The difference in the defrost cycle durations is shown in **Figure 6.3**. During each defrost-cycle the mass flow rate of the inlet exhaust air increases significantly from the mass flow rates measured during the exchange-cycle.

6.2. Analysis - One HEE unit with defrost

6.2.1. Frost management and ventilation

The use of defrost cycles effectively mitigate the formation of frost for all cores at the tested inlet supply air temperatures. The ERV core saw little to no change in the inlet exhaust air mass flow rate during the exchange-cycle for both tested inlet supply air temperatures. While there was a small decrease in the inlet exhaust air mass flow rates during the exchange-cycles for the MERV1, MERV2 and HRV cores when T_1 was equal to −35°C, the defrost-cycles adequately managed any accumulated frost.

As seen in **Figure 6.3** the supply of outdoor air is interrupted during the defrost-cycle. For the ventilation of low-rise residential buildings, according to [58] when ventilation is intermittent it is required that the time-average supply air volumetric flow rate over the period of three hours meet or exceed the rate specified in Eq. (4.12). **Table 6.1** shows the time-averaged supply air volumetric flow rate for one HEE unit with HRV core with defrost at inlet supply air temperatures of −25°C and −35°C. As previously mentioned, these inlet supply air temperatures were selected to demonstrate the two different factory-set defrost schedules (as shown in **Figure 3.7**) of the HEE unit.

Table 6.1 - The effect of defrost-cycle duration after 3 hours on the time-averaged supply air flow rate for the HRV core

Inlet supply air temp. T_1	Cycle duration per 3 hours [mins]		Supply air flow rate [L/s]	
	Exchange-cycle	Defrost-cycle	Exchange-cycle	Time-averaged
above −5°C	180	n/a	32.5*	32.5
−25°C	144	36	32.5	26.0
−35°C	128.5	51.5	32.3	23.1

* based on supply air volumetric flow rate measurements during exchange-cycle when T_1 = −25°C

The results show a decrease in the supply of outside air as a result of the cumulative duration of the defrost-cycles over the 3 hour tests. This decrease during times of cold inlet supply air temperatures might pose a challenge for the indoor air quality. If the HEE unit is selected based on the supply air volumetric flow rates when defrosting is not a concern (i.e. inlet supply air temperatures above −5°C), the ventilation requirements might not be met during times when a defrost-cycle is required. On the contrary, if the HEE unit is selected based on the flow rates when T_1 = −35°C, considering defrost-cycles, it might result in over ventilation for periods when defrost is not required.

6.2.2. Sensible and latent heat transfer effectiveness

The sensible and latent heat transfer effectiveness (**Table 6.2**) of each core at both tested inlet supply air temperatures were calculated for the last exchange-cycle of each 3 hour test. This was to minimize the influence of the starting conditions on the performance indices.

Table 6.2: Adjusted sensible and latent heat transfer effectiveness with defrost

Core	Adj. Sensible Effectiveness, ε'_s [-]		Adj. Latent Effectiveness, ε'_l [-]	
	$T_1 = -25°C$	$T_1 = -35°C$	$T_1 = -25°C$	$T_1 = -35°C$
ERV	0.78 ± 0.01	0.77 ± 0.01	0.61 ± 0.01	0.59 ± 0.01
MERV1	0.76 ± 0.01	0.77 ± 0.00	0.52 ± 0.01	0.48 ± 0.00
MERV2	0.76 ± 0.01	0.76 ± 0.01	0.46 ± 0.01	0.43 ± 0.01
HRV	0.83 ± 0.01	0.84 ± 0.01	0.02 ± 0.00	0.02 ± 0.00

* Average values plus-minus standard deviation for the evaluation period

The HRV core had the highest ε'_s values for both tested inlet supply air temperatures. The adjusted sensible heat transfer effectiveness of the vapour-permeable cores (ERV, MERV1 and MERV2) were nearly the same for T_1 equal to −25°C. The same result was observed for the inlet supply air temperature of −35°C. The adjusted sensible heat transfer effectiveness of each core were similar at T_1 equal to −35°C compared to −25°C for each core.

The latent heat transfer effectiveness for the ERV core was the highest compared to the other cores for both tested inlet supply air temperatures. The ε'_l for all vapour-permeable cores were lower for T_1 equal to −35°C compared to −25°C. The ε'_l values for the HRV core were the lowest due to the core's impermeability to water vapour.

7. RESULTS AND ANALYSIS OF TWO HEE UNITS WITH ALTERNATING DE-FROST

7.1. Results - Two HEE units with alternative defrost

The following section presents the results for two HEE units with ERV, MERV1, and HRV cores, operating for 3 hours with alternating defrost at the inlet supply air temperatures of −25°C and −35°C.

The two HEE units operate according to the schedule presented in **Figure 3.7**. The two HEE units operate in three modes: the heat/moisture exchange mode, the defrost mode and the standby mode. When one HEE unit starts the heat/moisture exchange mode the other HEE unit starts the defrost mode and then enters the standby mode waiting to be activated. The durations of each mode (heat/moisture exchange mode, defrost mode and standby mode) are based on the factory-set time periods (**Table 3.1**).

7.1.1. Outlet supply air temperature

Figure 7.1 shows the measured outlet supply air temperature for two HEE units with alternating defrost for cores ERV and HRV at $T_1 = -25°C$ and $T_1 = -35°C$. The results for core MERV1 can be found in APPENDIX C (**Figure C.4**).

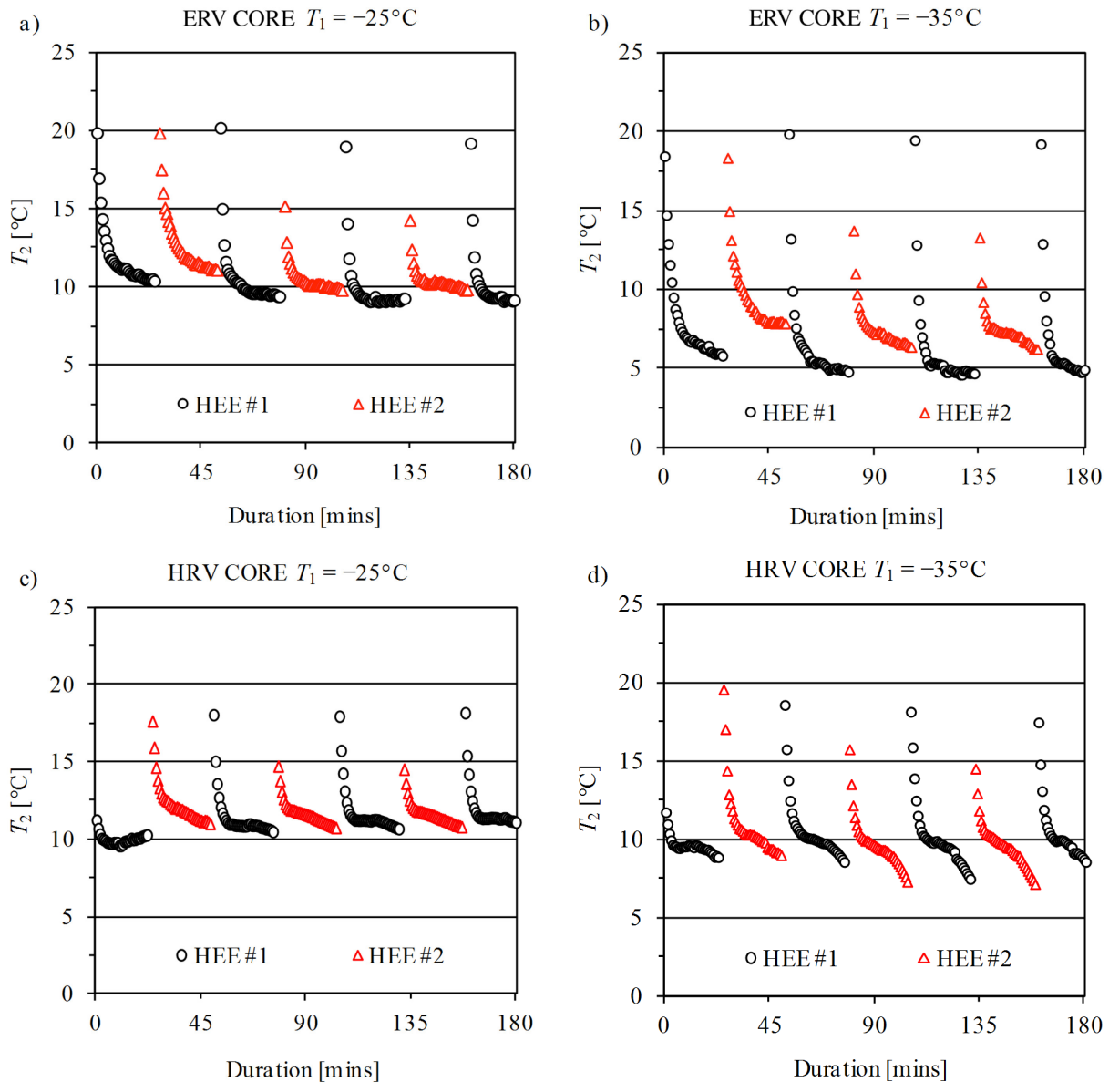

Figure 7.1: Measured outlet supply air temperature for two HEE units with alternating defrost for ERV and HRV cores at $T_1 = -25°C$ and $T_1 = -35°C$

The results in **Figure 7.1** are only for the heat/moisture exchange mode; measurements collected during the defrost mode and standby mode were omitted.

The outlet supply air temperature decreases significantly during the initial moments of each exchange cycle for both HEE units and for all cores. This is in keeping with the results of the tests with one HEE unit with defrosting enabled. These high initial outlet supply air temperatures are primarily due to the cores, HEE units and ducting being heated up during the defrost cycle and standby period by the relatively warm exhaust air and surrounding ambient air, respectively.

After the initial cooling period the outlet supply air temperatures for all cores were relatively stable for $T_1 = -25°C$. The HRV core had highest outlet supply air temperature compared to all tested cores.

When T_1 was equal to −35°C, the outlet supply air temperatures for the HRV core started to decrease over time beyond the initial plateau; exhibiting a clear inflection point. For the MERV1 core, when $T_1 = -35°C$ the outlet supply air temperature does not reach a plateau and instead continued to decrease over time. The outlet supply air temperature measurements for the ERV core at $T_1 = -35°C$ were lower than for $T_1 = -25°C$; however there was minimal decrease in the measurement after the initial cooling period.

Alternating between HEE units during the defrost cycles allowed for the continuous recovery of heat from the exhaust airstream.

7.1.2. Outlet supply air humidity ratio

Figure 7.2 shows the outlet supply air humidity ratio for two HEE units with alternating defrost for cores ERV and MERV1 at $T_1 = -25°C$ and $T_1 = -35°C$. The results for the HRV core can be found in APPENDIX C (**Figure C.5**).

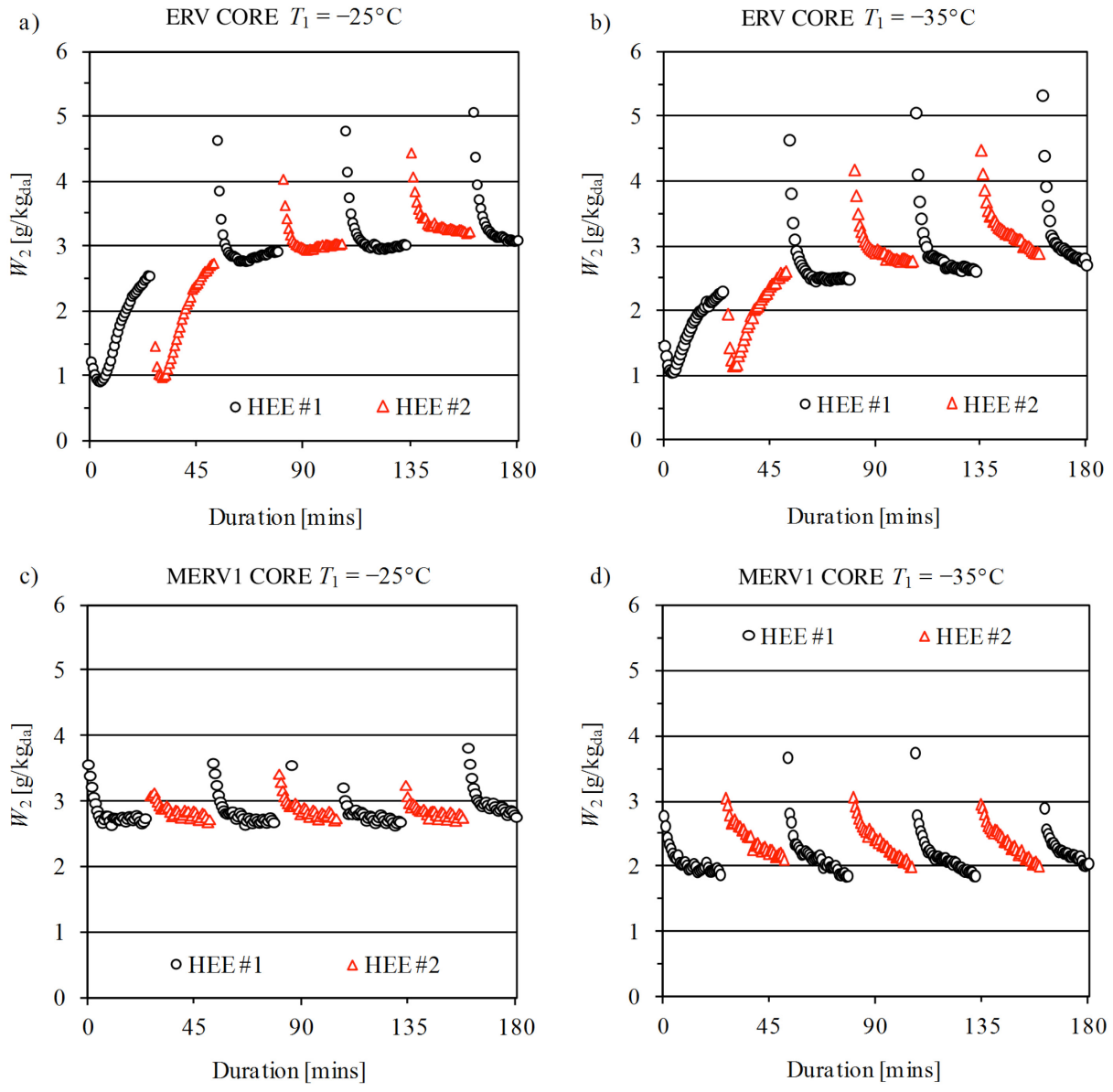

Figure 7.2: Outlet supply air humidity ratio for two HEE units with alternating defrost for ERV and MERV1 cores at $T_1 = -25°C$ and $T_1 = -35°C$

The results in **Figure 7.2** are only for the exchange cycle; measurements collected during the defrost cycle and standby period were omitted.

The initial conditions had a considerable effect on the outlet supply air humidity ratio for the ERV core at both test inlet supply air temperatures. As previously seen, this is primarily due to the absorption of moisture by the core. Cores MERV1 and HRV did not experience the same ramp-up in outlet supply air humidity ratio mostly due to the non-absorbent core materials.

Once the measurements reached a repeatable pattern (and the effects of the initial conditions were not longer a factor) the outlet supply air humidity ratio measurements for the ERV core were the highest compared to both the HRV and MERV1 cores at both tested inlet supply air temperatures. The outlet supply air humidity ratio for the HRV tests were very low due to the impermeability of the core to water vapour.

At the inlet supply air temperature of −25°C, the outlet supply air humidity ratio measurement for all cores reached a repeatable plateau after the effects of the defrost cycle and stand-by period were no longer a factor. When $T_1 = -35°C$ the measurements for all cores do not reach a plateau and instead are found to be constantly decreasing until the initiation of the next defrost cycle.

7.1.3. Air mass flow rates

Figure 7.3 shows the inlet supply and inlet exhaust air mass flow rates for two HEE units with HRV cores operating with alternating defrost. The results for the ERV and MERV1 cores can be found in APPENDIX C (**Figure C.6** and **Figure C.7**). The first number following the mass flow rate symbol, $\dot{m}$, indicates the HEE while the second number indicates the airflow.

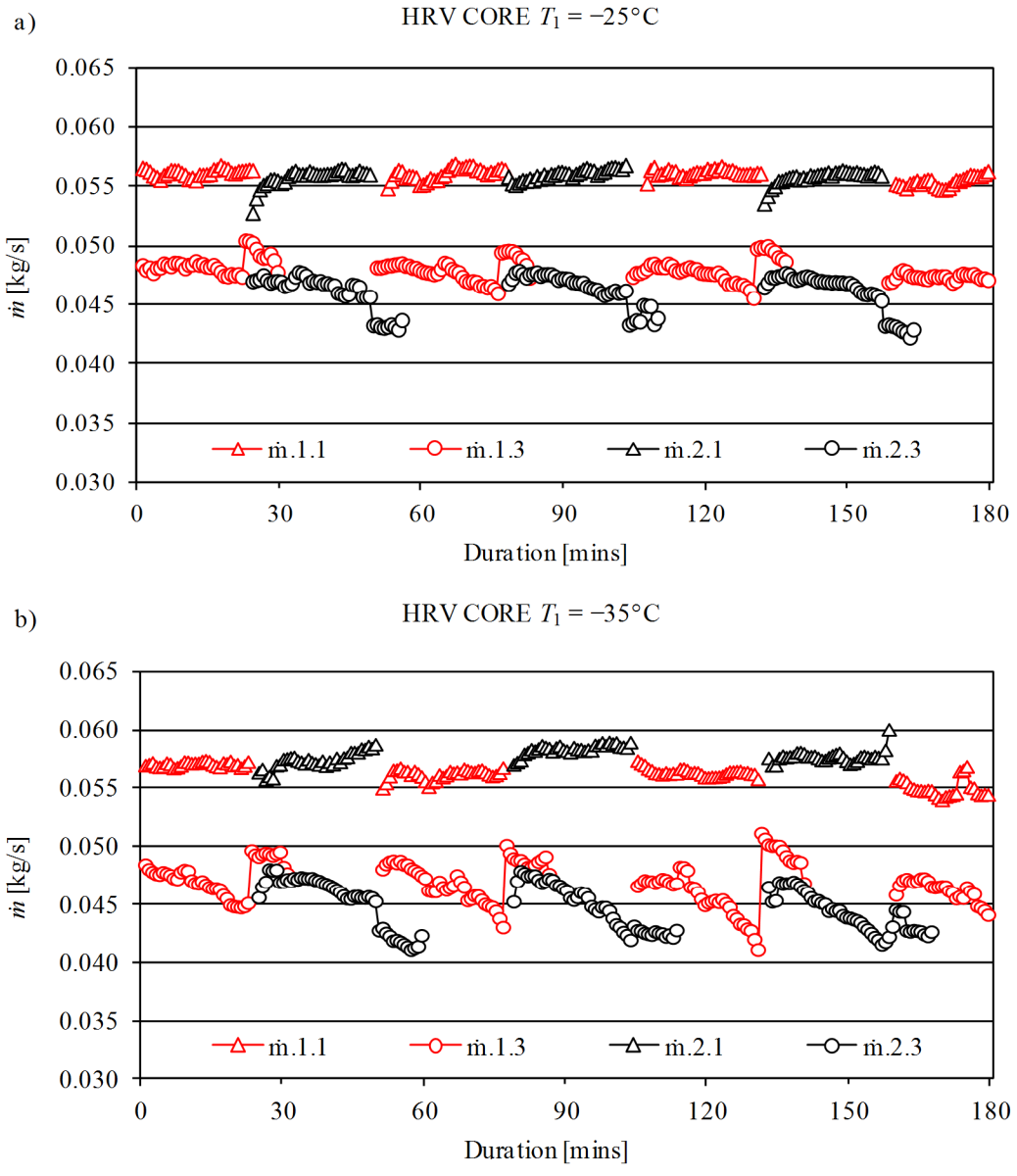

Figure 7.3: Inlet supply and exhaust air mass flow rates for two HEE units with alternating defrost for a HRV core at a) T_1 = −25°C and b) T_1 = −35°C

The mass flow rate of the exhaust air increased for HEE#1 when the exchanger was in the defrost cycle. However, the opposite was true for HEE#2. The mass flow rate of the exhaust air decreased for HEE#2 when the exchanger was in the defrost cycle. The difference might be due to the configuration of the air ducts leading to and from each HEE unit. When the air is redirected for the defrost cycle the mass flow rate of air could have been effected by the new path. Since the experimental setup, more specifically the ducting, to and from the two HEE was not identical it could explain the difference in the behaviour of the mass flow rate of the exhaust air.

There was little change is the exhaust air mass flow rate during the operating cycle for core ERV at both tested inlet supply air temperatures. This was observed for MERV1 and HRV cores, however only when $T_1 = -25°C$. There was a decrease in the exhaust air mass flow rate for both the HRV and MERV1 cores during the operating cycle at $T_1 = -35°C$.

For greater clarity, **Figure 7.4** shows a close-up of the inlet supply and inlet exhaust air mass flow rate results for ERV core at $T_1 = -25°C$. The graph shows the inlet supply and inlet exhaust air mass flow rates during one exchange mode (EX), defrost mode (DF), and standby mode (SB) for each HEE unit.

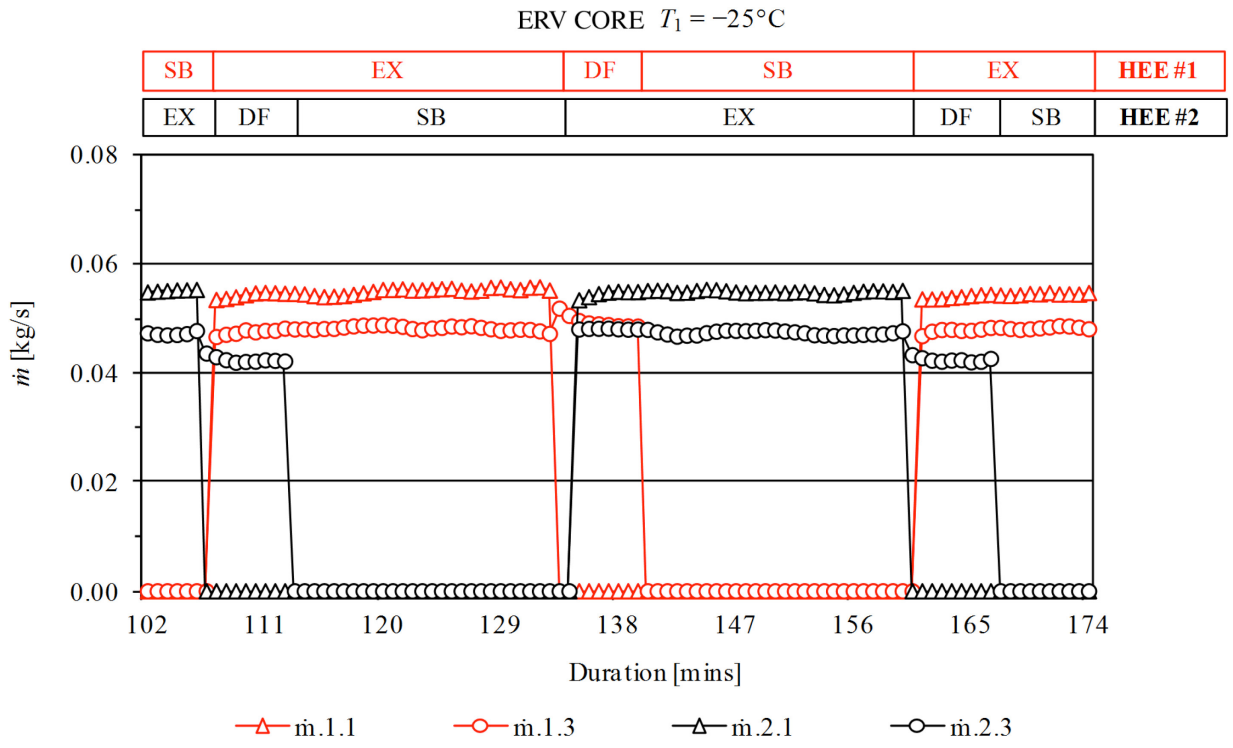

Figure 7.4: Inlet supply and exhaust air mass flow rates for two HEE with alternating defrost: ERV core at $T_1 = -25°C$

7.2. Analysis – Two HEE units with alternating defrost

7.2.1. Frost management and ventilation

The combination of the defrost cycle and stand-by period adequately managed the removal of frost in all cores while keeping the ventilation system in operation. The system provided a continuous supply of supply air as a result of the alternating between HEE units. As a result there was no reduction in the time-average supply air volumetric flow rates, as witnessed for the one HEE tests with defrost. This may prove to be useful when sizing HEE units for residential applications because the amount of air supplied to the home (time average volumetric flow rate) does not change when there is a defrost-cycle.

7.2.2. Sensible and latent heat transfer effectiveness

Table 7.1 and **Table 7.2** show the average adjusted sensible and latent heat transfer effectiveness, respectively, for both HEE units with alternating defrost. The adjusted effectiveness of the cores were evaluated during the last 6 minutes of the third exchange cycle at each tested inlet supply air temperature. The end of the third exchange cycle was selected to minimize the effects of the initial test conditions, caused by the thermal mass and moisture absorption of the cores, on the adjusted effectiveness values.

Table 7.1: Adjusted sensible heat transfer effectiveness with alternating defrost

Core	Adjusted Sensible Effectiveness, ε'_s [-] *			
	$T_1 = -25°C$		$T_1 = -35°C$	
	HEE #1	HEE #2	HEE #1	HEE #2
ERV	0.82 ± 0.1	0.74 ± 0.1	0.82 ± 0.1	0.74 ± 0.1
MERV1	0.82 ± 0.1	0.72 ± 0.0	0.75 ± 0.1	0.69 ± 0.1
HRV	0.83 ± 0.1	0.78 ± 0.1	0.86 ± 0.0	0.78 ± 0.1

* Average values plus-minus standard deviation for the evaluation period

Table 7.2: Adjusted latent heat transfer effectiveness with alternating defrost

Core	Adjusted Latent Effectiveness, ε'_1 [-] *			
	$T_1 = -25°C$		$T_1 = -35°C$	
	HEE #1	HEE #2	HEE #1	HEE #2
ERV	0.60 ± 0.1	0.57 ± 0.1	0.56 ± 0.1	0.53 ± 0.2
MERV1	0.56 ± 0.1	0.49± 0.1	0.41 ± 0.1	0.40 ± 0.1
HRV	0.04 ± 0.0	0.02 ± 0.0	0.05± 0.0	0.01 ± 0.0

* Average values plus-minus standard deviation for the evaluation period

The inlet supply air temperature did not influence the adjusted sensible heat transfer effectiveness for both HEE units for the ERV and HRV cores. There was a decrease in ε'_s for the

MERV1 core at $T_1 = -35°C$ when compared to $T_1 = -25°C$. The HRV core had the highest ε'_s values for the corresponding HEE unit. The ERV core was the middle-performing core, while the MERV1 core had the lowest ε'_s.

The inlet supply air temperature influenced the adjusted latent heat transfer effectiveness for both HEE units with ERV and MERV1 cores. The ε'_l for the ERV and MERV1 cores were lower at colder inlet supply air temperatures. The ε'_l for the HRV core remained very low for both HEE units and inlet supply air temperatures due to the vapour impermeability of the core material.

There was a significant discrepancy in the effectiveness (sensible and latent) values for the two HEE units with the same cores. The sensible and latent heat transfer effectiveness values calculated for HEE #1 where higher than the values for HEE #2. For comparison, the average inlet supply and exhaust air conditions along with the resulting average outlet supply air conditions during the evaluation periods for core ERV at $T_1 = -35°C$ are shown in **Table 7.3**.

Table 7.3: Average measurements during effectiveness evaluation periods for two HEE units with alternating defrost with core ERV at $T_1 = -35°C$

	Measurement*		HEE #1	HEE #2
Inlet supply air conditions	T_1	[°C]	−37.2 ± 0.1	−37.3 ± 0.1
	W_1	[g/kg$_{da}$]	0.06 ± 0.00	0.06 ± 0.00
	$\dot{V}_1$	[L/s]	39.9 ± 0.3	38.4 ± 0.4
Inlet exhaust air conditions	T_3	[°C]	22.5 ± 0.1	22.4 ± 0.1
	W_3	[g/kg$_{da}$]	5.41 ± 0.11	5.56 ± 0.11
	$\dot{V}_3$	[L/s]	39.1 ± 0.2	38.1 ± 0.4
Outlet supply air conditions	T_2	[°C]	4.7 ± 0.1	6.5 ± 0.2
	W_2	[g/kg$_{da}$]	2.64 ± 0.02	2.95 ± 0.05
	$\dot{V}_2$	[L/s]	43.8 ± 0.3	37.1 ± 0.4

* The values are the average of the measurements collected during the evaluation period

The average measurements during the effectiveness evaluation period show that both HEE units had very similar inlet supply and inlet exhaust air conditions. The resulting outlet supply air temperature and humidity ratio were only slightly higher for HEE #2. The largest discrepancy between the two HEE units was the outlet supply air volumetric flow rate. **Figure 7.5** shows the volumetric flow rates during the evaluation period for the two HEE units with core ERV at $T_1 = -35$C.

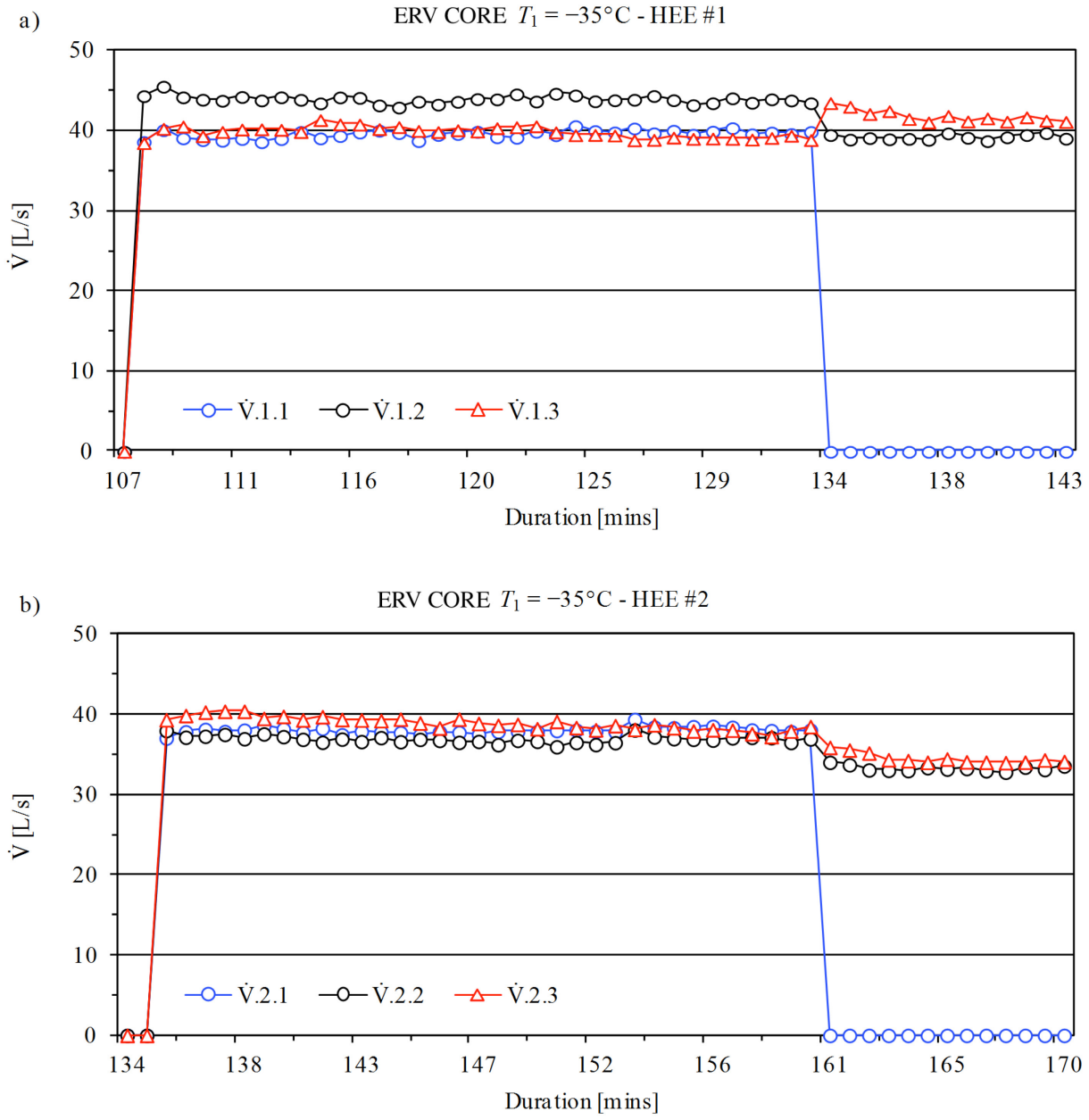

Figure 7.5: Volumetric flow rate measurements for two HEE units with alternating defrost for ERV core at $T_1 = -35°C$

Figure 7.5a shows that there was a nearly 10% increase in the supply airstream volumetric flow rate before and after HEE#1. **Figure 7.5**b shows that there was little change in the supply air-stream volumetric flow rate for HEE#2. The average change in volumetric flow rates for both

airstreams for both HEE units at the tested inlet supply air temperatures during the evaluation period are tabulated in **Table 7.4**.

Table 7.4: Change in volumetric air flow rate of supply and exhaust airstreams

Core	$\Delta\dot{V}$ of supply/exhaust airstreams [L/s] *			
	$T_1 = -25°C$		$T_1 = -35°C$	
	HEE #1	HEE #2	HEE #1	HEE #2
ERV	+4.7 / −3.0	−0.8 / +2.0	+3.9 / −2.0	−1.3 / +2.4
MERV1	+4.4 / −1.9	+1.0 / +0.4	+4.6 / −1.7	−1.6 / +2.6
HRV	+3.3 / −0.8	−2.0 / +3.3	+4.5 / −1.1	−1.5 / +3.1

* Average values for the evaluation period

The supply airstream volumetric air flow rates increased for all tests for HEE #1, while the exhaust airstream volumetric air flow rates increased for all tests for HEE #2. This increase in air flow rate could be attributed to leakage between airstreams across the exchanger core or between test surroundings and ducts. The relatively higher increase in the supply airstream volumetric air flow rate for HEE#1 is the primary reason behind the larger values for both the sensible and latent heat transfer effectiveness when compared to HEE #2.

7.2.3. Simultaneous Air Supply

There will be an increase in the amount of air supplied to a house when, at the same time one HEE is in exchange mode and the other HEE is in defrost mode (refer to **Figure 7.4**). During these periods, the outside air supplied by one HEE is combined with the air that is being used during the recirculation defrost of the second HEE. Consequently, it is necessary to consider this increase in airflow when designing the HVAC system, this is especially true for duct sizing. Duct size should ensure that the airflow rates are below the threshold at which drafts are noticeable in order to maintain thermal comfort.

8. CONCLUSIONS AND RECOMMENDATIONS

8.1. Conclusions

This thesis investigated the performance of air-to-air heat/energy exchangers in very cold climates. More specifically, it investigated the use of vapour-permeable cores and alternating recirculation defrost cycles to proactively and retroactively manage core frosting, respectively.

Measuring the reduction in the mass flow rate of the exhaust airstream was effective for evaluating the core frosting at all test conditions. As frost formed in the exchanger cores there was a corresponding decrease in the measured exhaust air mass flow rates. By comparing the reduction in the exhaust air mass flow rate between cores it was found that the use of vapour-permeable cores delayed the onset of core frosting

The rate of core frosting was dependant on the inlet supply air temperature. The rate of decrease in the mass flow rate of the exhaust air was higher at lower inlet supply air temperatures. However, It was found that the higher the adj. latent heat transfer effectiveness of the core the lower the rate of decrease in the exhaust air mass flow rate.

The adjusted sensible and latent heat transfer effectiveness for all cores decreased as core frosting was allowed to continue. The rate of decrease in the adjusted sensible and latent heat transfer effectiveness as a function of the exhaust air mass flow rates were not dependent on the inlet supply air temperature. Rather the inlet supply air temperature played more of a role in the total decrease in the exhaust air mass flow rate and ultimately the total decrease in the adj. effectiveness.

Frost formation impeded the transfer of heat between the two airstreams. The UA values for all cores except for ERV decrease over the duration of the tests where core frosting was allowed to continue uncontrolled. The rates of decrease in the UA values for the cores were higher at lower

inlet supply air temperatures, indicating that more frost results in a larger decrease the heat transfer between cores.

Recirculation defrost effectively managed the formation of frost in all tested exchanger cores for the duration of the tests at inlet supply air temperature down to −35°C. However, the use of recirculation defrost intermittently interrupts the supply of outdoor air resulting in reduced ventilation rates. The use of two heat/energy exchangers with alternating recirculation defrost adequately managed core frosting while providing a continuous supply of outdoor air.

8.2. Design and Operation Recommendations

The results and conclusions of this thesis can be used to optimize the design and operation of air-to-air heat/energy exchangers in northern climates. Recommendations have been summarized below:

- Vapour-permeable cores should be utilized in northern Canada and for regions where core frosting is a concern. The use of vapour-permeable cores will not only recover moisture for humidification but also reduce the need for frost management.
- Recirculation defrost schedules should better reflect the operational requirements. Heat/energy exchanger currently available come with factory-set defrost schedules which are enacted based on the inlet supply air temperatures. Meaning, the initiation of a defrost cycle is not based on whether there is actually frost present in the core. It is recommended the use of a measured variable directly associated with core frosting, i.e. pressure drop across the core or drop in exhaust air flow rate, be used instead to determine if a defrost cycle is required.
- Air-to-air heat/energy exchangers should be installed and operate in a conditioned space in order to reduce the amount of heat loss from the unit and ducts to the surrounding air.

This is a particularly difficult task in northern Canada where basement space is not available. Greater consideration during the design stage should be given to accommodating the unit and required ducting in a conditioned space.

- In agreement with the findings in [59], air leakage between the supply and exhaust airstreams as well as the surrounding ambient air can significantly affect the performance of a heat/energy exchanger. Significant attention should be made to ensuring that ducting is sealed and thermally insulated. Unintentional air leakage and heat transfer within the heat/energy exchanger can significantly reduce the efficiency and in turn reduce the amount of energy recovered.
- Current product rating procedures for residential air-to-air heat/energy exchangers are not sufficient for applications in northern Canada. The required testing conditions do not match the conditions that are experienced in these regions. Typically, residential air-to-air heat/energy heat exchangers are rated at inlet supply air temperatures of −25°C and above. However, considering that the outdoor air temperature in Iqaluit, Nunavut is below −25°C for nearly a quarter of the year, it is easy to see that testing at lower inlet supply air temperatures is required.
- The use of two exchangers with alternating recirculation defrost not only was able to mitigate the frost formation but was also able to supply continuous outside air. This operation mode reduces the need to oversize the exchangers to compensate for the drop ventilation cause by recirculation defrost in conventional systems. Continuous outdoor air supply is also beneficial when the system works in tandem with other HVAC equipment. Allowing for more predicable control and operation.

- One potential benefit of a heat/energy exchanger system that provides continuous outdoor air supply is that the system could be used in tandem with a solar thermal system. The proposed system is able to use 100% of the solar pre-heated air for the duration it is available. However, for conventional systems the solar pre-heated air would have to by-pass the exchanger system during the periods of recirculation defrost.

8.3. Future Work

The results and conclusions of this thesis have answered multiple questions regarding the use of heat/energy exchangers in Northern Canada. It hopefully will also serve as for further research in the field:

- While a laboratory setting allows for greater control of testing conditions it is not sufficient or realistic for real-world applications. In order to gain a better understand of the performance of vapour-permeable cores and alternating defrost in northern Canada, both methods of frost management should be field tested.
- One limitation of the experiments conducted for this thesis was that the relative humidity of the inlet exhaust air remained constant. The inlet exhaust air relative humidity was selected because it represented what would be typically found in residential buildings, however fluctuations do occur when people are cooking or taking a shower. Therefore, further testing should be conducted with higher relatively humidity levels to see how vapour-permeable cores and alternating defrost perform under these conditions.
- There is a variety of residential heating and ventilation equipment used in northern Canada. How these pieces of equipment work together to form a system is key when designing residential homes. Therefore further work is required in the integration of alternating

defrost and vapour-permeable cores with existing or new heating and cooling systems. System integration also need to be considered for solar thermal applications. More specifically how the overall system, inclusive of the proposed heat/energy exchanger system, responds to different outlet supply air temperatures from a solar thermal collector.

- Long term testing of vapour-permeable cores is required to test the durability and structural integrity of cores over time. This is very important considering that the cores are exposed to cyclical freeze thaw conditions.

REFERENCES

[1] Inuit Tapiriit Kanatami, "Maps of Inuit Nunangat." [Online]. Available: https://www.itk.ca/publication/maps-inuit-nunangat-inuit-regions-canada. [Accessed: 27-Nov-2015].

[2] Statistics Canada, "Census of Population Program Datasets - 2011 National Household Survey," *no. 99-011-X2011027*, 2011. .

[3] National Energy Board, "Energy Facts - Energy Use in Canada's North," 2011.

[4] J. Kruse, B. Poppel, L. Abryutina, G. Duhaime, S. Martin, M. Poppel, M. Kruse, E. Ward, P. Cochran, and V. Hanna, "Survey of Living Conditions in the Arctic (SLiCa)," in *Barometers of Quality of Life Around the Globe*, 2008, pp. 107–134.

[5] Statistics Canada, "Focus on Geography Series, 2011 Census - Census subdivision of Iqaluit," *no. 98-310-XWE2011004*, 2012. [Online]. Available: https://www12.statcan.gc.ca/census-recensement/2011/as-sa/fogs-spg/Facts-csd-eng.cfm?Lang=eng&GK=CSD&GC=6204003. [Accessed: 27-Nov-2015].

[6] Nunavut Housing Corporation, "The GN Long-Term Comprehensive Housing and Homelessness Strategy Tamapta."

[7] Statistics Canada, "An analysis of the housing needs in Nunavut : Nunavut Housing Needs Survey," 2010.

[8] M. Rousseau, M. Manning, M. N. Said, S. M. Cornick, and M. C. Swinton, "Characterization of Indoor Hygrothermal Conditions in Houses in Different Northern Climates," in *Thermal Performance of Exterior Envelopes of Whole Buildings X*, 2007.

[9] P. C. Dawson, "Examining the impact of Euro-Canadian architecture on Inuit families living in Arctic Canada," in *4th International Space Syntax Symposium*, 2003.

[10] Nunavut Housing Corporation, "Nunavut Housing Needs Survey Backgrounder Nunavut Housing Needs Survey Backgrounder," 2010.

[11] CMHC, "Canadian Housing Observer 2008," 2008.

[12] S. G. Donaldson, J. Van Oostdam, C. Tikhonov, M. Feeley, B. Armstrong, P. Ayotte, O. Boucher, W. Bowers, L. Chan, F. Dallaire, R. Dallaire, E. Dewailly, J. Edwards, G. M. Egeland, J. Fontaine, C. Furgal, T. Leech, E. Loring, G. Muckle, T. Nancarrow, D. Pereg, P. Plusquellec, M. Potyrala, O. Receveur, and R. G. Shearer, "Environmental contaminants and human health in the Canadian Arctic," *Sci. Total Environ.*, vol. 408, no. 22, pp. 5165–234, Oct. 2010.

[13] T. Kovesi, N. L. Gilbert, C. Stocco, D. F. Peng, R. E. Dales, M. Guay, and J. D. Miller, "Indoor air quality and the risk of lower respiratory tract infections in young Canadian Inuit children," *Can. Med. Assoc. J.*, vol. 177, no. 2, pp. 155–160, 2007.

[14] T. Kovesi, C. Zaloum, C. Stocco, D. Fugler, R. E. Dales, A. Ni, N. Barrowman, N. L. Gilbert, and J. D. Miller, "Heat recovery ventilators prevent respiratory disorders in Inuit children," *Indoor Air*, vol. 19, no. 6, pp. 489–499, Dec. 2009.

[15] T. Marsik and R. Johnson, “Use of Simulink to evaluate the air-quality and energy performance of HRV-equipped residences in Fairbanks, Alaska,” *Energy Build.*, vol. 40, pp. 1605–1613, Jan. 2008.

[16] J. Rose, T. R. Nielsen, J. Kragh, and S. Svendsen, “Quasi-steady-state model of a counter-flow air-to-air heat-exchanger with phase change,” *Appl. Energy*, vol. 85, no. 5, pp. 312–325, May 2008.

[17] a. Mardiana-Idayu and S. B. Riffat, “Review on heat recovery technologies for building applications,” *Renew. Sustain. Energy Rev.*, vol. 16, no. 2, pp. 1241–1255, Feb. 2012.

[18] A. Mardiana and S. B. Riffat, “Review on physical and performance parameters of heat recovery systems for building applications,” *Renew. Sustain. Energy Rev.*, vol. 28, pp. 174–190, 2013.

[19] L. Z. Zhang and J. L. Niu, “Energy requirements for conditioning fresh air and the long-term savings with a membrane-based energy recovery ventilator in Hong Kong,” *Energy*, vol. 26, pp. 119–135, 2001.

[20] M. Nasif, R. AL-Waked, G. Morrison, and M. Behnia, “Membrane heat exchanger in HVAC energy recovery systems, systems energy analysis,” *Energy Build.*, vol. 42, pp. 1833–1840, Oct. 2010.

[21] B. K. Ouazia, M. Julien, M. C. Swinton, and M. Manning, “Assessment of the Enthalpy Performance of Houses Using Energy Recovery Technology,” *ASHRAE Trans.*, vol. 112, no. 1, pp. 26–34, 2006.

[22] C. G. Barringer and C. A. McGugan, “Effects of Residential air-to-air Heat and Moisture Exchangers on indoor humidity.pdf,” *ASHRAE Trans.*, vol. 95, no. Part 2, pp. 461–474, 1989.

[23] R. N. Huizing, “Coated Membranes for Enthalpy Exchange and Other Applications,” US 2012/0061045 A1, 2012.

[24] J. L. Niu and L. Z. Zhang, “Membrane-based Enthalpy Exchanger : material considerations and clarification of moisture resistance,” *J. Memb. Sci.*, vol. 189, pp. 179–191, 2001.

[25] Y. Zhang, Y. Jiang, L. Z. Zhang, Y. Deng, and Z. Jin, “Analysis of thermal performance and energy savings of membrane based heat recovery ventilator,” *Energy*, vol. 25, no. 6, pp. 515–527, Jun. 2000.

[26] J. Min and M. Su, “Performance analysis of a membrane-based energy recovery ventilator: Effects of outdoor air state,” *Appl. Therm. Eng.*, vol. 31, pp. 4036–4043, Dec. 2011.

[27] P. Taylor, J. Nie, J. Yang, L. Fang, and X. Kong, “Experimental evaluation of enthalpy efficiency and gas-phase contaminant transfer in an enthalpy recovery unit with polymer membrane foils Experimental evaluation of enthalpy efficiency and gas-phase contaminant transfer in an enthalpy recovery unit with,” *Sci. Technol. Built Environ.*, vol. 21, pp. 150–159, 2015.

[28] L.-Z. Zhang, “Progress on heat and moisture recovery with membranes: From

fundamentals to engineering applications," *Energy Convers. Manag.*, vol. 63, pp. 173–195, Nov. 2012.

[29] W. J. Fisk, R. E. Chant, K. M. Archer, D. Hekmet, F. J. Offerman III, and B. S. Pederson, "Onset of freezing in residential air-to-air heat exchangers," *ASHRAE Trans.*, vol. 91, no. Part 1B, pp. 145–158, 1985.

[30] R. Ostin, "A Study of Heat Exchange under Frosting conditions," *Heat Recover. Syst. CHP*, vol. 12, no. 2, pp. 89–103, 1992.

[31] D. W. Schulte and R. H. Howell, "The Effects of Air Turbulence on the rate of Frost Growth on a Horizontal Plate," *ASHRAE Trans.*, vol. 88, no. pt. 2, pp. 201–217, 1982.

[32] M. Rafati Nasr, M. Fauchoux, R. W. Besant, and C. J. Simonson, "A review of frosting in air-to-air energy exchangers," *Renew. Sustain. Energy Rev.*, vol. 30, pp. 538–554, 2014.

[33] Y. Hayashi, A. Aoki, S. Adachi, and K. Hori, "Study of Frost Properties Correlating with Forst Formation Types," *J. Heat Transfer*, vol. 99, pp. 239–345, 1977.

[34] D. L. O'Neal and D. R. Tree, "A Review of Frost Formation in Simple Geometries," *ASHRAE Trans.*, vol. 90, pp. 267–281, 1985.

[35] B. W. Jones and Parker J. D., "Frost Formation with Varying Environmental Parameters," *J. Heat Transfer*, vol. 97, pp. 255–259, 1975.

[36] A. Lüer and H. Beer, "Frost deposition in a parallel plate channel under laminar flow conditions," *Int. J. Therm. Sci.*, vol. 39, no. 1, pp. 85–95, Jan. 2000.

[37] R. Ostin and S. Andersson, "Frost growth parameters in a forced air stream," *Int. J. Heat Mass Transf.*, vol. 34, no. No. 4/5, pp. 1009–1017, 1991.

[38] L. Z. Zhang and Y. Jiang, "Heat and mass transfer in a membrane-based energy recovery ventilator," *J. Memb. Sci.*, vol. 163, no. 1, pp. 29–38, Oct. 1999.

[39] E. G. Phillips, R. E. Chant, D. R. Fisher, and B. C. Bradley, "Comparison of Freezing Control Strategies for Residential Air-to-Air Heat Recovery Ventilators," *ASHRAE Trans.*, pp. 484–490, 1989.

[40] E. G. Phillips, D. R. Fisher, R. E. Chant, and B. C. Bradley, "Freeze-control strategy and air-to-air energy recovery performance," *ASHRAE Journal*, pp. 44–49, Dec-1992.

[41] Venmar AVS, "Product Sheet: Venmar AVS HRV EKO 1.5," no. 91414. 2012.

[42] J. Kragh, J. Rose, and S. Svendsen, "Mechanical ventilation with heat recovery in cold climates," in *Proceeding of the seventh Nordic symposium on building physics in nordic countries*, 2005, pp. 1–8.

[43] M. Kotol, "A low-energy Building under Arctic Conditions," *9th Nord. Symp. Build. Phys.*, 2011.

[44] P. Vladykova, C. Rode, J. Kragh, and M. Kotol, "Low-Energy House in Arctic Climate : Five Years of Experience," *J. Cold Reg. Eng.*, vol. 26, pp. 79–100, 2012.

[45] J. Kragh, J. Rose, T. R. Nielsen, and S. Svendsen, "New counter flow heat exchanger designed for ventilation systems in cold climates," *Energy Build.*, vol. 39, pp. 1151–1158,

Nov. 2007.

[46] Y. I. Aristov, I. V. Mezentsev, and V. A. Mukhin, “A new approach to regenerating heat and moisture in ventilation systems,” *Energy Build.*, vol. 40, pp. 204–208, Jan. 2008.

[47] ASHRAE, “Method of Testing Air-to-Air Heat/Energy Exchangers,” *ANSI/ASHRAE Standard 84*, 2013.

[48] T. J. Sokira and W. Jaffe, *Brushless DC Motors - Electronics Commutation and Controls*. Blue Ridge Summit: TAB Books Inc., 1990.

[49] Venmar AVS, “Product Sheet: Venmar AVS ERV EKO 1.5,” no. 120309. 2012.

[50] Canadian Standards Association, “Standard laboratory methods of test for rating the performance of heat/energy-recovery ventilators,” 2009.

[51] American Society of Heating Refrigerating and Air-Conditioning Engineers, “Standard Method for Temperature Measurement,” *ANSI/ASHRAE Stand. 41.1*, 2013.

[52] American Society of Heating Refrigerating and Air-Conditioning Engineers, “Standard Method for Measurement of Moist Air Properties,” *ANSI/ASHRAE Stand. 41.6*, 1994.

[53] American Society of Heating Refrigerating and Air-Conditioning Engineers, “Standard Methods for Laboratory Air-flow Measurement,” *ANSI/ASHRAE Stand. 41.2*, 1987.

[54] ASHRAE, “Standard Method for Pressure Measurement,” *ANSI/ASHRAE Stand. 41.3*, 1989.

[55] American Society of Heating Refrigerating and Air-Conditioning Engineers, “Engineering Analysis of Experimental Data,” *ASHRAE Guidel. 2*, 2010.

[56] Natural Resources Canada, “Canada - Permafrost,” *The National Atlas of Canada 5th Edition*, 1995. [Online]. Available: http://ftp2.cits.rncan.gc.ca/pub/geott/atlas/archives/english/5thedition/environment/land/mcr4177.pdf. [Accessed: 28-Nov-2015].

[57] U.S. Department of Energy, “EnergyPlus Weather Data.” [Online]. Available: http://apps1.eere.energy.gov/buildings/energyplus/cfm/weather_data3.cfm/region=4_north_and_central_america_wmo_region_4/country=3_canada/cname=CANADA.

[58] ASHRAE, “Ventilation and Acceptable Indoor Air Quality in Low-Rise Residential Buildings,” *ANSI/ASHRAE Standard 62-2*, 2013.

[59] H. Manz, H. Huber, and D. Helfenfinger, “Impact of air leakages and short circuits in ventilation units with heat recovery on ventilation efficiency and energy requirements for heating,” *Energy Build.*, vol. 33, pp. 133–139, 2001.

APPENDIX A. SENSOR CALIBRATION

A.1. Thermocouple Calibration

In order to calibrate the temperature measurement systems, all thermocouples were placed in an environmental chamber set at a constant temperature. The reference temperature was measured using a Vaisala HMT333 hygrometer. The calibration offset was determined by comparing the average temperature measurements for each thermocouple to the reference temperature measurement. The calculated calibration offsets for each thermocouple are listed in **Table A.1**.

Table A.1: Thermocouple calibration offsets

Thermocouple	Offset [°C]	Thermocouple	Offset [°C]	Thermocouple	Offset [°C]
T.1.1.1	-0.1	T.1.4.1	+0.1	T.2.3.1	+0.1
T.1.1.2	+0.1	T.1.4.2	-0.6	T.2.3.2	+0.2
T.1.1.3	+0.0	T.1.4.3	-0.2	T.2.3.3	+0.0
T.1.1.4	+0.2	T.1.4.4	-0.9	T.2.3.4	-0.2
T.1.1.5	+0.1	T.1.4.5	-0.3	T.2.3.5	+0.1
T.1.1.6	-0.3	T.1.4.6	-0.7	T.2.3.6	+0.0
T.1.1.7	-0.2	T.1.4.7	-0.2	T.2.3.7	+0.1
T.1.1.8	+0.0	T.1.4.8	-0.2	T.2.3.8	-0.1
T.1.2.1	+0.1	T.2.1.1	+0.9	T.2.4.1	+0.7
T.1.2.2	-0.1	T.2.1.2	+0.8	T.2.4.2	+0.8
T.1.2.3	-0.1	T.2.1.3	+0.9	T.2.4.3	+0.5
T.1.2.4	-0.2	T.2.1.4	+0.8	T.2.4.4	+0.8
T.1.2.5	+0.1	T.2.1.5	+1.1	T.2.4.5	+0.6
T.1.2.6	-0.1	T.2.1.6	+0.7	T.2.4.6	+0.6
T.1.2.7	-0.1	T.2.1.7	+1.4	T.2.4.7	+0.9
T.1.2.8	-0.1	T.2.1.8	+1.0	T.2.4.8	+0.7
T.1.3.1	-0.1	T.2.2.1	+0.0		
T.1.3.2	-0.1	T.2.2.2	+0.3		
T.1.3.3	-0.2	T.2.2.3	+0.1		
T.1.3.4	+0.1	T.2.2.4	+0.0		
T.1.3.5	-0.6	T.2.2.5	+0.1		
T.1.3.6	-0.2	T.2.2.6	+0.7		
T.1.3.7	-0.5	T.2.2.7	+0.4		
T.1.3.8	-0.1	T.2.2.8	+0.3		

A.2. Airflow Measurement Station Calibration

The airflow measurement stations were calibrated in the Solar Simulator and Environmental Chamber facility at Concordia University. The measurement stations were tested at different airflow rates. At each tested airflow rate the calculated airflow rate was determined using the manufacturer's flow equation and the corresponding average measured differential pressures.

Manufacturer's flow equation: $Q\left[{m^3}/{_S}\right] = 0.204\sqrt{\frac{\Delta p[Pa]}{249.09}}$

The calculated airflow rates were then compared to the airflow measurements of orifice flow meter (PSE) at the facility (**Figure A.1** and **Figure A.2**). A correction factor for the manufacturer's flow equation was developed for each measurement station by comparing these results. The correction factors are summarised in **Table A.2** and were applied to the manufacturer's flow equation.

Table A.2: Correction Factors for airflow measurement stations

Measurement Station	Correction Factor
P.1.1	1.0134
P.1.2	1.0401
P.1.3	1.0961
P.1.4	1.0303
P.2.1	1.0509
P.2.2	1.0153
P.2.3	1.0219
P.2.4	1.0821

a)

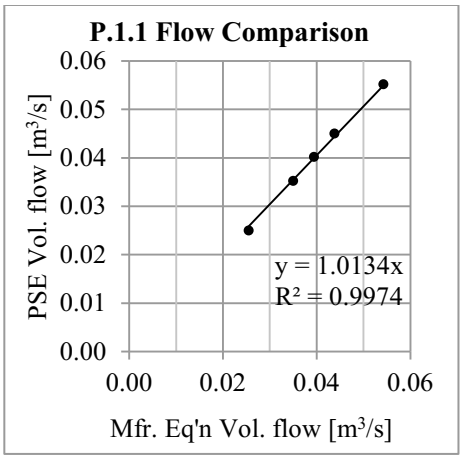

b)

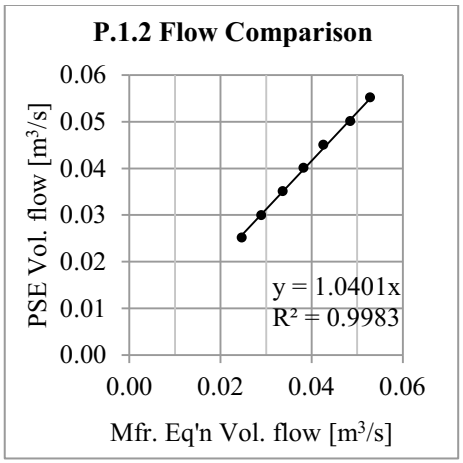

c)

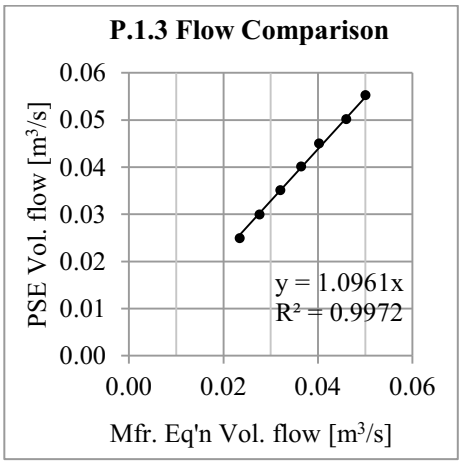

d)

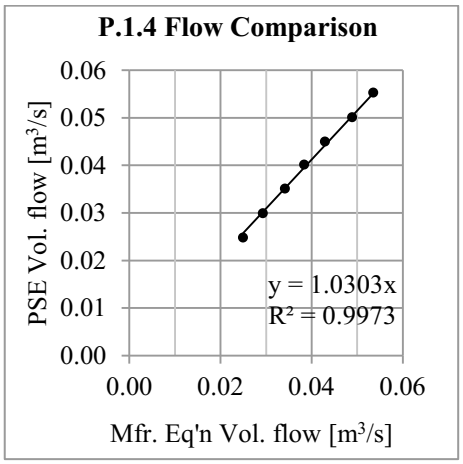

Figure A.1: HEE #1 airflow measurement stations flow comparisons: a) inlet supply, b) outlet exhaust, c) inlet exhaust and d) outlet exhaust airflow measurement stations.

a)

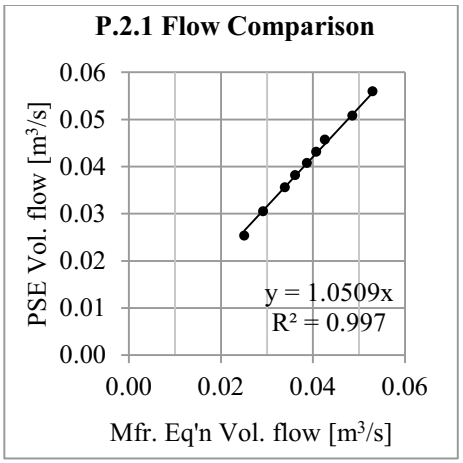

b)

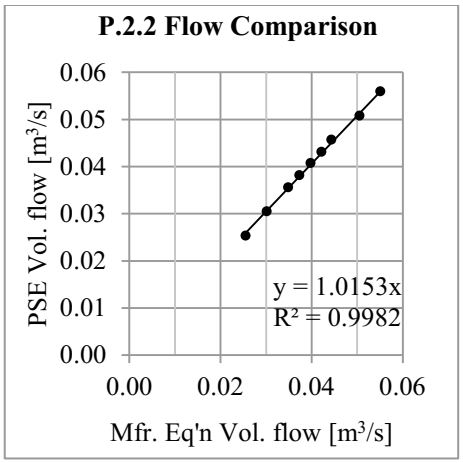

c)

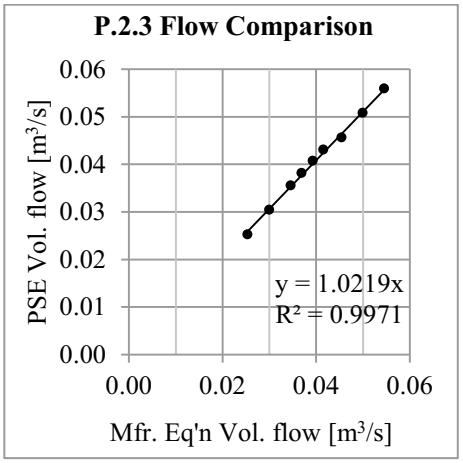

d)

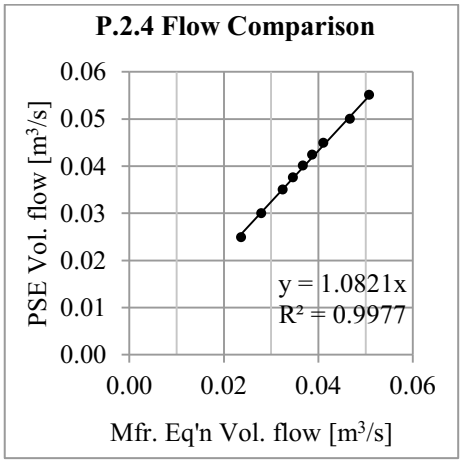

Figure A.2: HEE #2 airflow measurement stations flow comparisons: a) inlet supply, b) outlet exhaust, c) inlet exhaust and d) outlet exhaust airflow measurement stations.

APPENDIX B. MEASUREMENT UNCERTAINTY AND PROPAGATION OF ERROR

The overall uncertainty of all measured and calculated variables are summarized in **Table 4.4** and the calculations are shown in the following sections.

B.1. Average air temperature

The following analysis is based on measurement data collected during the test of core ERV at $T_1 = -10$°C without defrost.

Data reduction equation:

The average air temperature, $\bar{T}$ is calculated using the equation below:

$$\bar{T} = \frac{T_1 + T_2 + T_3 + T_4 + T_5 + T_6 + T_7 + T_8}{8}$$

Partial derivatives:

The partial derivative of the data reduction equation with respect to each air temperature is below:

$$\frac{\partial \bar{T}}{\partial T_1} = \frac{\partial \bar{T}}{\partial T_2} = \frac{\partial \bar{T}}{\partial T_3} \cdots \frac{\partial \bar{T}}{\partial T_8} = \frac{1}{8}$$

Standard Deviation Equations:

The standard deviation of $\bar{T}$ for random and bias errors are calculated separately:

$$S_{\bar{T}_{random}} = \sqrt{\sum_{i=1}^{8} \left(\frac{\partial \bar{T}}{\partial T_i} S_{T_{i,random}} \right)^2}$$

$$S_{\bar{T}_{bias}} = \sqrt{\sum_{i=1}^{8} \left(\frac{\partial \bar{T}}{\partial T_i} S_{T_{i,bias}} \right)^2}$$

Where:

$S_{T_{i,random}} = \pm 0.10$℃ (based on measurement data)

$S_{T_{i,bias}} = \pm 0.50℃$ (based on manufacturer's specifications)

The results of the analysis concluded the following:

$S_{\bar{T}_{random}} = \pm 0.04℃$

$S_{\bar{T}_{bias}} = \pm 0.18℃$

The overall uncertainty of $\bar{T}$is shown below:

$$U_{\bar{T}} = \sqrt{\left(Z \cdot S_{\bar{T}_{random}}\right)^2 + \left(Z \cdot S_{\bar{T}_{bias}}\right)^2} = \pm 0.4℃$$

Where:

Z = 2: 95.5% of the data will be within ±2 $S_{\bar{T}}$of the mean

B.2. Saturation Pressure

The following analysis is based on measurement data collected during the test of core ERV at T1 = −10°C without defrost.

Data reduction equation:

Saturation pressure, Psat, is calculated using the equation below:

$(\bar{T} < 0°C)$ $P_{sat} = e^{\left(\frac{C_1}{T_{RHT}} + C_2 + C_3 T_{RHT} + C_4 {T_{RHT}}^2 + C_5 {T_{RHT}}^3 + C_6 {T_{RHT}}^4 + C_7 \ln T_{RHT}\right)}$

Where:

T_{RHT} – air temperature measured by hygrometer (this is different than average of thermocouple measurements)

C_1 = -5.6745359E+03

C_2 = 6.3925247E+00

C_3 = -9.6778430E-03

C_4 = 6.2215701E-07

C_5 = 2.0747825E-09

C_6 = -9.4840240E-13

C_7 = 4.1635019E+00

Partial derivatives:

The partial derivative of the data reduction equation with respect to air temperature less than 0°C is below:

$$\frac{\partial P_{sat}}{\partial T_{RHT}} = \left(-\frac{C_1}{{T_{RHT}}^2} + C_3 + 2C_4 T_{RHT} + 3C_5 {T_{RHT}}^2 + 4C_6 {T_{RHT}}^3 + \frac{C_7}{T_{RHT}}\right) e^{\left(\frac{C_1}{T_{RHT}} + C_2 + C_3 T_{RHT} + C_4 {T_{RHT}}^2 + C_5 {T_{RHT}}^3 + C_6 {T_{RHT}}^4 + C_7 \ln T_{RHT}\right)}$$

Standard Deviation Equations:

The standard deviation of P_{sat} for random and bias errors are calculated separately:

$$S_{P_{sat,random}} = \sqrt{\left(\frac{\partial P_{\text{sat}}}{\partial T_{RHT}} S_{\text{RHT,random}}\right)^2} \qquad S_{P_{sat,bias}} = \sqrt{\left(\frac{\partial P_{sat}}{\partial T_{RHT}} S_{RHT,bias}\right)^2}$$

Where:

$S_{RHT,random}$ = ±0.14°C (based on measurement data)

$S_{RHT,bias}$ = ±0.2°C (based on manufacturer's specifications)

The results of the analysis concluded the following:

$S_{P_{sat,random}} = \pm 3.1\ Pa$

$S_{P_{sat,bias}} = \pm 4.4\ Pa$

The random and bias standard deviations for saturation pressure are the averages of values calculated for each measurement (n = 360) of the inlet supply air temperature during the testing of core ERV at T_1 = -10C.

The overall uncertainty of Psat is shown below:

$$U_{P_{sat}} = \sqrt{\left(Z \cdot S_{P_{sat,random}}\right)^2 + \left(Z \cdot S_{P_{sat,bias}}\right)^2} = \pm 10.7\ Pa$$

Where:

Z = 2: 95.5% of the data will be within ±2 $S_{P_{sat}}$ of the mean

B.3. Humidity Ratio

The following analysis is based on measurement data collected during the test of core ERV at T1 = −10°C without defrost.

Data reduction equation:

The humidity ratio, *w*, is calculated using the equation below:

$$w = 0.62198 \frac{\varphi * P_{sat}}{100 * P_{atm} - \varphi * P_{sat}}$$

Partial derivatives:

The partial derivatives of the data reduction equation with respect to relative humidity, φ, and saturation pressure, Psat, are below:

$$\frac{\partial w}{\partial \varphi} = 0.62198 \frac{100 P_{sat} P_{atm}}{(100 P_{atm} - \varphi P_{sat})^2}$$

$$\frac{\partial w}{\partial P_{sat}} = 0.62198 \frac{100 \varphi P_{atm}}{(100 P_{atm} - \varphi P_{sat})^2}$$

Standard Deviation Equations:

The standard deviation of *w* for random and bias errors are calculated separately:

$$S_{w_{random}} = \sqrt{\left(\frac{\partial w}{\partial \varphi} S_{\varphi,\text{random}}\right)^2 + \left(\frac{\partial w}{\partial \text{Psat}} S_{\text{Psat,random}}\right)^2}$$

$$S_{w_{bias}} = \sqrt{\left(\frac{\partial w}{\partial \varphi} S_{\varphi,\text{bias}}\right)^2 + \left(\frac{\partial w}{\partial \text{Psat}} S_{\text{Psat,bias}}\right)^2}$$

Where:

$S_{\varphi,random}$ = ±0.60 %RH (based on measurement data)

$S_{\varphi,bias}$ = ±1.25 %RH (based on manufacturer's specifications)

$S_{Psat,random}$ = ±3.1 Pa (calculated in previous section)

$S_{Psat,bias}$ = ±4.4 Pa (calculated in previous section)

The results of the analysis concluded the following:

$S_{w_{random}} = \pm 1.42 \times 10^{-7}\ kg/kg_{da}$

$S_{w_{bias}} = \pm 3.91 \times 10^{-7}\ kg/kg_{da}$

The random and bias standard deviations for humidity ratio are the averages of values calculated for each measurement (n = 360) of the inlet supply air relative humidity during the testing of core ERV at T_1 = -10C.

The overall uncertainty of w is shown below:

$$U_{\mathrm{w}} = \sqrt{\left(Z \cdot S_{w_{random}}\right)^2 + \left(Z \cdot S_{w_{bias}}\right)^2} = \pm 8.33\ \times 10^{-7} \frac{kg}{kg_{da}} or\ \ \pm 0.00083\ \frac{g}{kg_{da}}$$

Where:

Z = 2: 95.5% of the data will be within ±2 S_w of the mean

B.4. Volumetric flow rate

The following analysis is based on measurement data collected during the test of core ERV at T1 = −10°C without defrost.

Data reduction equations:

The volumetric flow rate, Q is calculated using the manufacturer's equation that has been calibrated for each air flow measurement station (Sensor Calibration). For this uncertainty analysis the calibrated equation for air station P.2.1 (inlet supply air) was used:

$$Q = 0.215 \sqrt{\frac{P}{249.09}}$$

Where:

P – Measured pressure, [Pa]

Partial derivatives:

The partial derivative of the data reduction equation with respect to the measured pressure, P is below:

$$\frac{\partial Q}{\partial P} = \frac{0.215}{500\sqrt{\frac{P}{250}}}$$

Standard Deviation Equations:

The standard deviation of Q for random and bias errors are calculated separately:

$$S_{Q_{random}} = \sqrt{\left(\frac{\partial Q}{\partial P} S_{\mathrm{P,random}}\right)^2}$$

$$S_{Q_{bias}} = \sqrt{\left(\frac{\partial Q}{\partial P} S_{\mathrm{P,bias}}\right)^2}$$

Where:

$S_{P,random}$ = ±0.20 Pa (based on measurement data)

$S_{P,bias}$ = ±0.11 Pa (based on manufacturer's specifications and calibration tests)

The results of the analysis using the data collected during the core ERV at $T_1 = -10$°C tests concluded the following:

$S_{Q_{random}} = \pm 0.0003 \ \frac{m^3}{s}$

$S_{Q_{bias}} = \pm 0.0006 \ \frac{m^3}{s}$

The overall uncertainty of Q is shown below:

$$U_{\mathrm{Q}} = \sqrt{\left(Z \cdot S_{Q_{random}}\right)^2 + \left(Z \cdot S_{Q_{bias}}\right)^2} = \pm 0.0013 \frac{m^3}{s}$$

Where:

Z = 2: 95.5% of the data will be within ±2 S_P of the mean

B.5. Mass flow rate

The following analysis is based on measurement data collected during the test of core ERV at T1 = −10°C without defrost.

Data reduction equations:

The air mass flow rate, m-dot is calculated as follows:

$$\dot{m} = Q\left(\frac{P_{atm}}{287 \cdot \bar{T}}\right)$$

Partial derivatives:

The partial derivatives of the data reduction equation with respect to volumetric flow rate, Q and average temperature, $\bar{T}$ are below:

$$\frac{\partial \dot{m}}{\partial Q} = \frac{101300}{287 \cdot \bar{T}}$$

$$\frac{\partial \dot{m}}{\partial \bar{T}} = -\frac{101300 \cdot Q}{287 \cdot \bar{T}^2}$$

Standard Deviation Equations:

The standard deviation of $\dot{m}$ for random and bias errors are calculated separately:

$$S_{\dot{m}_{random}} = \sqrt{\left(\frac{\partial \dot{m}}{\partial Q} S_{\mathrm{Q,random}}\right)^2 + \left(\frac{\partial \dot{m}}{\partial \bar{T}} S_{\bar{T},\mathrm{random}}\right)^2}$$

$$S_{\dot{m}_{bias}} = \sqrt{\left(\frac{\partial \dot{m}}{\partial Q} S_{\mathrm{Q,bias}}\right)^2 + \left(\frac{\partial \dot{m}}{\partial \bar{T}} S_{\bar{T},\mathrm{bias}}\right)^2}$$

Where:

$S_{Q_{random}} = \pm 0.0003\ \frac{m^3}{s}$ (calculated in previous section)

$S_{Q_{bias}} = \pm 0.0006\ \frac{m^3}{s}$ (calculated in previous section)

$S_{\bar{T}_{random}} = \pm 0.04°C$ (calculated in previous section)

$S_{\bar{T}_{Bias}} = \pm 0.18°C$ (calculated in previous section)

The results of the analysis using the data collected during the core ERV at $T_1 = -10°C$ tests concluded the following:

$S_{\dot{m}_{random}} = \pm 7.63 \times 10^{-4} \frac{\text{kg}}{s}$

$S_{\dot{m}_{bias}} = \pm 4.20 \times 10^{-4} \frac{\text{kg}}{s}$

The overall uncertainty of $\dot{m}$ is shown below:

$$U_{\dot{m}} = \sqrt{\left(Z \cdot S_{\dot{m}_{random}}\right)^2 + \left(Z \cdot S_{\dot{m}_{bias}}\right)^2} = \pm 0.002 \frac{\text{kg}}{s}$$

Where:

Z = 2: 95.5% of the data will be within ±2 $S_{\dot{m}}$ of the mean

B.6. Sensible heat transfer effectiveness

The following analysis is based on measurement data collected during the test of core ERV at T1 = −10°C without defrost.

Data reduction equation:

The sensible effectiveness, ε_s is calculated as follows:

$$\varepsilon_s = \frac{\dot{m}_s c_{pa}\left(T_{s,in} - T_{s,out}\right)}{\dot{m}_{min} c_{pa}\left(T_{s,in} - T_{ex,in}\right)}$$

Partial derivatives:

The partial derivatives of the data reduction equation with respect to mass flow rates and temperatures are below:

$$\frac{\partial \varepsilon_s}{\partial \dot{m}_s} = \frac{c_{pa}\left(T_{s,in} - T_{s,out}\right)}{\dot{m}_{min} c_{pa}\left(T_{s,in} - T_{ex,in}\right)}$$

$$\frac{\partial \varepsilon_s}{\partial \dot{m}_{min}} = -\frac{\dot{m}_s c_{pa}\left(T_{s,in} - T_{s,out}\right)}{c_{pa}\left(T_{s,in} - T_{ex,in}\right)} * \frac{1}{(\dot{m}_{min})^2}$$

$$\frac{\partial \varepsilon_s}{\partial T_{s,out}} = -\frac{\dot{m}_s c_{pa}}{\dot{m}_{min} c_{pa}\left(T_{s,in} - T_{ex,in}\right)}$$

$$\frac{\partial \varepsilon_s}{\partial T_{s,in}} = \frac{\left(\dot{m}_s c_{pa}\right)\left(\dot{m}_{min} c_{pa}\right)\left(T_{s,out} - T_{ex,in}\right)}{\left[\dot{m}_{min} c_{pa}\left(T_{s,in} - T_{ex,in}\right)\right]^2}$$

$$\frac{\partial \varepsilon_s}{\partial T_{ex,in}} = \frac{\left(\dot{m}_s c_{pa}\right)\left(\dot{m}_{min} c_{pa}\right)\left(T_{s,in} - T_{s,out}\right)}{\left[\dot{m}_{min} c_{pa}\left(T_{s,in} - T_{ex,in}\right)\right]^2}$$

Standard Deviation Equations:

The standard deviation of ε_s for random and bias errors are calculated separately:

$$S_{\varepsilon_{s_{random}}} = \sqrt{\left(\frac{\partial \varepsilon_s}{\partial \dot{m}_s} S_{\dot{m},\mathrm{rand}}\right)^2 + \left(\frac{\partial \varepsilon_s}{\partial \dot{m}_{min}} S_{\dot{m},\mathrm{rand}}\right)^2 + \left(\frac{\partial \varepsilon_s}{\partial \bar{T}_{s,out}} S_{\bar{T}_{\mathrm{rand}}}\right)^2 + \left(\frac{\partial \varepsilon_s}{\partial \bar{T}_{s,in}} S_{\bar{T}_{\mathrm{rand}}}\right)^2 + \left(\frac{\partial \varepsilon_s}{\partial \bar{T}_{ex,in}} S_{\bar{T}_{\mathrm{rand}}}\right)^2}$$

$$S_{\varepsilon_{s_{bias}}} = \sqrt{\left(\frac{\partial \varepsilon_s}{\partial \dot{m}_s} S_{\dot{m},\text{bias}}\right)^2 + \left(\frac{\partial \varepsilon_s}{\partial \dot{m}_{min}} S_{\dot{m},\text{bias}}\right)^2 + \left(\frac{\partial \varepsilon_s}{\partial \bar{T}_{s,out}} S_{\bar{T}\text{bias}}\right)^2 + \left(\frac{\partial \varepsilon_s}{\partial \bar{T}_{s,in}} S_{\bar{T}\text{bias}}\right)^2 + \left(\frac{\partial \varepsilon_s}{\partial \bar{T}_{ex,in}} S_{\bar{T}\text{bias}}\right)^2}$$

Where:

$S_{\dot{m}_{random}} = \pm 7.63 \times 10^{-4} \ \frac{\text{kg}}{s}$ (calculated in previous section)

$S_{\dot{m}_{bias}} = \pm 4.20 \times 10^{-4} \ \frac{\text{kg}}{s}$ (calculated in previous section)

$S_{\bar{T}_{random}} = \pm 0.04°C$ (calculated in previous section)

$S_{\bar{T}_{Bias}} = \pm 0.18°C$ (calculated in previous section)

The results of the analysis using the data collected during the core ERV at $T_1 = -10$°C tests concluded the following:

$S_{\varepsilon_{s_{random}}} = \pm 0.02$

$S_{\varepsilon_{s_{bias}}} = \pm 0.01$

The overall uncertainty of ε_s is shown below:

$$U_{\varepsilon_s} = \sqrt{\left(Z \cdot S_{\varepsilon_{s_{random}}}\right)^2 + \left(Z \cdot S_{\varepsilon_{s_{bias}}}\right)^2} = \pm 0.04$$

Where:

Z = 2: 95.5% of the data will be within ±2 S_{ε_s} of the mean

B.7. Latent heat transfer effectiveness

The following analysis is based on measurement data collected during the test of core ERV at T1 = −10°C without defrost.

Data reduction equation:

The sensible effectiveness, ε_l is calculated as follows:

$$\varepsilon_l = \frac{\dot{m}_s(W_{s,in} - W_{s,out})}{\dot{m}_{min}(W_{s,in} - W_{ex,in})}$$

Partial derivatives:

The partial derivatives of the data reduction equation with respect to mass flow rates and temperatures are below:

$$\frac{\partial \varepsilon_l}{\partial \dot{m}_s} = \frac{(W_{s,in} - W_{s,out})}{\dot{m}_{min} c_{pa}(W_{s,in} - W_{ex,in})}$$

$$\frac{\partial \varepsilon_l}{\partial \dot{m}_{min}} = -\frac{\dot{m}_s(W_{s,in} - W_{s,out})}{(T_{s,in} - W_{ex,in})} * \frac{1}{(\dot{m}_{min})^2}$$

$$\frac{\partial \varepsilon_s}{\partial W_{s,out}} = -\frac{\dot{m}_s}{\dot{m}_{min}(W_{s,in} - W_{ex,in})}$$

$$\frac{\partial \varepsilon_s}{\partial W_{s,in}} = \frac{\dot{m}_s \cdot \dot{m}_{min}(W_{s,out} - W_{ex,in})}{[\dot{m}_{min}(W_{s,in} - W_{ex,in})]^2}$$

$$\frac{\partial \varepsilon_s}{\partial W_{ex,in}} = \frac{\dot{m}_s \cdot \dot{m}_{min}(W_{s,in} - W_{s,out})}{[\dot{m}_{min} c_{pa}(W_{s,in} - W_{ex,in})]^2}$$

Standard Deviation Equations:

The standard deviation of ε_l for random and bias errors are calculated separately:

$$S_{\varepsilon_{l_{random}}} = \sqrt{\left(\frac{\partial \varepsilon_l}{\partial \dot{m}_s} S_{\dot{m},\text{rand}}\right)^2 + \left(\frac{\partial \varepsilon_l}{\partial \dot{m}_{min}} S_{\dot{m},\text{rand}}\right)^2 + \left(\frac{\partial \varepsilon_l}{\partial \text{W}_{s,out}} S_{\text{W}_{\text{rand}}}\right)^2 + \left(\frac{\partial \varepsilon_l}{\partial \text{W}_{s,in}} S_{\text{W}_{\text{rand}}}\right)^2 + \left(\frac{\partial \varepsilon_l}{\partial \text{W}_{ex,in}} S_{\text{W}_{\text{rand}}}\right)^2}$$

$$S_{\varepsilon_{l_{bias}}} = \sqrt{\left(\frac{\partial \varepsilon_l}{\partial \dot{m}_s} S_{\dot{m},\text{bias}}\right)^2 + \left(\frac{\partial \varepsilon_l}{\partial \dot{m}_{min}} S_{\dot{m},\text{bias}}\right)^2 + \left(\frac{\partial \varepsilon_l}{\partial W_{s,out}} S_{W_{\text{bias}}}\right)^2 + \left(\frac{\partial \varepsilon_l}{\partial W_{s,in}} S_{W_{\text{bias}}}\right)^2 + \left(\frac{\partial \varepsilon_l}{\partial W_{ex,in}} S_{W_{\text{bias}}}\right)^2}$$

Where:

$S_{\dot{m}_{random}} = \pm 7.63 \times 10^{-4} \ \frac{\text{kg}}{s}$ (calculated in previous section)

$S_{\dot{m}_{bias}} = \pm 4.20 \times 10^{-4} \ \frac{\text{kg}}{s}$ (calculated in previous section)

$S_{\text{W}_{random}} = \pm 1.42 \times 10^{-7} \ kg/kg_{da}$ (calculated in previous section)

$S_{\text{W}_{Bias}} = \pm 3.91 \times 10^{-7} \ kg/kg_{da}$ (calculated in previous section)

The results of the analysis using the data collected during the core ERV at $T_1 = -10°\text{C}$ tests concluded the following:

$S_{\varepsilon_{l_{random}}} = \pm 0.015$

$S_{\varepsilon_{l_{bias}}} = \pm 0.008$

The overall uncertainty of ε_l is shown below:

$$U_{\varepsilon_l} = \sqrt{\left(Z \cdot S_{\varepsilon_{l_{random}}}\right)^2 + \left(Z \cdot S_{\varepsilon_{l_{bias}}}\right)^2} = \pm 0.03$$

Where:

Z = 2: 95.5% of the data will be within ±2 S_{ε_l} of the mean

APPENDIX C. SUPPLEMENTARY RESULTS

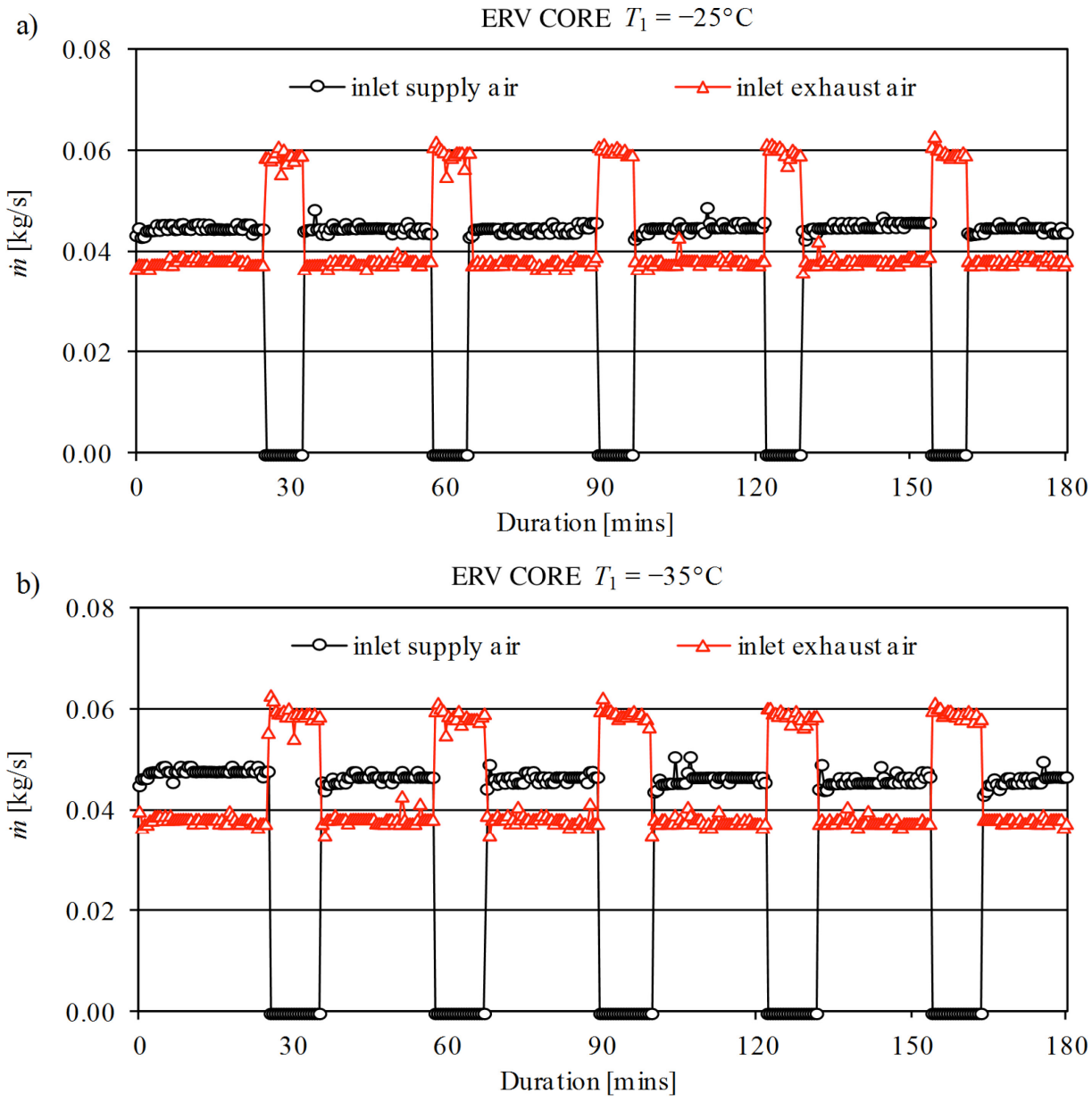

Figure C.1: Inlet supply and exhaust air mass flow rates versus time for a single HEE with defrost enabled for core ERV at a) $T_1 = -25°C$ and b) $T_1 = -35°C$

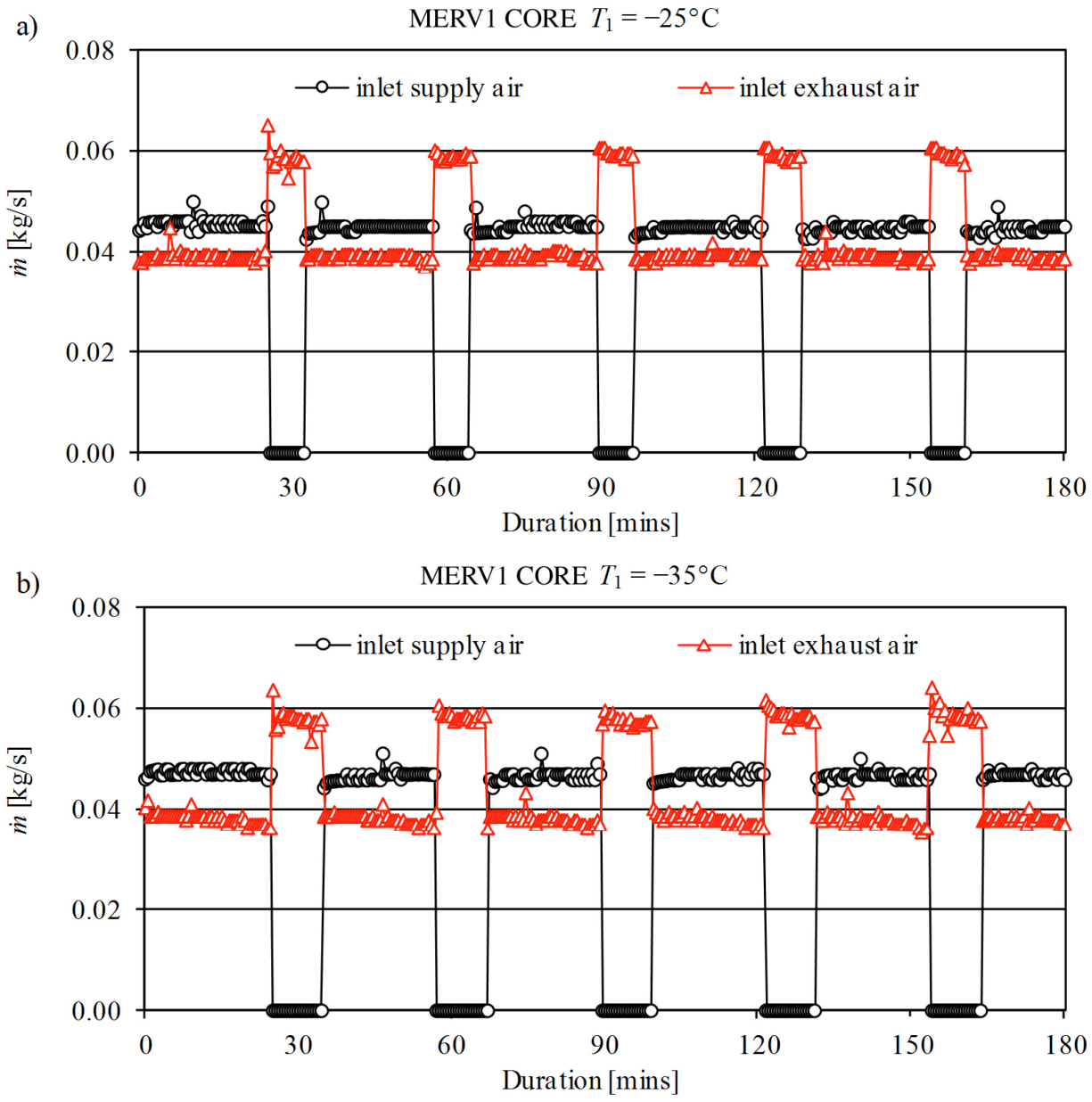

Figure C.2: Inlet supply and exhaust air mass flow rates versus time for a single HEE with de-frost enabled for core MERV1 at a) T_1= −25°C and b) T_1= −35°C

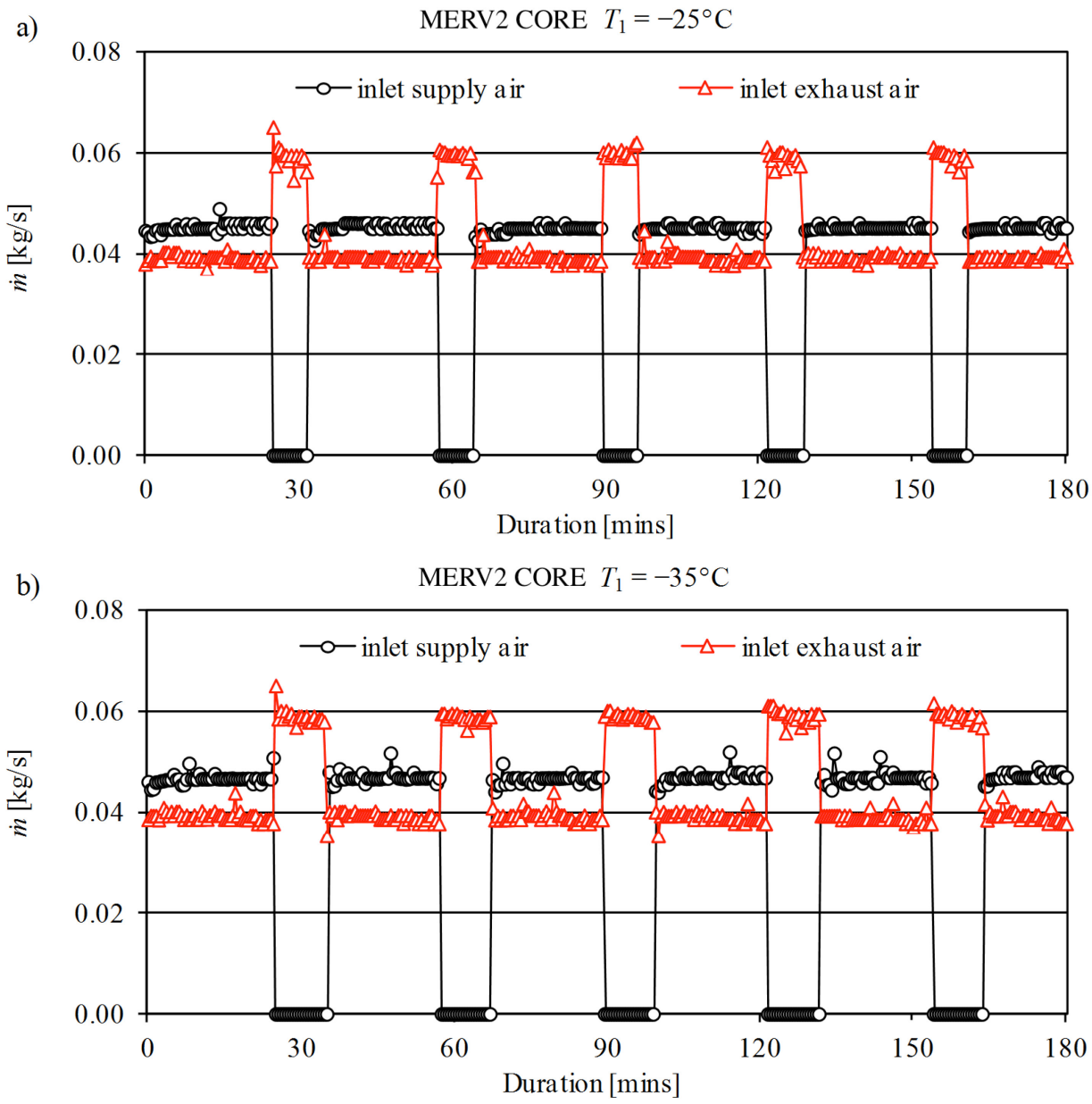

Figure C.3: Inlet supply and exhaust air mass flow rates versus time for a single HEE with de-frost enabled for core MERV2 at a) T_1= −25°C and b) T_1= −35°C

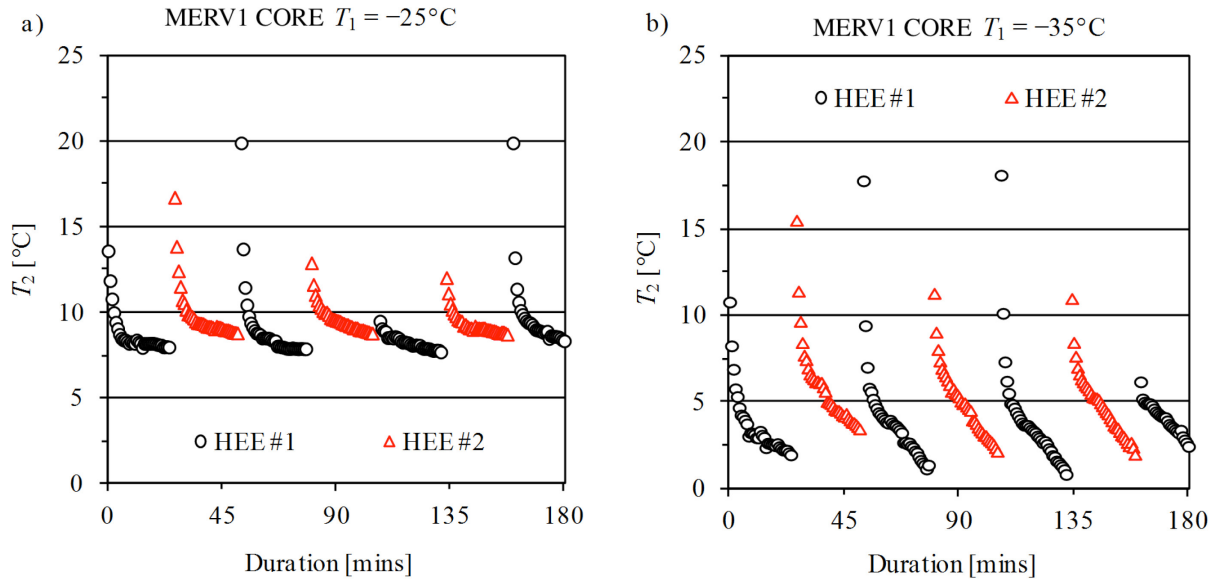

Figure C.4: Measured outlet supply air temperature for two HEE units with alternating defrost for a) MERV1 core at $T_1 = -25°C$ and b) MERV1 core at $T_1 = -35°C$

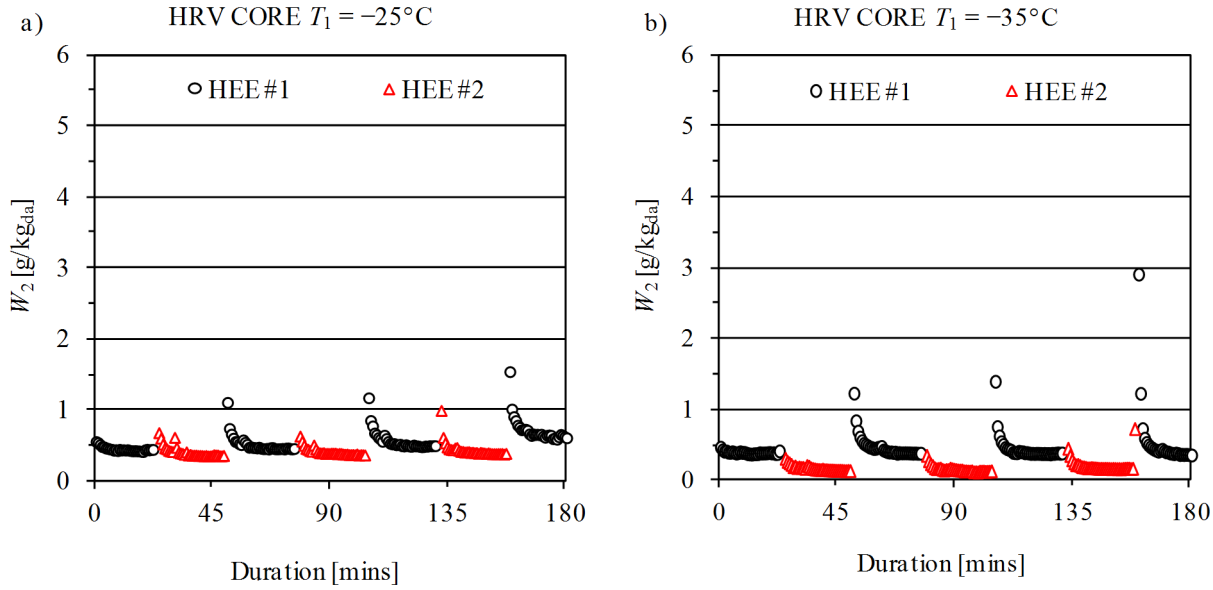

Figure C.5: Outlet supply air humidity ratio for two HEE units with alternating defrost for a) HRV core at $T_1 = -25°C$ and b) HRV core at $T_1 = -35°C$

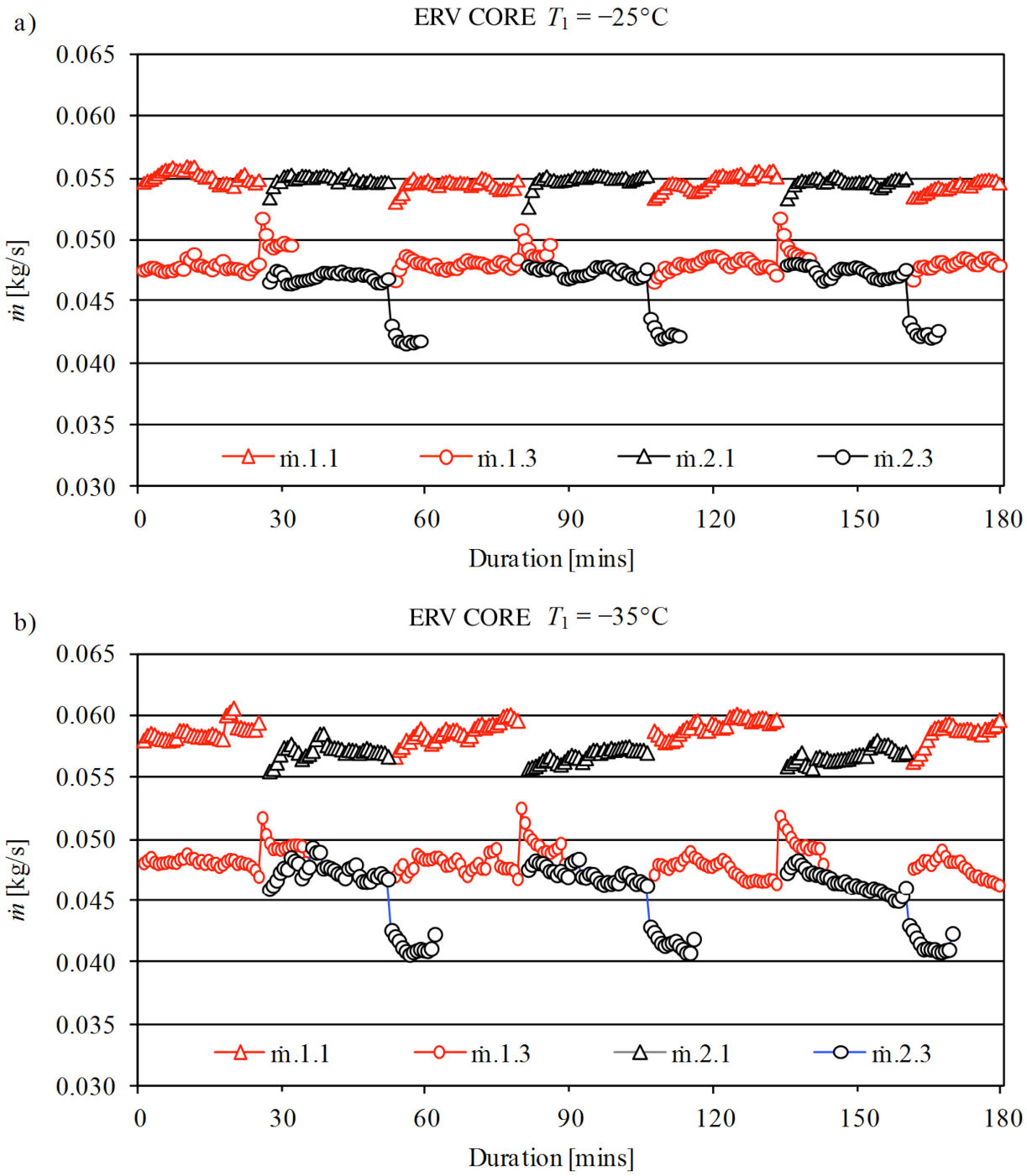

Figure C.6: Inlet supply and exhaust air mass flow rates versus time for two HEE units with alternating defrost core ERV at a) $T_1 = -25°C$, b) $T_1 = -35°C$

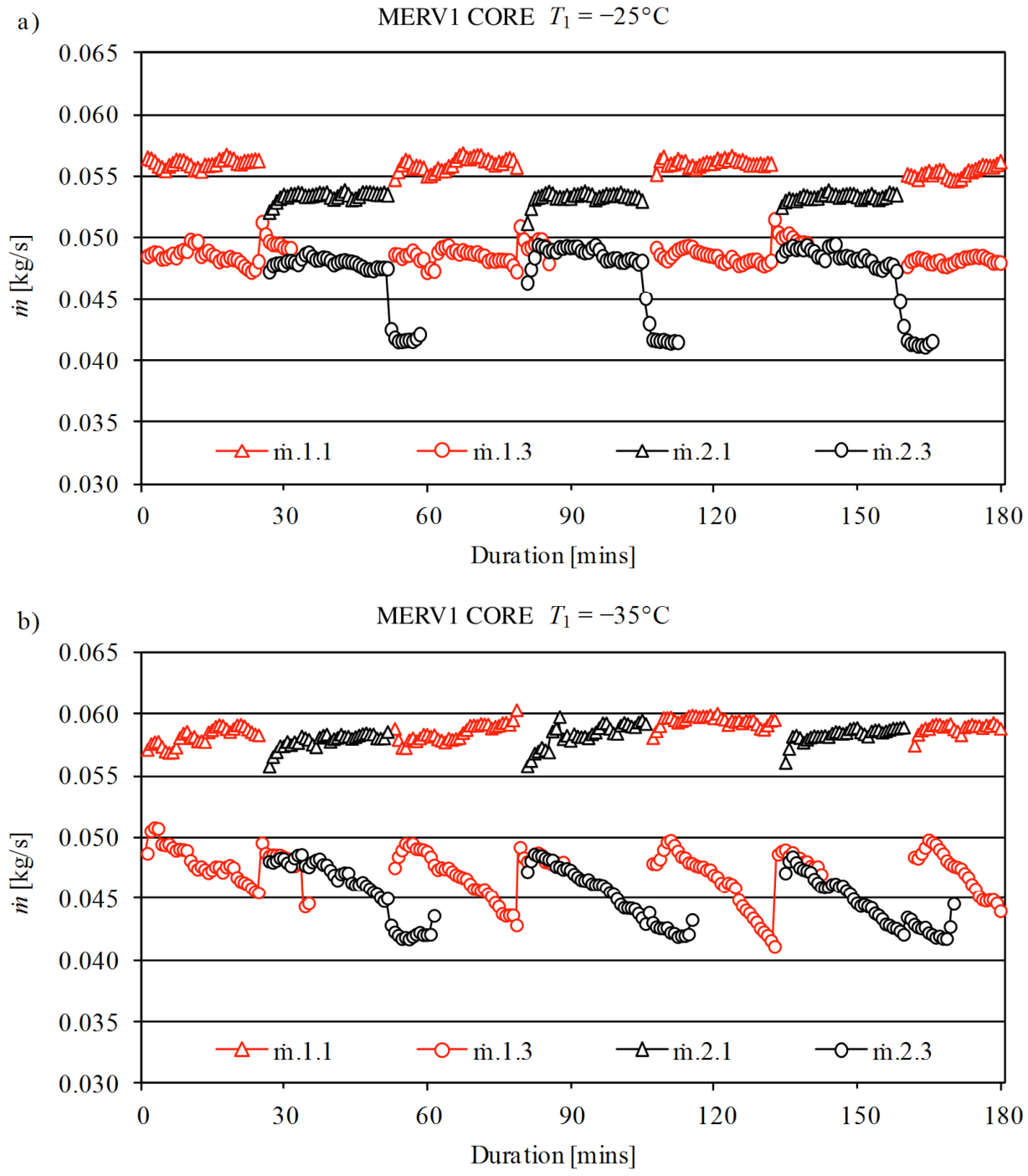

Figure C.7: Inlet supply and exhaust air mass flow rates versus time for two HEE units with alternating defrost core MERV1 at a) $T_1 = -25°C$, b) $T_1 = -35°C$